Technische Universität München
Institut für Energietechnik

Professur für Thermofluiddynamik

State Space Modeling of Thermoacoustic Systems with Application to Intrinsic Feedback

Thomas Michael Emmert

Vollständiger Abdruck der von der Fakultät für Maschinenwesen der Technischen Universität München zur Erlangung des akademischen Grades eines

DOKTOR – INGENIEURS

genehmigten Dissertation.

Vorsitzender:
Univ.-Prof. Dr.-Ing. habil. Boris Lohmann
Prüfer der Dissertation:
Univ.-Prof. Wolfgang Polifke, Ph.D.
Univ.-Prof. Dr.-Ing. Jonas Moeck

Die Dissertation wurde am 24.05.2016 bei der Technischen Universität München eingereicht und durch die Fakultät für Maschinenwesen am 22.09.2016 angenommen.

Abstract

One way to cope with the complexity of thermoacoustic systems is network modeling. The full system is partitioned into a network of interconnected subsystems. Each of the subsystems can be modeled independently with adequate complexity. In particular, linearized models have proven to predict the propagation of acoustic perturbations very well in many cases. There have been a lot of different model structures associated with the individual methods to retrieve linear acoustic models. Analytical derivations typically involved time delays, linearized PDEs used to be evaluated in frequency domain directly inside of the FEM software and LES system identification resulted in discrete time filters. We have adapted and developed a framework called taX which unifies all types of linear acoustic models based on linear system theory and state space modeling. Besides providing a standardized basis for linear acoustic models, there is a generic interconnection algorithm for state space network models. It evaluates the interconnections between the subsystem models and results in one joint linear state space model. Consequently, eigenvalues of the connected system can be computed by solving a standard or generalized linear eigenvalue problem. This leads especially for large systems to a tremendous speed improvement over the classical multiplicative coupling in frequency domain. In the latter case, a nonlinear eigenvalue problem needed to be solved instead.

A continuous time linear state space system is stable, if the real parts of all eigenvalues are less than zero. Consequently, it is easy to determine the stability of a linear acoustic network model if it is modeled by state space systems. But the eigenvalues of a network model can only be computed, if all subsystem models are fully specified. In complex systems such as gas turbines it would be favorable to draw conclusions about the stability just by investigating isolated parts of the system. It is of interest to provide a stability criterion which helps to discriminate between burners which are more or less prone to instability. Such a criterion is given by the instability potentiality, which is based on sound power amplification and corresponding to the small gain theorem.

Common perception was that instability in thermoacoustic systems happens due to acoustic eigenmodes becoming unstable. This idea is based on the assumption that the amplification of acoustic cavity modes by the flame may exceed the damping by acoustic losses inside the device and at the boundaries. But recently it was discovered that thermoacoustic systems with velocity sensitive flames may exhibit unstable eigenmodes even if non reflective boundary conditions enforce that no cavity modes exist. Those intrinsic thermoacoustic (ITA) modes are caused by an intrinsic feedback: Heat release fluctuations of the flame act as a volume source and generate upstream traveling acoustic waves. Those acoustic waves in turn cause a velocity perturbation at the burner mouth, which excites the flame dynamics. Therefore, these ITA modes are distinct from the acoustic modes of the system and they also exist in full gas burner test rigs with

reflective boundaries. The thorough investigation of the interconnection of state space models for acoustics and flame allows to identify and discriminate between ITA and acoustic cavity modes of a full system. This paradigm shift in the interpretation of thermoacoustic instability brings an explanation for apparently paradox behavior such as the destabilization of a combustor test rig by raising the acoustic losses at the downstream end using a perforated plate.

Kurzfassung

Ein Weg zur Beherrschung der Komplexität in thermo-akustischen Systemen ist die Netzwerk Modellierung. Das Gesamtsystem wird in miteinander verbundene Teilsysteme aufgeteilt. Jedes Teilsystem kann mit der jeweils lokal notwendigen Komplexität modelliert werden. Dabei haben sich speziell linearisierte Modelle als gut geeignet erwiesen um die akustische Wellenausbreitung abzubilden. In Abhängigkeit der unterschiedlichen Methoden um lineare akustische Modelle zu gewinnen, gab es eine Vielzahl verschiedener Modellstrukturen. Analytische Herleitungen münden typischer Weise in Zeitverzügen, lineariserte partielle Differentialgleichungen wurden direkt in der FEM Software im Frequenzbereich ausgewertet und LES in Kombination mit System Identifikationsalgorithmen resultiert in zeitdiskreten Filtern. Aufbauend auf linearer System Theorie und Zustandsraum Modellen haben wir eine Werkzeugsammlung namens taX entwickelt, die eine vereinheitlichte Modellierung erlaubt. Neben der standardisierten Basis für lineare akustische Modelle, gibt es einen generischen Verbindungsalgorithmus für Zustandsraum Modelle. Dieser wertet die Verbindungen zwischen den Teilsystemen aus und liefert als Ergebnis ein zusammengefasstes lineares Zustandsraum Modell zurück. Folglich können die Eigenwerte des verbundenen Gesamtsystems durch die Lösung eines linearen Eigenwert Problems bestimmt werden. Speziell für große Systeme ist diese Vorgehensweise um viele Größenordnungen effizienter als die herkömmliche multiplikative Kopplung im Frequenzraum. In letzterem Fall muss stattdessen ein nichtlineares Eigenwert Problem gelöst werden.

Ein zeitkontinuierliches lineares Zustandsraum Modell ist stabil, wenn die Realteile aller Eigenwerte negativ sind. Dementsprechend ist es einfach die Stabilität von linearen akustischen Netzwerk Modellen zu bestimmen, sofern sie als Zustandstraum Modell vorliegen. Allerdings funktioniert das nur, wenn alle Teilsysteme des Netzwerk Modelles vollständig definiert vorliegen. In komplexen Systemen, wie Gas Turbinen ist es vorteilhaft, wenn man in der Lage ist Schlüsse über die Stabilität von einzelnen Teilsystemen zu ziehen, ohne das Gesamtsystem komplett zu berücksichtigen. Es ist hoch Interessant ein Stabilitätskriterium zu finden, das eine Unterscheidung zwischen Brennern zu lässt, die mehr oder weniger stark zu Instabilität neigen. Solch ein Kriterium wird durch die "Instability Potentiality" gegeben, welche auf akustischer Leistungsverstärkung basiert und dem Small Gain Theorem entspricht.

Die herkömmliche These war, dass Instabilität von themoakustischen Systemen allein durch instabile akustische Eigenmoden verursacht wird. Dieses Konzept basiert auf der Annahme, dass die Verstärkung von akustischen Moden durch die Flamme größer sein kann als die Dämpfung durch akustische Verluste im Inneren der Maschine und an den Rändern. Vor kurzem wurde entdeckt, dass thermoakustische Systeme mit geschwindigkeits sensitiven Flammen auch dann Eigenmoden besitzen, wenn das System durch nicht reflektierende Ränder gar keine akustischen Moden hat. Diese intrinsischen thermo-akustischen (ITA) Moden werden durch eine intrinsis-

che Rückkopplung verursacht: Wärmefreisetzungsschwankungen der Flamme wirken wie eine Volumen Quelle und erzeugen stromauf propagierende Schallwellen. Diese Schallwellen erzeugen ihrerseits eine Geschwindigkeitsstörung am Brenner Auslass, die die Flammendynamik anregt. Folglich sind ITA Moden phänomenologisch von akustischen Moden verschieden und sie existieren auch in echten Gas Brenner Teststänten mit reflektierenden Rändern. Die präzise Untersuchung der Verbindung der Zustandsraum Modelle für die Akustik und die Flamme erlaubt eine klare Unterscheidung zwischen ITA und akustischen Moden eines kompletten Systems. Dieser Paradigmenwechsel in der Interpretation von thermoakustischer Instabilität erlaubt eine Erklärung für scheinbar paradoxe Situationen wie die Destabilisierung eines Brenner Versuchsstandes durch die Erhöhung akustischer Verluste mit einer perforierten Platte als Terminierung.

Contents

1 Introduction

Prediction and optimization of thermoacoustic stability is important in many applications as diverse as domestic heaters, gas turbines or rocket engines. Thermoacoustic instability may occur, when acoustic perturbations in a system are amplified. The resulting elevated amplitudes of pressure and velocity oscillations increase wear and emissions and may ultimately even destroy a system. For instance, liners of gas turbines may break and combustor face plates may melt as shown in Fig. 1.1. In rocket engines, thermoacoustic instability may even destroy the entire device. In order to avoid thermoacoustic instability, the operational range of systems needs to be restrained. For example in lean premixed combustion gas turbines, thermoacoustic resonances enforce a trade off between low $N0_x$ emissions and the tolerable sound pressure level [1]. Thus, there is a large interest to develop tools to efficiently simulate and predict the dynamics of thermoacoustic systems and to enhance the understanding of the causes for thermoacoustic instability.

Modeling and simulation of thermoacoustic systems is typically very hard and computationally expensive for two reasons. The first issue is that multi scale processes are involved in the generation and propagation of acoustic waves. On the one hand, acoustic flow noise is often generated by turbulence or combustion, which are very small scale phenomena. On the other hand, acoustic waves are weakly damped as they propagate in confined systems and therefore interactions within large domains like entire HVAC systems or gas turbines need to be taken into account. The second issue is that thermoacoustic systems may require multi physics simulations. This is the case if combustion is involved. For instance in gas turbines or rocket engines, acoustic waves can interact with the combustion process, which may cause thermoacoustic instabilities.

Even though multi scale and multi physics phenomena may be involved in some parts of a thermoacoustic system, the propagation of acoustic waves typically remains linear in most other parts. Therefore it is of interest not to model the entire thermoacoustic system with one single

[1] Reproduced with kind permission of Prof. Sikke Klein

Figure 1.1: Damages of a gas turbine liner (left) and combustor face plate (right) due to thermoacoustic instability.[1]

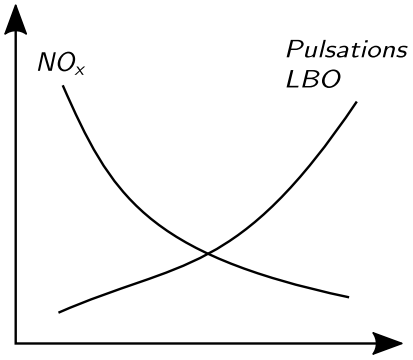

Figure 1.2: Trade off between NO_x emissions and lean blow out (LBO) due to thermoacoustic oscillations.

type of model that captures all possible effects, but rather to subdivide the system into a network of interconnected subsystems. Each subsystem, can then be modeled with suitable complexity and the interconnected model is supposed to retrieve the overall thermoacoustic dynamics.

The manuscript is structured as follows: At first an introduction to thermoacoustic network modeling is presented. Special emphasis is put on the difference between classical frequency domain methods and newer state space modeling approaches. Due to the identity of frequency and time domain in state space models, we can easily determine the stability of such systems. In order to do so, an algorithm to connect two linear state space systems, which retrieves one joint state space system is presented and explained. This procedure has the huge advantage, that linear eigenvalue problems can be solved to determine the stability of thermoacoustic network models. The classical frequency domain approaches need to solve a nonlinear eigenvalue problem, which is much less computationally efficient. Furthermore, the network models can be simulated in time and used as a boundary condition for LES simulations. By doing so, the acoustic environment of an entire combustion test rig can be simulated jointly with a nonlinear high fidelity combustion simulation [2] at reasonable computational costs.

Subsequently acoustic energy and sound power based stability criteria are elaborated. There is a stability criterion called "instability potentiality" respectively "whistling potential". It can be linked to a system theoretic method called the small gain theorem. Unfortunately, the criterion does not directly prove to be useful for stability investigations on premixed flames, because it is very conservative and over predicts instability. However, it may be used to identify burner configurations, which minimize sound power amplification.

Finally the dynamics of premixed combustion systems are investigated. It is shown, that an intrinsic feedback between flame and burner causes intrinsic thermoacoustic (ITA) eigenmodes of full combustion test rig systems, which are clearly distinct from acoustic cavity modes of the system. This has several important implications for the theory of thermoacoustic combustion instability. First of all, thermoacoustic combustion systems possess more eigenmodes than just the acoustic cavity modes. When thermoacoustic instability occurs, it does not necessarily need to be an acoustic mode which becomes unstable due to the driving of the flame, as traditional theories assume. It may just as well be an ITA eigenmode, which becomes unstable due to the

coupling with the acoustic boundaries. The theory of ITA eigenmodes in combustion systems explains seemingly paradox phenomena such as the destabilization of a combustion test rig by applying a dissipative perforated plate termination.

A summary of achievements condenses the contributions of the author to the respective developments and publications. Eventually the outlook presents potentials for further development in the pursuit of providing better tools for the modeling of thermoacoustic systems.

2 Thermoacoustic Network Modeling

Thermoacoustic network modeling is a state of the art technique to model the thermoacoustic dynamics of large confined systems. It is based on a subdivision of a system into interconnected subsystems, which locally model the generation and propagation of acoustic perturbations [3]. Interfaces need to be defined, where the system is split into subsystem models. Subsequently the subsystem models are connected by an interconnection algorithm. The resulting aggregated thermoacoustic network model can for example be solved for frequency responses, and their linear stability properties can be determined.

There are two modeling paradigms for the interfaces and the connection of subsystem models. The first one is simply an averaged balance of the acoustic state on the interface. As it does not presume the wave number vector or the frequency of the modes involved, it naturally ties into time and frequency domain investigations [4–6]. The second one is the classical frequency domain network modeling, which presumes the structure of the wave number vector on the interface and the complex frequency of oscillation [7–10]. Depending on the modeling paradigm, the interconnection of the systems is different and the resulting interconnected system is different as well. This has important implications especially for the efficiency of the computation of eigenmodes.

Subsequently, the interface and interconnection design is presented. The differences between higher order frequency domain and universal coupling are discussed. A brief introduction to linear models in general is given, followed by a section, which presents methods to retrieve such models of acoustic and thermoacoustic systems. In the context of network modeling, the interconnection algorithm is a key technology. Therefore, the state space interconnection algorithm is presented and differences to the classical frequency domain methods are emphasized. The nature of the model, state space or classical frequency domain, determines how the system is solved. Thus we discuss implications for the efficiency of the computation of eigenvalues.

2.1 Interface Design

The process of subdividing the system raises the need for well defined interfaces between subsystems. There is a distinction between planar wave and so called higher order mode interfaces.

Plane wave interfaces presume that the wave propagation on the interface is one dimensional. This condition is necessarily valid, if the smallest acoustic wave length involved is larger than the diameter D of the interface. This corresponds to acoustically compact interfaces: $\mathrm{He} = (Df)/c \ll 1$. In different words, if the maximum frequency of interest is less than the cut on frequency of a duct section with the cross section of the respective interface, there are

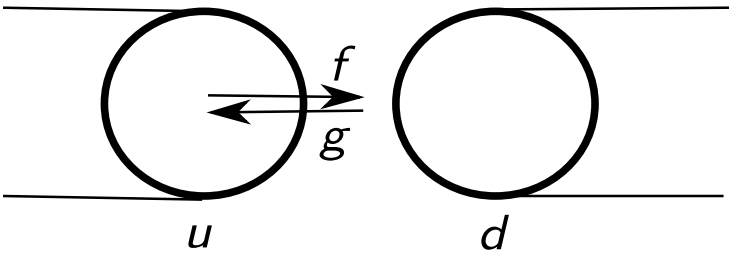

Figure 2.1: Plane wave interface between subsystems u and d.

just plane waves propagating. The averaged acoustic state variables across the interface are

$$u'_u = u'_d; \quad p'_u = p'_d, \tag{2.1}$$

where u', p' are the axial acoustic velocity and pressure oscillations and the subscripts u, d denote the up and downstream system at the respective interface. A different set of state variables are expressed by Riemann invariants

$$f = (p'/(\rho c) + u')/2; \quad g = (p'/(\rho c) - u')/2, \tag{2.2}$$

of the linearized Euler equations. The resulting coupling condition is

$$f_u = f_d; \quad g_u = g_d, \tag{2.3}$$

as shown in Fig. 2.1. For planar waves, the simple coupling of the state at the interface and the classical frequency domain network method result in the same equations.

The term higher order modes relates to the mode shapes of a duct section above cut on but here we generalize it and use the expression to charactarize any non-planar wave interface. For non-planar waves, there is a difference between the simple coupling of averaged states on the plane and the classical frequency domain method.

2.1.1 Higher Order Frequency Domain Coupling

The classical way to realize a thermoacoustic network simulation code is to couple the individual subsystems in frequency domain by evaluating the frequency response of the subsystem at the given frequency. The corresponding waves traveling in the same direction on both sides of the interface between two connected annular subsystems must have the same wave number vector. This wave number vector consists of an axial and an azimuthal component [11] as depicted in Fig. 2.2. There is a symmetry condition in azimuthal direction imposed:

$$k_\phi = \pm m \quad , m = 1, 2, 3, \ldots \tag{2.4}$$

This restricts the azimuthal wave number to be real and discrete on the interface. The axial wave number component is a function of the frequency:

$$k_{x\pm} = \frac{k}{1-M^2}\left(-M \pm \sqrt{1-\left(\frac{k_\phi}{Rk}\right)^2 (1-M^2)}\right) \tag{2.5}$$

with $k = \omega/c$ and R the middle radius of the annulus.

There are several issues with this definition:

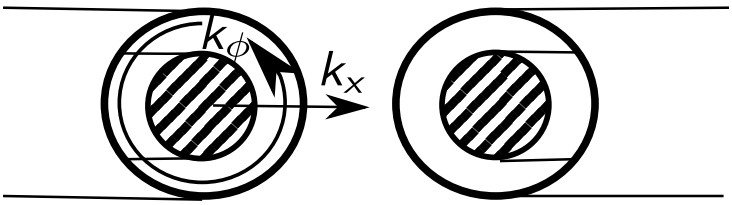

Figure 2.2: Higher order annular acoustic subsystem interface with wave number vector coupling.

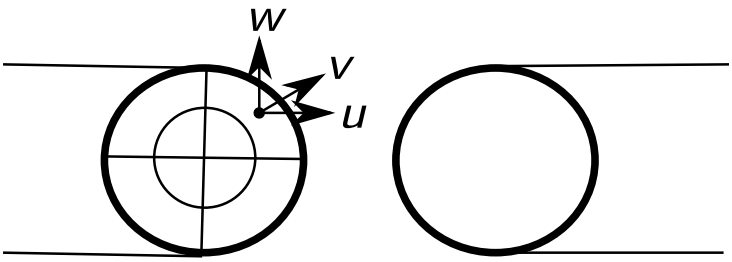

Figure 2.3: Higher order acoustic subsystem interface with mass, momentum, species and energy coupling.

- The symmetry condition is justified for modes shapes of marginally stable, neither growing nor decaying, azimuthal eigenmodes in annular duct sections. However the direction of propagation of the acoustic wave fronts in principal axis k is not orthogonal to the surface of the interface. Therefore, the symmetry condition does not necessarily hold in the case of growth or decay of a mode or transient time domain simulation.

- The second shortcoming is that the interface relies on $k_{x\pm}$, which is a function of ω. Therefore, it is not possible to construct subsystem models with constant coefficients independent of ω such as state space models. This implies, that eigenvalues of such a system cannot be obtained by solving a standard linear eigenvalue problem.

- Depending on the investigated frequency range and problem, it is possible that multiple azimuthal wave numbers need to be considered. This makes the handling complicated, as it is difficult to determine the maximum order of m.

2.1.2 Universal Higher Order Coupling

Instead of presuming the mode shape on the higher order interface, it is possible to divide it into patches and to couple the averaged acoustic (and species if applicable) state variables as depicted in Fig. 2.3. The number of the patches can be increased up to the point, where the coupling is on a cell by cell basis between the domains of the subsystems. This procedure would be similar to aero acoustic solvers, which couple a solid body and its oscillations with a system of linearized PDEs for the acoustic propagation.

2.2 Linear Subsystem Models

Having chosen a decomposition of a thermoacoustic system with plane wave or universal interfaces, linear subsystem models for the parts of a linear network model can be defined. For simplicity, the derivation is limited to plane wave interfaces. In this case, the models are independent of the different interface and interconnection modeling paradigms introduced in the previous section. At first an introduction to linear dynamic models and system theory is given. Subsequently, several procedures for retrieving such models from acoustic systems are presented. Eventually, the interconnection of subsystems is presented for both, the classical frequency domain and the state space systems.

2.2.1 General Properties of Linear Models

A linear dynamic model $\mathtt{f}$ (function not the acoustic wave) relates some input time series $u(t)$ with an output $y(t)$. Typical inputs are incident acoustic Riemann invariants f, g also called characteristic wave amplitudes (CWA) or acoustic velocity fluctuations. Outputs may be emitted CWA or pressure fluctuations. The most general expression for such a model is given by the convolution of the input with the impulse response function $G(\tau)$, also known as *Green's function*, of the model $\mathtt{f}$:

$$y(t) = \mathtt{f}(u(t)) = G(\tau) \star u(t) = \int_{-\infty}^{\infty} G(\tau)\, u(t-\tau)\, \mathrm{d}\tau\,. \tag{2.6}$$

The past values of the input time series are convolved with the impulse response function G. If the system is causal, the output $y(t)$ only depends on past inputs $u(t-\tau; \tau \geq 0)$ and the convolution reduces to

$$y(t) = \int_{0}^{\infty} G(\tau)\, u(t-\tau)\, \mathrm{d}\tau\,. \tag{2.7}$$

The convolution integral is linear as it satisfies additivity (superposition)

$$\mathtt{f}(u_1 + u_2) = \mathtt{f}(u_1) + \mathtt{f}(u_2) \tag{2.8}$$

and homogeneity of degree 1

$$\mathtt{f}(a u(t)) = a\mathtt{f}(u(t))\,. \tag{2.9}$$

The *Laplace transform* is defined to be

$$\mathscr{L}\{\mathtt{f}(t)\} = \int_{-\infty}^{\infty} \mathtt{f}(t) e^{-st}\, \mathrm{d}t = F(s)\,. \tag{2.10}$$

We use the definition $s = j\omega + \sigma$ of the Laplace variable, where ω is the angular frequency and σ is the growth rate. In the Laplace domain, the convolution becomes a multiplication of the Laplace transformed input and output time series and the so called *transfer function* $G(s)$, which is the Laplace transform of the Green's function:

$$\mathscr{L}\{y(t)\} = y(s) = \mathscr{L}\{G(\tau) \star u(t))\} = \mathscr{L}\{G(\tau)\} \cdot \mathscr{L}\{u(t))\} = G(s) \cdot u(s)\,. \tag{2.11}$$

Commonly, linear systems are examined using impulse, step and frequency responses. The frequency response of a linear model is retrieved by evaluating the transfer function at a set of

discrete frequencies ω. Similar, the impulse response is computed from evaluating the impulse response function at a set of delays τ. However it is important to notice, that the responses of a linear system characterize properties of the corresponding linear model. Usually, they are not linear models by themselves.

2.2.2 Polynomial Transfer Function Models

There is a large class of linear dynamic models, which may be described by a linear differential equation in time

$$b_0 y(t) + b_1 \dot{y}(t) + b_2 \ddot{y}(t) + \ldots + b_m \frac{\mathrm{d}^m y(t)}{\mathrm{d}^m t} = a_0 u(t) + a_1 \dot{u}(t) + a_2 \ddot{u}(t) + \ldots + a_n \frac{\mathrm{d}^n u(t)}{\mathrm{d}^n t}, \quad (2.12)$$

The transfer function of such models can easily be determined by applying Laplace transform into frequency domain, where the model is expressed by a rational polynomial in s

$$G(s) = \frac{a_0 + a_1 s + a_2 s^2 + \ldots + a_n s^n}{b_0 + b_1 s + b_2 s^2 + \ldots + b_m s^m}. \quad (2.13)$$

Subsequently, the input output relation is solved by integration of the convolution equation (2.7) using the inverse Laplace transformation of the transfer function to obtain the corresponding Green's function.

2.2.3 State Space Models

There is a generalization of polynomial transfer function models by so called *state space* models. Instead of modeling systems with one dimensional rational polynomials of high order, it is possible to represent the same dynamics with a high dimensional system of equations of first order:

$$\begin{aligned} E\dot{x} &= Ax + Bu \\ y &= Cx + Du \end{aligned} \quad (2.14)$$

where x is the state vector and $ABCDE$ are the system matrices with constant coefficients. B relates the inputs to the time derivative of the state and C maps the state on the ouputs. The so called feedthrough matrix D directly links inputs u and outputs y, as it typically happens in acoustically compact subsystems. The dynamics of the model are given by A and E. Depending on the source of the model (see section 2.3), the state vector x may or may not have an explicit physical signification like a pressure distribution inside the subsystem.

The transfer function $G(s)$ of every state space model can be determined uniquely by Laplace transform. It is given by a rational polynomial in s

$$y(s) = \underbrace{\left(C(Es - A)^{-1}B + D\right)}_{G(s)} u(s). \quad (2.15)$$

The opposite translation from a polynomial transfer function to a state space model exists as well, but it is not unique. One generic way to achieve such a translation is given by the controllable canonical form [2, 12]:

$$\dot{x} = \begin{bmatrix} 0 & 1 & & \\ & \ddots & \ddots & \\ & & 0 & 1 \\ -a_0 & -a_1 & \dots & -a_{m-1} \end{bmatrix} x + \begin{bmatrix} 0 \\ \vdots \\ 0 \\ 1 \end{bmatrix} u \tag{2.16}$$
$$y = \begin{bmatrix} b_0 - b_n a_0, & b_1 - b_n a_1, & \dots, & b_{n-1} - b_n a_{m-1} \end{bmatrix} x + b_n u .$$

In the derivations shown above just single input, single output (SISO) systems are considered. However, the extension to multiple input, multiple output systems (MIMO) is straight forward and will be used in the following without further notice. Then the inputs u and outputs y are vectors instead of scalars and B, C, D are matrices instead of vectors or scalars.

2.3 Methods to Retrieve Linear Acoustic and Thermoacoustic Models

The purpose of linear thermoacoustic network modeling is to cope with the different levels of complexity in distinct parts of the corresponding system. By dividing the system into interconnected parts, each subsystem can then be modeled by a modeling procedure that is as simple as possible, while capturing the relevant effects.

In the following sections, models retrieved from 1D duct acoustics, $n-\tau$ flame models, 2d/3D linearized PDEs and system identification are briefly discussed. Most emphasis is put on the 1D models as they provide the most valuable insights without adding superfluous complexity.

2.3.1 1D Duct Acoustic

In a homogeneous perfect gas, the propagation of acoustic waves can be modeled by an isentropic compression. In the simplest case of a thermoacoustic system, there is one dimensional wave propagation. Analytical solutions exist for a variety of acoustically compact ($He = fd/c \ll 1$) elements, such as area or temperature discontinuities and for duct sections. Assuming a fluid at rest, the one dimensional propagation of acoustic waves in a duct section is described by the linearized continuity and momentum equation [13]:

$$\frac{\partial}{\partial t} \begin{bmatrix} \frac{p'}{\bar{\rho} c} \\ u' \end{bmatrix} = \begin{bmatrix} 0 & -c\frac{\partial}{\partial x} \\ -c\frac{\partial}{\partial x} & 0 \end{bmatrix} \begin{bmatrix} \frac{p'}{\bar{\rho} c} \\ u' \end{bmatrix} \tag{2.17}$$

The linear system of differential equations is not diagonal and therefore, the two equations are coupled. In order to transform the system to diagonal form, Laplace transformation is applied:

$$s \begin{bmatrix} \frac{p'}{\bar{\rho} c} \\ u' \end{bmatrix} = \begin{bmatrix} 0 & -c\frac{\partial}{\partial x} \\ -c\frac{\partial}{\partial x} & 0 \end{bmatrix} \begin{bmatrix} \frac{p'}{\bar{\rho} c} \\ u' \end{bmatrix} \tag{2.18}$$

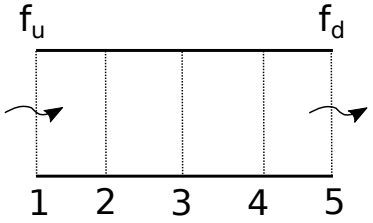

Figure 2.4: Discretized duct section.

and then the system of equations is solved for its eigenvalues

$$\det\begin{bmatrix} s & -c\frac{\partial}{\partial x} \\ -c\frac{\partial}{\partial x} & s \end{bmatrix} = 0; \quad s_{1,2} = \pm c\frac{\partial}{\partial x} \tag{2.19}$$

and eigenvectors, also called Riemann invariants, of the differential operator are found by substituting $s_{1,2}$:

$$c\frac{\partial}{\partial x}\begin{bmatrix} -1 & -1 \\ -1 & -1 \end{bmatrix}\begin{bmatrix} \frac{p'}{\bar{\rho}c} \\ u' \end{bmatrix} \Rightarrow \left(\frac{p'}{\bar{\rho}c} + u'\right) \equiv 2f \tag{2.20}$$

$$c\frac{\partial}{\partial x}\begin{bmatrix} 1 & -1 \\ -1 & 1 \end{bmatrix}\begin{bmatrix} \frac{p'}{\bar{\rho}c} \\ u' \end{bmatrix} \Rightarrow \left(\frac{p'}{\bar{\rho}c} - u'\right) \equiv 2g\,. \tag{2.21}$$

Thus there is a transformation to generalized coordinates

$$\begin{bmatrix} \frac{p'}{\bar{\rho}c} \\ u' \end{bmatrix} = \begin{bmatrix} 1 & 1 \\ 1 & -1 \end{bmatrix}\begin{bmatrix} f \\ g \end{bmatrix}. \tag{2.22}$$

The system of differential equations is subsequently transformed to generalized coordinates:

$$\frac{\partial}{\partial t}\begin{bmatrix} 1 & 1 \\ 1 & -1 \end{bmatrix}\begin{bmatrix} f \\ g \end{bmatrix} = \begin{bmatrix} 0 & -c\frac{\partial}{\partial x} \\ -c\frac{\partial}{\partial x} & 0 \end{bmatrix}\begin{bmatrix} 1 & 1 \\ 1 & -1 \end{bmatrix}\begin{bmatrix} f \\ g \end{bmatrix} \tag{2.23}$$

$$\frac{\partial}{\partial t}\begin{bmatrix} f \\ g \end{bmatrix} = \begin{bmatrix} \frac{1}{2} & \frac{1}{2} \\ \frac{1}{2} & -\frac{1}{2} \end{bmatrix}\begin{bmatrix} 0 & -c\frac{\partial}{\partial x} \\ -c\frac{\partial}{\partial x} & 0 \end{bmatrix}\begin{bmatrix} 1 & 1 \\ 1 & -1 \end{bmatrix}\begin{bmatrix} f \\ g \end{bmatrix} \tag{2.24}$$

$$\frac{\partial}{\partial t}\begin{bmatrix} f \\ g \end{bmatrix} = \begin{bmatrix} -c\frac{\partial}{\partial x} & 0 \\ 0 & c\frac{\partial}{\partial x} \end{bmatrix}\begin{bmatrix} f \\ g \end{bmatrix}. \tag{2.25}$$

Thus the propagation of acoustic waves in ducts can be expressed by two independent advection equations:

$$\frac{\partial f}{\partial t} = -c\frac{\partial f}{\partial x} \quad ; \qquad \frac{\partial g}{\partial t} = c\frac{\partial g}{\partial x} \tag{2.26}$$

Solutions for the f-wave are of the form $f(x,t) = f(t - x/c)$. With boundary condition $f|_{x=0} = f_u$ and output definition $f|_{x=l} = f_d$ as shown in Fig. 2.4.

2.3.1.1 Analytical Solution

The analytic solution for the propagation of acoustic waves through a duct section of length l is:

$$f_d = f_u(t - l/c)\,. \tag{2.27}$$

In analogy the solution for g-waves is:

$$g_u = g_d(t - l/c)\,. \tag{2.28}$$

Thus the incident waves leave the duct section after a delay $\tau = l/c$. In Laplace domain, the solution is given by the classical result of the scattering matrix of a duct section:

$$\begin{bmatrix} g_u(s) \\ f_d(s) \end{bmatrix} = \underbrace{\begin{bmatrix} 0 & e^{-s\tau} \\ e^{-s\tau} & 0 \end{bmatrix}}_{G(s)} \begin{bmatrix} f_u(s) \\ g_d(s) \end{bmatrix} \tag{2.29}$$

This scattering matrix can be interpreted as a matrix of transfer functions $G(s)$. Unfortunately the exact solution in Laplace domain is a harmonic function of the frequency $s = j\omega + \sigma$. As there exist very efficient solvers for algebraic eigenvalue problems (see 2.5), it is of interest to approximate the exact solution of the delay either directly by a state space system or by a polynomial, which may subsequently be converted to a state space system.

2.3.1.2 Padé Approximation

It is possible to develop a series expansion of the exponential expression in the delay transfer functions. This method results in a rational polynomial in s and is called Padé approximation. For instance, the polynomial transfer function of order 2 in numerator and denominator is:

$$e^{-s\tau} \approx \frac{1 - \frac{\tau}{2}s + \frac{\tau^2}{12}s^2}{1 + \frac{\tau}{2}s + \frac{\tau^2}{12}s^2}\,. \tag{2.30}$$

This transfer function can be translated to matrix representation as shown in section 2.2.3. Unfortunately, the resulting transfer function tends to become unstable with increasing order of approximation. The Matlab manual of Padé approximation suggests not to go beyond an order of 9. This effectively limits the application of the Padé approximation, to nondimensionalized delays $\tau\omega < 3$ [6].

2.3.1.3 Spatially Discretized State Space System

Instead of solving the differential equation (2.26) analytically, it is possible to spatially discretize the duct as shown in Fig. 2.4 and to directly aim for a state space system. Previous works of Mangesius et al. [14] and Blumenthal [15] used to discretize in space and time, whereas here, we remain continuous time. Using a first order upwind finite difference scheme:

$$\frac{\mathrm{d}f_j}{\mathrm{d}t} = -c\frac{f_j - f_{j-1}}{\Delta x}\,. \tag{2.31}$$

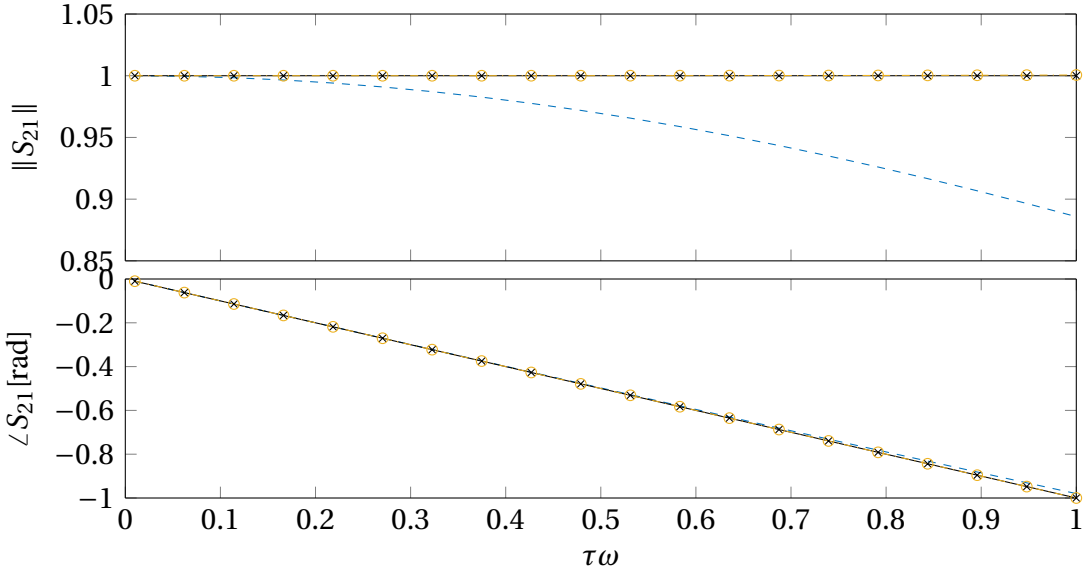

Figure 2.5: Frequency response of f_u to f_d: First order upwind (- - -), third order upwind (-⊖-) and analytic solution (—×—) .

We choose a resolution $\Delta x = L/4$ and define a short hand $a \equiv c/\Delta x$. By those definitions, the state space system (2.14) which models the f-wave duct dynamics is:

$$\frac{\mathrm{d}}{\mathrm{d}t}\begin{bmatrix} f_2 \\ f_3 \\ f_4 \\ f_5 \end{bmatrix} = \begin{bmatrix} -a & 0 & 0 & 0 \\ a & -a & 0 & 0 \\ 0 & a & -a & 0 \\ 0 & 0 & a & -a \end{bmatrix}\begin{bmatrix} f_2 \\ f_3 \\ f_4 \\ f_5 \end{bmatrix} + \begin{bmatrix} a \\ 0 \\ 0 \\ 0 \end{bmatrix}[f_u] \tag{2.32}$$
$$[f_d] = [0 \quad 0 \quad 0 \quad 1]\, x + [0]\, f_u .$$

The state space system of the g-waves is retrieved accordingly.

By choosing higher order integration schemes e.g. third order upwind and by using a higher resolution, The precision of the state space model can be increased. Typically a resolution of 10 points per wavelength for both f and g is a reasonable choice to achieve high accuracy. Therefore the order of the duct model should be chosen $N/2 = 10\tau\omega_{max}$.

Fig. 2.5 shows how well the model is performing compared to the analytical solution.

2.3.2 Simplistic n-τ Flame Models

There is a widely used low order flame model in thermoacoustic systems called the $n-\tau$ flame. It presumes, that the flame reacts to a velocity perturbation u' at the burner mouth with a delayed heat release fluctuation $\dot{Q}'$. The input u' at a time $t-\tau$ is multiplied by a fixed value n to result in the output $\dot{Q}'(t)$:

$$\dot{Q}'(t) = n u'(t-\tau) \quad \left(= \int_0^\tau \underbrace{n\delta(\theta-\tau)}_{G(\tau)} u'(t-\theta)\,\mathrm{d}\theta \right). \tag{2.33}$$

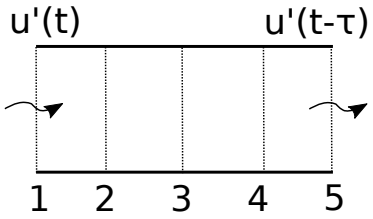

Figure 2.6: Discretized delay.

The exact solution in Laplace domain is:

$$Q'(s) = \underbrace{ne^{-s\tau}}_{G(s)} u'(s)\,. \tag{2.34}$$

Similar to the 1D wave propagation in ducts in the previous section 2.3.1, it would be possible to use Padé approximation on the exact solution. However, it is better to directly retrieve a state space model due to the limitations of the Padé approximation discussed above. It is possible to express the delay by an advection equation:

$$\frac{\partial x}{\partial t} + \frac{\partial x}{\partial \theta} = 0\,. \tag{2.35}$$

The artificial state x of the delayed input signal is transported at speed 1 along $\theta = 0 \ldots \tau$ with inlet boundary condition $x(t)|_{\theta=0} = u'(t)$. The downstream boundary is the output $u'(t-\tau) = x(t)|_{\theta=\tau}$. Subsequently θ is discretized, e.g. $\Delta\theta = \tau/4$ as shown in Fig. 2.6, with a first order upwind scheme:

$$\frac{\mathrm{d}x_j}{\mathrm{d}t} = \frac{x_j - x_{j-1}}{\Delta\theta}\,. \tag{2.36}$$

The full $n-\tau$ model eventually is described by a system of ODEs with input $x_1 = u\,(= u')$ and output definition $(\dot{Q}' =)\ y = nx_5$

$$\begin{aligned}
\frac{\mathrm{d}}{\mathrm{d}t}\begin{bmatrix} x_2 \\ x_3 \\ x_4 \\ x_5 \end{bmatrix} &= \begin{bmatrix} 4/\tau & 0 & 0 & 0 \\ -4/\tau & 4/\tau & 0 & 0 \\ 0 & -4/\tau & 4/\tau & 0 \\ 0 & 0 & -4/\tau & 4/\tau \end{bmatrix} \begin{bmatrix} x_2 \\ x_3 \\ x_4 \\ x_5 \end{bmatrix} + \begin{bmatrix} -4/\tau \\ 0 \\ 0 \\ 0 \end{bmatrix} u \\
y &= \begin{bmatrix} 0 & 0 & 0 & n \end{bmatrix} x + \begin{bmatrix} 0 \end{bmatrix} u\,.
\end{aligned} \tag{2.37}$$

It is possible to use a second or third order upwind scheme to discretize the differential equation, which improves the accuracy (2.35). Additionally, the resolution may be increased, which also raises the accuracy of the delay approximation. A good approximation is obtained, if a delayed input wave is discretized by a third order upwind scheme and a resolution of 10 points: $N = 10\omega\tau$. In contrast to Padé approximation, there are no stability issues with increasing order, because the state space system is well conditioned.

2.3.3 2D/3D Spatially Discretized Linearized PDEs

If the geometry of the subsystem is more complicated, but the acoustic waves do not affect the mean flow, linearized partial differential equations (PDEs) can be used to account for the

wave propagation [16, 17]. Such PDEs are given for instance by the Helmholtz, linearized Euler and linearized Navier-Stokes equations [18, 19]. Models can effectively be retrieved using finite element method (FEM) tools like Comsol Multiphysics or FreeFEM. The geometry of the system, the mean flow, the mesh used for the discretization and the discretization scheme need to be specified.

Standard FEM schemes are not well suited to solve advection diffusion problems as given by linearized flow equations. The resulting models are not asymptotically stable and possess unstable unphysical eigenmodes. It is possible to improve such schemes by stream line diffusion or Galerkin least squares stabilization methods, but this comes at the price of an arbitrary stabilization parameter. The specification of this parameter is critical as it considerably influences the results and there is no generic method to estimate a good value. In contrast to that, discontinuous Galerkin FEM and finite Volume methods are not subject to those issues. Discontinuous Galerkin methods invoke an up winding parameter as well, but the result is insensitive to the exact value. It follows that for modeling acoustic systems, discontinuous Galerkin FEM methods are superior to standard FEM.

In order to couple the FEM model with a thermoacoustic network code, there are two classical and one new method to be presented in the following sections.

2.3.3.1 Evaluation of Impedances

It is possible to solve the linearized PDE model inside the FEM software and to couple the resulting impedances with the network code in frequency domain [19, 20]. This procedure is very inefficient, as in every iteration of any computation the entire FEM model needs to be solved.

2.3.3.2 State Space from Modal Reduction

The next method is to extract a reduced order state space system from the FEM model using a modal reduction approach [4, 5, 21]. The eigenmodes of the FEM Model are computed inside the FEM software and a state space model is constructed based on the modes. This method is computationally very efficient, but it comes at the price of the modal reduction. Depending on the system, the eigenmodes may or may not be good Ansatz functions to model the transmission of acoustic waves through a system. Additionally, modal reduction does not converge with increasing order.

2.3.3.3 Direct State Space Export

Eventually a linear state space model as given in Eq. (2.14) is directly retrieved by exporting the system matrices from the FEM software as shown by Meindl et al. [22]. Inside the subsystem domain, 3D wave propagation may occur, whereas the interfaces remain acoustically compact and plane.

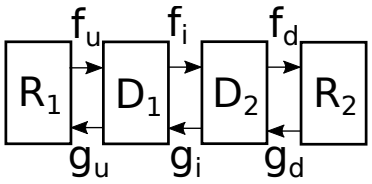

Figure 2.7: Interconnection of two duct sections and two reflective ends.

Following the direct export of the state space system, instead of modal reduction, any suitable model order reduction algorithm may be applied to the system.

The system matrices of models resulting from linearized PDEs are very sparse. In order to take advantage of the sparsity, we have reimplemented the functionality of matlab control system toolbox, which relies on full matrices. The resulting sparse state space (sss) custom toolbox is developed in a cooperation with the Lehrstuhl für Regelungstechnik at TUM [23].

2.3.4 System Identification from LES or Experiment Time Series Data

Eventually, if there is strong bidirectional interaction between acoustic waves and mean flow like in the case of domains where combustion takes place, nonlinear LES simulations or even experiments need to be carried out. The system is excited with acoustic waves from the up- and downstream section and time series of the incident and emitted plane waves are measured. In experiments this measurement is achieved using the multi microphone method, whereas in CFD the plane waves can be extracted by averaging across planes in the simulation domain. Linearized models for the scattering of acoustic waves in the domain may be retrieved from the input, output time series and system identification techniques [24–28].

2.4 Interconnection

Thermoacoustic network models are constituted by a set of interconnected subsystems. In order to solve for the properties of the underlying full system, the interconnections between the subsystems need to be evaluated. As already introduced in section 2.1, there are two modeling paradigms for the interconnection of thermoacoustic network models. It is the classical frequency domain methods and the state space modeling. The respective interconnection algorithms will be introduced in the following sections on a generic network model shown in Fig. 2.7. The model consists of a closed $R_1 = 1$ and an open end $R_2 = -1$ and two duct sections D_1, D_2 of equal length $l/2$ with upstream (u), intermediary (i) and downstream (d) acoustic interfaces.

2.4.1 Frequency Domain Interconnection

As we have seen in section 2.2.1, the transformation of linear models from time into frequency domain resolves the convolution with a Green's function into a multiplication with the transfer

function. Thus it is possible to transform all linear subsystem models to frequency domain and evaluate the interconnection by a set of algebraic equations. The two duct models are:

$$\begin{bmatrix} g_u(s) \\ f_i(s) \end{bmatrix} = \begin{bmatrix} 0 & e^{-s\tau} \\ e^{-s\tau} & 0 \end{bmatrix} \begin{bmatrix} f_u(s) \\ g_i(s) \end{bmatrix}; \quad \begin{bmatrix} g_i(s) \\ f_d(s) \end{bmatrix} = \begin{bmatrix} 0 & e^{-s\tau} \\ e^{-s\tau} & 0 \end{bmatrix} \begin{bmatrix} f_i(s) \\ g_d(s) \end{bmatrix} \tag{2.38}$$

with $\tau = l/(2c)$ and the reflection coefficients:

$$f_u = g_u; \quad g_d = -f_d. \tag{2.39}$$

By appending all the scattering matrices we obtain a multiple input, multiple output system of open loop transfer functions:

$$\begin{bmatrix} f_u \\ g_u \\ f_i \\ g_i \\ f_d \\ g_d \end{bmatrix} = \underbrace{\begin{bmatrix} 0 & 1 & 0 & 0 & 0 & 0 \\ 0 & 0 & 0 & e^{-s\tau} & 0 & 0 \\ e^{-s\tau} & 0 & 0 & 0 & 0 & 0 \\ 0 & 0 & 0 & 0 & 0 & e^{-s\tau} \\ 0 & 0 & e^{-s\tau} & 0 & 0 & 0 \\ 0 & 0 & 0 & 0 & -1 & 0 \end{bmatrix}}_{G(s)} \begin{bmatrix} f_u \\ g_u \\ f_i \\ g_i \\ f_d \\ g_d \end{bmatrix} \tag{2.40}$$

The system is closed on the left hand side by subtracting the matrix of transfer functions from unity:

$$\begin{bmatrix} 1 & -1 & 0 & 0 & 0 & 0 \\ 0 & 1 & 0 & -e^{-s\tau} & 0 & 0 \\ -e^{-s\tau} & 0 & 1 & 0 & 0 & 0 \\ 0 & 0 & 0 & 1 & 0 & -e^{-s\tau} \\ 0 & 0 & -e^{-s\tau} & 0 & 1 & 0 \\ 0 & 0 & 0 & 0 & 1 & 1 \end{bmatrix} \begin{bmatrix} f_u \\ g_u \\ f_i \\ g_i \\ f_d \\ g_d \end{bmatrix} = I - G(s) = 0 \tag{2.41}$$

Non trivial solutions for f_x, g_x exist if the resulting closed loop transfer function matrix is rank deficient. Values s that lead to rank deficiency are eigenvalues of the system:

$$\det \begin{bmatrix} 1 & -1 & 0 & 0 & 0 & 0 \\ 0 & 1 & 0 & -e^{-s\tau} & 0 & 0 \\ -e^{-s\tau} & 0 & 1 & 0 & 0 & 0 \\ 0 & 0 & 0 & 1 & 0 & -e^{-s\tau} \\ 0 & 0 & -e^{-s\tau} & 0 & 1 & 0 \\ 0 & 0 & 0 & 0 & 1 & 1 \end{bmatrix} = \det(I - G(s)) = 0 \tag{2.42}$$

The characteristic equation of the system is also called dispersion relation:

$$1 + e^{4s\tau} = 0 \tag{2.43}$$

Using the definition of the Laplace variable $s = j\omega + \sigma$, we can solve for the real and imaginary part independently:

$$1 + \cos(\omega 4\tau) e^{\sigma 4\tau} = 0; \quad \sin(\omega 4\tau) e^{\sigma 4\tau} = 0 \tag{2.44}$$

According to the first condition, the system is a quarter wave resonator $\frac{\omega}{2\pi} = \frac{n+1/2}{4\tau} = (1/4 + n/2)\frac{c}{l}$ with $\sigma_n = 0$ for all whole numbers $n = 0, 1, 2, \ldots$. The second equation does not impose further restrictions as $\frac{\omega}{2\pi} = \frac{n/2}{4\tau}$ is part of the first condition.

2.4.2 Universal State Space Interconnection

If all subsystems of the acoustic network model as shown in Fig. 2.7 are modeled as state space systems, they can be connected by a universal interconnection algorithm for state space systems [29]. The algorithm is similar to the ones used by Matlab Control System Toolbox [30] and Octave Control Toolbox [31]. At first the theoretic derivation for the interconnection algorithm is presented, followed by the application to the minimal example in analogy to the previous frequency domain section.

2.4.2.1 Interconnection of State Space Models

At first the system matrices A, B, C, D, E of the systems $1, 2...N$ that shall be connected are block diagonally appended as exemplary shown for A:

$$\tilde{A} = \begin{bmatrix} A_1 & 0 & 0 & 0 \\ 0 & A_2 & 0 & 0 \\ 0 & 0 & \ddots & 0 \\ 0 & 0 & 0 & A_N \end{bmatrix}; \tag{2.45}$$

The corresponding state, input and output vectors are:

$$x = \begin{bmatrix} x_1 \\ x_2 \\ \vdots \\ x_N \end{bmatrix}; \quad \tilde{u} = \begin{bmatrix} u_1 \\ u_2 \\ \vdots \\ u_N \end{bmatrix}; \quad \tilde{y} = \begin{bmatrix} y_1 \\ y_2 \\ \vdots \\ y_N \end{bmatrix}. \tag{2.46}$$

The interconnection itself is expressed by the feedback equation

$$\tilde{u} = F\tilde{y} + u \tag{2.47}$$

where F is the feedback matrix, which contains mostly zeros and ones to indicate outputs $\tilde{y}$ which are internally connected to inputs $\tilde{u}$. The feedback equation of the resulting system of equations

$$\tilde{E}\dot{x} = \tilde{A}x + \tilde{B}\tilde{u} \tag{2.48}$$

$$\tilde{y} = \tilde{C}x + \tilde{D}\tilde{u} \tag{2.49}$$

$$\tilde{u} = F\tilde{y} + u. \tag{2.50}$$

can be solved for the input

$$\tilde{u} = (1 - F\tilde{D})^{-1}F\tilde{C}x + (1 - F\tilde{D})^{-1}u. \tag{2.51}$$

and the solution is substituted in order to obtain the system matrices of the interconnected state space system:

$$\begin{aligned} A &= \tilde{A} + \tilde{B}(1 - F\tilde{D})^{-1}F\tilde{C}; \\ B &= \tilde{B}(1 - F\tilde{D})^{-1}; \\ C &= \tilde{C} + \tilde{D}(1 - F\tilde{D})^{-1}F\tilde{C}; \\ D &= \tilde{D}(1 - F\tilde{D})^{-1}; \\ E &= \tilde{E}. \end{aligned} \tag{2.52}$$

2.4.2.2 SS Interconnection Minimal Example

The interconnection algorithm is now illustrated by the application to the minimal example shown in Fig. 2.7. Discretization and numbering is done in analogy to section 2.3.1.3 and Fig. 2.4. The state space representation of the duct models is given by:

$$\frac{\mathrm{d}}{\mathrm{d}t}\begin{bmatrix} f_2 \\ f_3 \end{bmatrix} = \begin{bmatrix} -a & 0 \\ a & -a \end{bmatrix}\begin{bmatrix} f_2 \\ f_3 \end{bmatrix} + \begin{bmatrix} a \\ 0 \end{bmatrix}[f_u] \tag{2.53}$$

$$[f_i] = \begin{bmatrix} 0 & 1 \end{bmatrix}\begin{bmatrix} f_2 \\ f_3 \end{bmatrix} + [0]\,[f_u] \tag{2.54}$$

$$\frac{\mathrm{d}}{\mathrm{d}t}\begin{bmatrix} f_4 \\ f_5 \end{bmatrix} = \begin{bmatrix} -a & 0 \\ a & -a \end{bmatrix}\begin{bmatrix} f_4 \\ f_5 \end{bmatrix} + \begin{bmatrix} a \\ 0 \end{bmatrix}[f_i] \tag{2.55}$$

$$[f_d] = \begin{bmatrix} 0 & 1 \end{bmatrix}\begin{bmatrix} f_4 \\ f_5 \end{bmatrix} + [0]\,[f_i]\,. \tag{2.56}$$

$$\frac{\mathrm{d}}{\mathrm{d}t}\begin{bmatrix} g_1 \\ g_2 \end{bmatrix} = \begin{bmatrix} a & -a \\ 0 & a \end{bmatrix}\begin{bmatrix} g_1 \\ g_2 \end{bmatrix} + \begin{bmatrix} 0 \\ -a \end{bmatrix}[g_i] \tag{2.57}$$

$$[g_u] = \begin{bmatrix} 1 & 0 \end{bmatrix}\begin{bmatrix} g_1 \\ g_2 \end{bmatrix} + [0]\,[g_i] \tag{2.58}$$

$$\frac{\mathrm{d}}{\mathrm{d}t}\begin{bmatrix} g_3 \\ g_4 \end{bmatrix} = \begin{bmatrix} a & -a \\ 0 & a \end{bmatrix}\begin{bmatrix} g_3 \\ g_4 \end{bmatrix} + \begin{bmatrix} 0 \\ -a \end{bmatrix}[g_d] \tag{2.59}$$

$$[g_i] = \begin{bmatrix} 1 & 0 \end{bmatrix}\begin{bmatrix} g_3 \\ g_4 \end{bmatrix} + [0]\,[g_d]\,. \tag{2.60}$$

Due to the numbering scheme, the acoustic states on the interfaces correspond to: $f_u = f_1$, $g_u = g_1$, $f_i = f_3$, $g_i = g_3$,$f_d = f_5$, $g_d = g_5$. States $2,4$ are internal states of duct D_1 respectively D_2. In addition to that, the boundaries are just feed-through conditions:

$$[f_u] = [1]\,[g_u]\,; \quad [g_d] = [-1]\,[f_d] \tag{2.61}$$

Appending the system matrices results in

$$\tilde{A} = \begin{bmatrix} -a & 0 & 0 & 0 & 0 & 0 & 0 & 0 \\ a & -a & 0 & 0 & 0 & 0 & 0 & 0 \\ 0 & 0 & -a & 0 & 0 & 0 & 0 & 0 \\ 0 & 0 & a & -a & 0 & 0 & 0 & 0 \\ 0 & 0 & 0 & 0 & a & -a & 0 & 0 \\ 0 & 0 & 0 & 0 & 0 & a & 0 & 0 \\ 0 & 0 & 0 & 0 & 0 & 0 & a & -a \\ 0 & 0 & 0 & 0 & 0 & 0 & 0 & a \end{bmatrix}; \quad \tilde{B} = \begin{bmatrix} a & 0 & 0 & 0 & 0 & 0 \\ 0 & 0 & 0 & 0 & 0 & 0 \\ 0 & a & 0 & 0 & 0 & 0 \\ 0 & 0 & 0 & 0 & 0 & 0 \\ 0 & 0 & 0 & 0 & 0 & 0 \\ 0 & 0 & 0 & 0 & -a & 0 \\ 0 & 0 & 0 & 0 & 0 & 0 \\ 0 & 0 & 0 & 0 & 0 & -a \end{bmatrix} \tag{2.62}$$

$$\tilde{C} = \begin{bmatrix} 0 & 0 & 0 & 0 & 0 & 0 & 0 & 0 \\ 0 & 1 & 0 & 0 & 0 & 0 & 0 & 0 \\ 0 & 0 & 0 & 1 & 0 & 0 & 0 & 0 \\ 0 & 0 & 0 & 0 & 1 & 0 & 0 & 0 \\ 0 & 0 & 0 & 0 & 0 & 0 & 1 & 0 \\ 0 & 0 & 0 & 0 & 0 & 0 & 0 & 0 \end{bmatrix}; \quad \tilde{D} = \begin{bmatrix} 0 & 0 & 0 & 1 & 0 & 0 \\ 0 & 0 & 0 & 0 & 0 & 0 \\ 0 & 0 & 0 & 0 & 0 & 0 \\ 0 & 0 & 0 & 0 & 0 & 0 \\ 0 & 0 & 0 & 0 & 0 & 0 \\ 0 & 0 & -1 & 0 & 0 & 0 \end{bmatrix} \tag{2.63}$$

$$x = \begin{bmatrix} f_2 \\ f_3 \\ f_4 \\ f_5 \\ g_1 \\ g_2 \\ g_3 \\ g_4 \end{bmatrix}; \quad \tilde{y} = \begin{bmatrix} f_u \\ f_i \\ f_d \\ g_u \\ g_i \\ g_d \end{bmatrix}; \quad \tilde{u} = \begin{bmatrix} f_u \\ f_i \\ f_d \\ g_u \\ g_i \\ g_d \end{bmatrix}; \quad u = [0] \tag{2.64}$$

The system is closed by the feedback equation (2.47):

$$\tilde{u} = \begin{bmatrix} 1 & 0 & 0 & 0 & 0 & 0 \\ 0 & 1 & 0 & 0 & 0 & 0 \\ 0 & 0 & 1 & 0 & 0 & 0 \\ 0 & 0 & 0 & 1 & 0 & 0 \\ 0 & 0 & 0 & 0 & 1 & 0 \\ 0 & 0 & 0 & 0 & 0 & 1 \end{bmatrix} \tilde{y} + [0]\, u \tag{2.65}$$

Due to the arrangement of $\tilde{u}$ and $\tilde{y}$, the feedback matrix F is unity in this particular case. It is an autonomous system, therefore thre are no remaining external in- or outputs u, y. Subsequently, the feedback equation is solved as given by eq. (2.51) and the system matrix is retrieved from eq. (2.52):

$$A = \begin{bmatrix} -a & 0 & 0 & 0 & a & 0 & 0 & 0 \\ a & -a & 0 & 0 & 0 & 0 & 0 & 0 \\ 0 & a & -a & 0 & 0 & 0 & 0 & 0 \\ 0 & 0 & a & -a & 0 & 0 & 0 & 0 \\ 0 & 0 & 0 & 0 & a & -a & 0 & 0 \\ 0 & 0 & 0 & 0 & 0 & a & -a & 0 \\ 0 & 0 & 0 & 0 & 0 & 0 & a & -a \\ 0 & 0 & 0 & a & 0 & 0 & 0 & a \end{bmatrix} \tag{2.66}$$

The system has an order of n=8. We are using the same duct resolution as in section 2.3.1, therefore the upper left 4x4 sub matrix, which is modeling the f wave dynamics, is identical to eq. (2.32).

A comparison of the eigenvalues of the analytic solution ×, the first order upwind scheme n=8 • as shown above, third order upwind n=8 ○ and high resolution third order upwind n=80 □ is shown in Fig. 2.8. The first quarter wave eigenvalue is approximated fairly well by all three state space systems. Whereas the highly resolved system □ matches all four eigenvalues in the given frequency range, the two systems of order n=8 •,○ exhibit highly damped modes. This corresponds well to the general behavior of the state space models in the frequency response plots

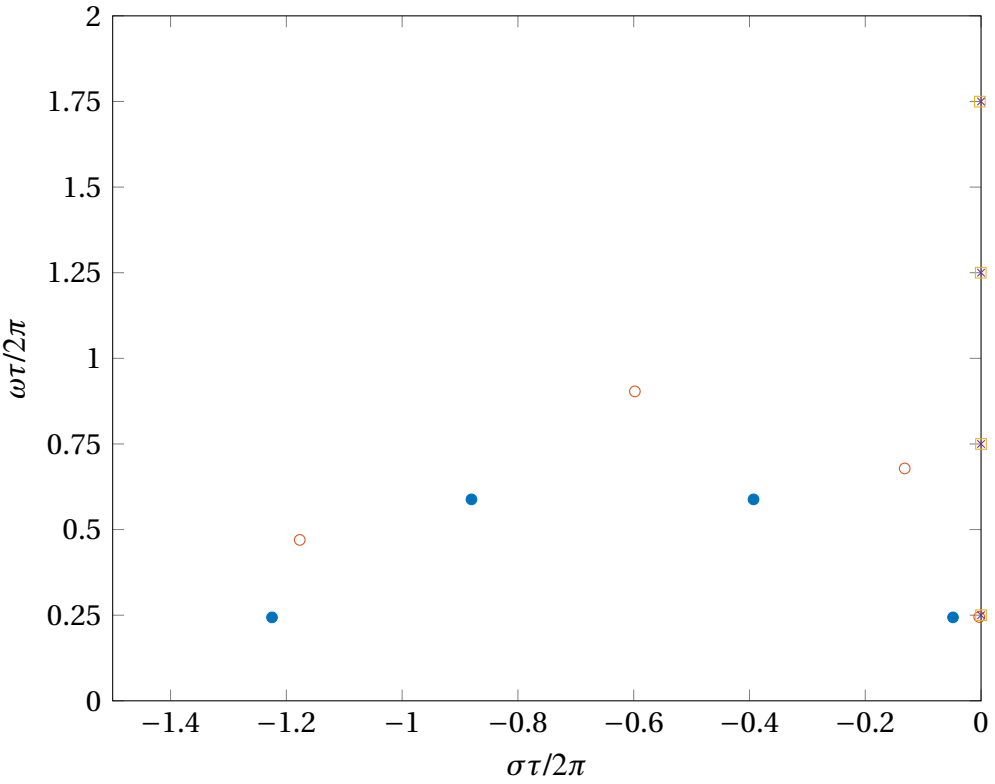

Figure 2.8: Eigenvalues of the minimal network system. Analytic solution ×, first order upwind n=8 •, third order upwind n=8 ○ and high resolution third order upwind n=80 □.

of the duct section let alone as shown in Fig. 2.5, where the gain decreases at high frequencies. The most important feature of the discretization scheme is that it is conservative in the sense that the resulting models are stable for analytically marginally stable systems.

2.5 Stability of Thermoacoustic Systems

One practical application of thermoacoustic network modeling is to determine the asymptotic stability of a system. It is achieved by computing the eigenvalues or poles of the linear system and to determine whether all poles are stable. This is the case if

$$\mathcal{R}e\{s_i\} < 0 \tag{2.67}$$

for all eigenvalues s_i of the system. Subsequently algorithms to compute eigenvalues for classical frequency domain models and state space models are presented.

2.5.1 Classical Frequency Domain Model Solver

As stated in section 2.4.1, the search for eigenvalues involves the search for zeros of the characteristic equation, also called dispersion relation:

$$\det(I - G(s)) = 0\,. \tag{2.68}$$

This is a nonlinear eigenvalue problem. The solution involves an iterative procedure which solves the optimization problem

$$\min_s \| \det(I - G(s)) \| . \tag{2.69}$$

From an initial value s^* a gradient descent algorithm is used to find the zeros one by one. With each iterative step, the determinant of the system needs to be computed, which is computationally very expensive for large systems. Depending on the smoothness of the dispersion relation, it may be difficult to find all eigenvalues, as gradient descent is just able to find local minima. Then it may be necessary to search the complex plane with many initial values s^* in order to find all eigenvalues in a certain region. Unfortunately, there is no way to determine whether all eigenvalues have been found. All in all, the procedure is computationally very expensive and inefficient.

2.5.2 State Space Model Eigenvalue Solver

In the case of state space systems, the eigenvalues are the poles of the dispersion relation as well. This time however it involves solving just for a non-hermitian generalized linear eigenvalue problem as opposed to the nonlinear eigenvalue problem for the classical methods [29].

$$(Es - A)x = 0 \tag{2.70}$$

There are very efficient standard procedures to solve this type of equation. For small systems, direct solvers can compute all eigenvalues in a single run. When the order of the system becomes large, iterative algorithms to compute a distinct number of eigenvalues close to some value s^* are the standard procedure. Such algorithms are given by Arnoldi methods [32]. This procedure involves solving a shifted and inverted eigenvalue problem of a matrix pencil $(A - Es^*)^{-1}$. The inversion of the matrix is not computed explicitly, as only the vector product with the inverted matrix is needed. This is achieved by an LU decomposition of the matrix pencil. For large systems the LU decomposition is very expensive and takes up most of the computational time compared to the Arnoldi iterations. Therefore we suggest to use a special LU algorithm tailored for sparse systems called MUMPS [33] for this step.

3 Sound Power Amplification and Acoustic Energy of Thermoacoustic Systems

In the previous section it was already shown how the linear stability of a thermoacoustic network model can be computed if models for the entire system are known. There are two reasons, why an investigation of acoustic energy or more general perturbation energy is of interest. At first, the linear stability of a thermoacoustic system does not enforce the stability of the underlying nonlinear system. This raises the need for proper Lyapunov function based nonlinear stability proofs [34]. Lyapunov functions are generalized energy functions, which are used to show the convergence of a system to a certain orbit respectively fix point. Secondly, thermoacoustic systems tend to be very complex with many nontrivial interactions. In order to handle the complexity, it is important to find a method to characterize the stability properties of individual subsystems like a single burner of a gas turbine. This is achieved by the instability potentiality criterion [35], which is based on sound power amplification.

3.1 Nonlinear Stability

It is a well known result from turbulence investigation, that the prediction of laminar-turbulent flow transition is under predicted by the stability of linearized perturbation models. There are cases when, even though those models predict linear stability, the flow transitions to turbulence. The effect that the system transitions from a linearly stable fix point to chaos or a limit cycle is called "triggering".

Trefethen et al. [36] have shown that this behavior relates to the great sensitivity of pseudospectra of the non-normal linearized matrix operator and the transient growth of perturbations. Schmid [37] gives a review about methods that have emerged from non-modal stability analysis. Gebhardt and Grossmann [38] have investigated a nonlinear model and shown that instability and chaotic behavior may occur if the linearized model is non-normal and there is so called nonlinear mixing. The nonlinearity mixes energy from those states that had transiently grown back into perturbations that are about to grow.

Those investigations relate to flow instability and turbulence, but especially flame models cause large non-normal effects. Thus the linear stability of a thermoacoustic model does not imply stability of the underlying nonlinear system. In order to prove nonlinear stability, a Lyapunov function [34], also called generalized energy function, for the state of a system around an orbit or fix point needs to be found. If such a function exists, then the system is stable. The generalized energy function needs to be positive definite and the proof is achieved by showing, that the

energy is monotonously decreasing over time departing from any given state x.

There exists a Lyapunov function for linear state space systems if and only if all eigenvalues of the system are strictly stable $\mathscr{R}e\{s_i\} < 0$. The generalized energy function is a quadratic form of the state:

$$E(x) = x^T P x, \tag{3.1}$$

where P is the energy norm and therefore a positive definite and symmetric matrix, which is retrieved by solving the so called Lyapunov equation:

$$PA + A^H P + Q = 0. \tag{3.2}$$

Here Q is an arbitrary positive definite and symmetric matrix and $-x^T Q x$ is the dissipation rate. There is an extension of this method to state space systems, that possess a descriptor matrix E given by Takaba et al. [39].

Instead of formulating an arbitrary Lyapunov function, it is possible to derive it directly from the physically motivated perturbation energy inside of an acoustic domain. There are several different suggestions for the definition of acoustic energy and sound power found in literature by Chu [40], Cantrell et al. [41], Morfey [42] Myers [43], more recently Giauque et al.[44] and Brear et al. [45]. The mathematically most elaborate definition was issued by Myers and is based on an infinite series expansion of the Navier-Stokes equations. He provides a proof that his definition of perturbation energy defined by first order terms is exact up to second order. However, as George et al. [46] point out, Myers definition of perturbation energy is positive definite, but not symmetric for non-zero mean flow, whereas Chu's definition is. Therefore Myers energy corollary is beautiful, but not suitable to construct a Lyapunov function, whereas Chu's is less elaborate, but more useful.

However, unlike total flow energy, perturbation energy is not a preserved quantity. It can be amplified or attenuated by the mean flow. In order to prove the stability of such a system, those interactions need to be accounted for in the energy balance as investigated by Blumenthal et al. [47]. This is achieved by the modeling of so called ports between the different domains of the network model in which individual generalized energy functions exist. There is substantial efforts to use Lyapunov functions in the context of network models under the topic of port-Hamiltonian systems and passivity based control [48].

3.2 Instability Potentiality and Small Gain Theorem

Instead of constructing a Lyapunov function from the internal state of a system, it is possible to state a stability criterion based on the input- output behavior. The theoretic basis was developed by Zames [49] and is called the small gain theorem. In system theory, the supremum of the norm of the outputs of a system $y = Sys(u)$ over all possible inputs u is called "gain".

$$g(Sys) = \sup \frac{\|Sys(u)\|}{\|u\|} \tag{3.3}$$

The gain of an interconnected system $Sys_1 \cdot Sys_2$ is bound by the product of the individual gains of Sys_1 and Sys_2. If the individual systems are stable and the gain is less than unity, then the

interconnected system is stable, hence the name "small gain theorem". Due to the gain acting as an upper bound, the small gain criterion is sufficient, but not necessary:

$$g(Sys_1 \cdot Sys_2) \leq g(Sys_1)g(Sys_2) < 1 \tag{3.4}$$

The proof of the theorem poses only few requirements that the norm must fulfill. Identity should be mapped to one, zero to zero and the norm should be continuously defined. The small gain theorem is closely related to the classical Nyquist stability criterion [50] and represents an extension to nonlinear multiple input, multiple output (MIMO) systems.

In the context of linear thermoacoustic systems, the maximum sound power amplification of the frequency response can be used as metric for the gain. This criterion is already known in the community as whistling potential [51] or instability potentiality [35, 52, 53]. In the following derivations, a link between sound power amplification and the scattering matrix of an acoustic system will be established. As mentioned in the previous section, there are several different definitions of perturbation energy and sound power transferred through an interface. Whereas Polifke [52] and Emmert et al. [35] used the low Mach definition for instantaneous sound power transfer respectively intensity fluctuations I':

$$I' = p'u', \tag{3.5}$$

we use the version of Morfey [42]:

$$I' = p'u' + \frac{u_0}{\rho_0 c^2} p'^2 + \frac{u_0^2}{c^2} p'u' + \rho_0 u_0 u'^2 \tag{3.6}$$

Aurégan et al. [51] have shown that it can be factored into the product of acoustic exergy fluctuations Π' and acoustic mass flux m' using the linearized equation of state for a perfect fluid $p' = c^2\rho'$:

$$I' = \Pi' m'; \tag{3.7}$$

$$m' = \rho_0 u' + \rho' u_0; \tag{3.8}$$

$$\Pi' = \frac{p'}{\rho_0} + u_0 u' \tag{3.9}$$

Acoustic waves f, g as defined in section 2.3.1 are used to split the exergy transfer and mass flux into two directions $\pm$:

$$\Pi' = \frac{p'}{\rho_0} + u_o \cdot u' = f(c + u_0) + g(c - u_0) = \Pi'_+ + \Pi'_- \tag{3.10}$$

$$\begin{aligned} m' =& \rho_0(f - g) + p'/c^2 u_0 \\ =& \frac{\rho_0}{c}(f(c + u_0) + g(u_0 - c)) = m'_+ + m'_- = \frac{\rho_0}{c}\Pi'_+ - \frac{\rho_0}{c}\Pi'_- \end{aligned} \tag{3.11}$$

With

$$\Pi'_+ = f(c + u_o); \quad m'_+ = \frac{\rho_0}{c}\Pi'_+, \tag{3.12}$$

$$\Pi'_- = g(c - u_o); \quad m'_- = -\frac{\rho_0}{c}\Pi'_-. \tag{3.13}$$

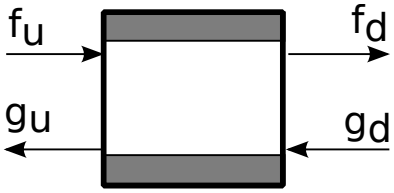

Figure 3.1: Two-port system with upstream (u) and downstream (d) ports.

Equations (3.7) (3.10) and (3.11) give:

$$I' = (\Pi'_+ + \Pi'_-)(\frac{\rho_0}{c}\Pi'_+ - \frac{\rho_0}{c}\Pi'_-) = \frac{\rho_0}{c}(\Pi'^2_+ - \Pi'^2_-) \tag{3.14}$$

Short term temporal averaging over one period of the product of real parts of harmonically oscillating quantities results in:

$$I = \frac{\rho_0}{2c}(\hat{\Pi}^H_+\hat{\Pi}_+ - \hat{\Pi}^H_-\hat{\Pi}_-) \tag{3.15}$$

where $\hat{\cdot}$ represents the complex amplitudes and $\cdot^H$ stands for the Hermitian (complex conjugate transpose). Spatial integration over one cross section assuming constant mean flow and plane waves gives the net acoustic sound power transferred across the interface:

$$W = AI = \frac{A\rho_0}{2c}(\hat{\Pi}^H_+\hat{\Pi}_+ - \hat{\Pi}^H_-\hat{\Pi}_-) = \tilde{\Pi}^H_+\tilde{\Pi}_+ - \tilde{\Pi}^H_-\tilde{\Pi}_- \tag{3.16}$$

with the normalized exergy fluctuations

$$\tilde{\Pi} = \sqrt{\frac{A\rho_0}{2c}}\hat{\Pi}. \tag{3.17}$$

The scattering matrix of a two port system (Fig. 3.1) models the dynamics between incident and emitted acoustic waves

$$\begin{bmatrix} g_u \\ f_d \end{bmatrix} = \begin{bmatrix} S_{11} & S_{12} \\ S_{21} & S_{22} \end{bmatrix} \begin{bmatrix} f_u \\ g_d \end{bmatrix}. \tag{3.18}$$

The vector of incident exergy fluctuations can be expressed by acoustic waves, mean flow indices u, d are shown explicitly only in the first matrix and are further omitted for ease of notation:

$$\tilde{\Pi}_+ = \begin{bmatrix} \sqrt{\frac{A\rho_0}{2c}}(c+u_0)\Big|_u & 0 \\ 0 & \sqrt{\frac{A\rho_0}{2c}}(c-u_0)\Big|_d \end{bmatrix} \begin{bmatrix} f_u \\ g_d \end{bmatrix} = \begin{bmatrix} (1+\mathrm{Ma})\sqrt{\frac{A\rho_0 c}{2}} & 0 \\ 0 & (1-\mathrm{Ma})\sqrt{\frac{A\rho_0 c}{2}} \end{bmatrix} \begin{bmatrix} f_u \\ g_d \end{bmatrix}$$

$$\begin{bmatrix} f_u \\ g_d \end{bmatrix} = \begin{bmatrix} \frac{1}{(1+\mathrm{Ma})\sqrt{\frac{A\rho_0 c}{2}}} & 0 \\ 0 & \frac{1}{(1-\mathrm{Ma})\sqrt{\frac{A\rho_0 c}{2}}} \end{bmatrix} \tilde{\Pi}_+ \tag{3.19}$$

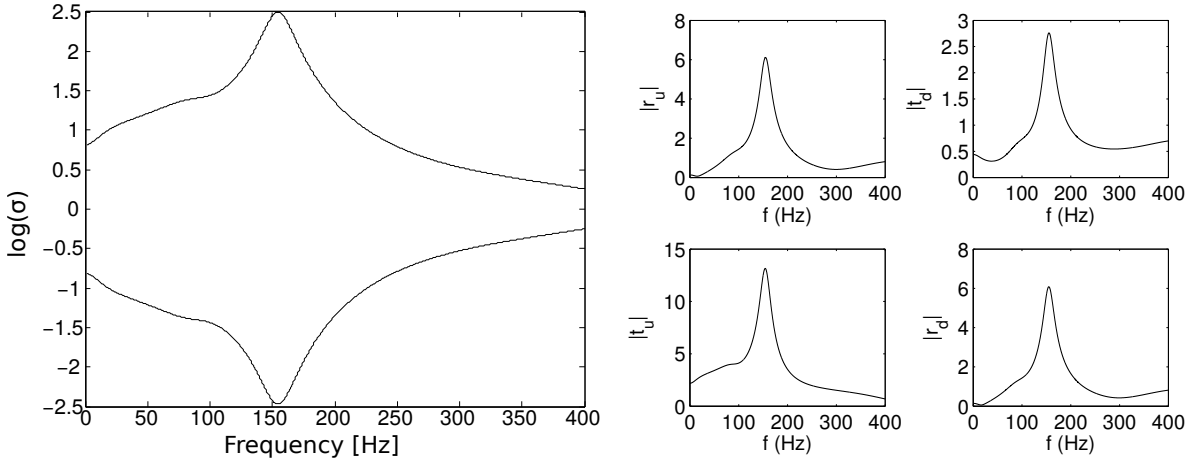

Figure 3.2: Instability potentiality of a typical turbulent premixed swirl flame and corresponding scattering matrix [35].

and eventually the vector of emitted acoustic exergy fluctuation flow is:

$$\begin{aligned}
\tilde{\Pi}_- &= \begin{bmatrix} (1-\mathrm{Ma})\sqrt{\frac{A\rho_0 c}{2}}\Big|_u & 0 \\ 0 & (1+\mathrm{Ma})\sqrt{\frac{A\rho_0 c}{2}}\Big|_d \end{bmatrix} \begin{bmatrix} g_u \\ f_d \end{bmatrix} \\
&= \begin{bmatrix} (1-\mathrm{Ma})\sqrt{\frac{A\rho_0 c}{2}} & 0 \\ 0 & (1+\mathrm{Ma})\sqrt{\frac{A\rho_0 c}{2}} \end{bmatrix} S \begin{bmatrix} f_u \\ g_d \end{bmatrix} \\
&= \begin{bmatrix} (1-\mathrm{Ma})\sqrt{\frac{A\rho_0 c}{2}} & 0 \\ 0 & (1+\mathrm{Ma})\sqrt{\frac{A\rho_0 c}{2}} \end{bmatrix} S \begin{bmatrix} \frac{1}{(1+\mathrm{Ma})\sqrt{\frac{A\rho_0 c}{2}}} & 0 \\ 0 & \frac{1}{(1-\mathrm{Ma})\sqrt{\frac{A\rho_0 c}{2}}} \end{bmatrix} \tilde{\Pi}_+ \\
&= V_- S V_+^{-1} \tilde{\Pi}_+ = \Sigma \tilde{\Pi}_+ .
\end{aligned} \tag{3.20}$$

The relation between emitted and incident acoustic exergy fluctuation flow is described by the exergy scattering matrix Σ.

The gain of the system is according to Eq. (3.3):

$$g = \sup \frac{\|\tilde{\Pi}_-^H \tilde{\Pi}_-\|}{\|\tilde{\Pi}_+^H \tilde{\Pi}_+\|} = \sup \frac{\|\tilde{\Pi}_+^H \Sigma^H \Sigma \tilde{\Pi}_+\|}{\|\tilde{\Pi}_+^H \tilde{\Pi}_+\|} \tag{3.21}$$

Without loss of generality, we choose normalized inputs such that $\|\tilde{\Pi}_+^H \tilde{\Pi}_+\| \equiv 1$

$$g = \sup_{\tilde{\Pi}_+} \|\tilde{\Pi}_+^H \Sigma^H \Sigma \tilde{\Pi}_+\| = \sup_{\omega \in R} \sigma(\Sigma(j\omega))) = \|\Sigma\|_\infty \tag{3.22}$$

and solutions can be expressed by the maximum eigenvalue of $\Sigma^H \Sigma$ respectively the maximum singular value of Σ. This definition corresponds to the so called H_∞ norm of the energy scattering matrix Σ. The basis vectors of the SVD are the orthogonal directions of minimum and maximum sound power amplification. The gain $g = \|\Sigma\|_\infty$ is called the instability potentiality of the system [35].

If the gain exceeds 1, the system amplifies sound power, if it is less than 1, the system attenuates sound power. Following this derivation, there is a naive stability criterion based on the small gain theorem: Assuming passive boundaries with a gain g of 1, burner and flame scattering matrices with a gain of less than 1 will result in a stable thermoacoustic system. As stated above, the criterion is sufficient but not necessary for stability and typically violated by systems involving a flame. Premixed flames exhibit scattering matrix resonance peaks, which exceed unity sound power amplification by far, as shown in Fig. 3.2. It is safe to assume, that an unstable burner system may be stabilized by coupling it with different acoustic boundaries [35].

Therefore, the instability potentiality is not suitable to prove stability of combustion systems. However it can be used as an optimization criterion to minimize the maximum sound power amplification of a burner and to figure out critical frequencies. On the other side, it may be useful to maximize the sound power amplification in applications such as thermoacoustic stacks in thermoacoustic engines.

The energy scattering matrix Σ is related to the acoustic scattering matrix S by a constant rescaling V_+, V_- as shown in Eq. (3.20). For low Mach numbers $\mathrm{Ma} \to 0$ it can even be shown, that $V_+ = V_-$ and the singular values of S and Σ are identical. Therefore, peaks in the frequency response of the scattering matrix are also peaks in sound power amplification. This is illustrated in Fig. 3.2, which shows the singular values and scattering matrix of a burner and flame system [35]. The physical reason for such peaks in acoustic power amplification at distinct frequencies are resonance phenomena inside of the system. One such phenomenon is given by the so called intrinsic thermoacoustic feedback of premixed flames, which will be investigated in the following chapter.

4 Intrinsic Thermoacoustic Feedback of Premixed Flames

It is a known phenomenon that there are peaks in the scattering matrix of premixed flames [54]. Bomberg et al. [55] have shown that the resonance mechanism, which causes these peaks, is caused by a flame intrinsic acoustic-flow-flame-acoustic feedback. Premixed flames respond to velocity fluctuations upstream of the flame at the burner mouth with a heat release modulation [35]. The resulting heat release fluctuations in turn act as a volume source and generate an upstream traveling acoustic wave. This wave closes the feedback as it causes a velocity perturbation at the burner mouth.

Flame intrinsic modes have since been reproduced and investigated by several research groups [35, 56–58]. Emmert et al. [35] have demonstrated that the flame intrinsic resonances are the cause for strong sound power amplification and in consequence for potential thermoacoustic instabilities. Eventually, Emmert et al. [59] have shown, that the flame intrinsic modes exist besides the acoustic modes and actually play an important role in full thermoacoustic systems like burner test rigs and supposedly also in entire gas turbines.

This result causes a paradigm shift in the analysis of thermoacoustic systems. Previous investigations [10, 60] attributed at the time inexplicable low frequency eigenmodes of thermoacoustic systems to some Helmholtz or longitudinal acoustic modes, but in fact they were caused by flame intrinsic resonance [22, 35]. We show that classical stabilization measures, such as to increase damping by a perforated plate termination in a burner test rig, may actually render the system more unstable [59]. Even though all acoustic modes are damped, intrinsic modes may be amplified.

The following derivations are based on state space modeling and preceded [59], where a classical frequency domain approach is used. For people, who have been working in the field, the argument using the classical frequency domain method is more intuitive and easier to understand. However the state space modeling has a clarity, which makes the existence of intrinsic thermoacoustic eigenmodes trivial. The dynamics of a full combustion systems with reflective boundaries are modeled using a low order acoustic network model [6, 29]. Such models are able to predict the dynamics and stability of thermoacoustic systems in experiments [4], [5], [27] and DNS simulations [58].

4.1 Low Order Combustor Test Rig Network Model

We investigate a linear acoustic network model that is depicted in Figure 4.1, with model parameters specified in Table 4.1. It is derived from a single burner test rig of the BRS Burner

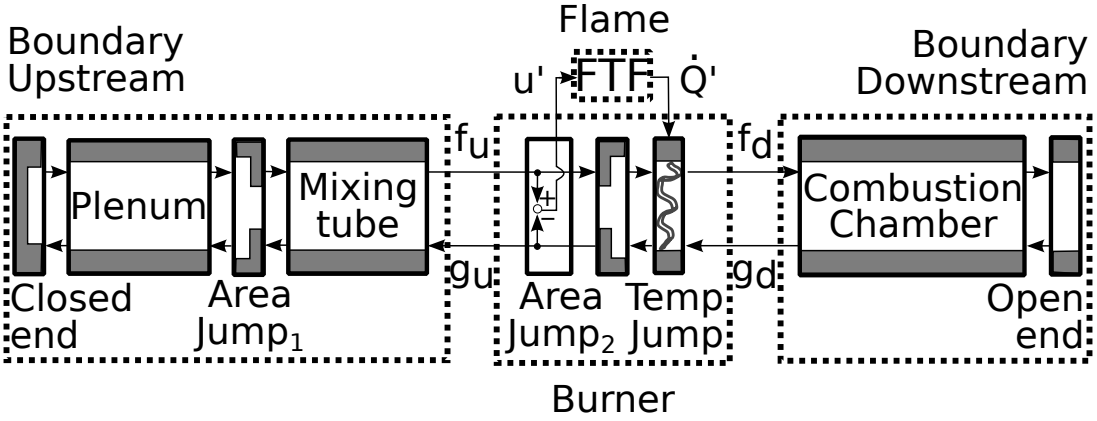

Figure 4.1: Scheme of the BRS test rig network model.

Table 4.1: Parameters of the BRS test rig network model.

Name	Parameters
Closed End	Reflection coefficient $r_C = 1$
	Inlet: $Mach = 0.0011$, $c = 343\,\frac{\mathrm{m}}{\mathrm{s}}$, $\rho = 1.2\,\frac{\mathrm{kg}}{\mathrm{m}^3}$
Plenum	Duct, $l_P = 0.17\,\mathrm{m}$
Area Jump 1	Area ratio $\alpha_1 = 29.76$
Mixing Tube	Duct, $l_M = 0.18\,\mathrm{m}$
Area Jump 2	Area ratio $\alpha_2 = 0.13$
Temperature Jump	Lin. energy equation, $\theta = (T_d - T_u)/T_u = 5.59$
Combustion Chamber	Duct, $l_C = 0.70\,\mathrm{m}$
Open End	Reflection coefficient $r_O = [-1, 0]$
FTF	Identified from LES by [27],
	see Figure 4.4

which was experimentally investigated by Komarek et al. [61] and Alemela et al. [62]. The model is very similar to the one used by Tay-Wo-Chong et al. [27] with a length of the combustion chamber $l_C = 0.7\,\mathrm{m}$, which we will refer to for validation purposes. Whereas the model of Tay-Wo-Chong et al. [27] was a classical frequency domain low order network model, here linear state space models as described in section 2 and [29] are used. Propagation of acoustic waves is modeled by 1D linearized Euler equations, which are spatially discretized using a third order upwind scheme. The frequency range of interest is up to 500 Hz, which is below the cut on frequency of the plenum $f_{cuton} = 1.84 \cdot c/2\pi \cdot r \approx 1000\,\mathrm{Hz}$, where the radius is $r = 0.10\,\mathrm{m}$. All area jumps are modeled as acoustically compact elements and in contrast to Tay's work without losses or correction factors. As in the work by Tay-Wo-Chong et al. [27], the swirler is assumed to be acoustically transparent and is therefore neglected. The acoustic boundary conditions are an upstream closed end and a downstream open end. In contrast to that, Tay considered on the downstream side a reflection coefficient of a perforated plate, which was not precisely determined and is in the range between -1 and 0. The acoustic flame model is derived from linearized jump equations and consists of an acoustically compact temperature jump with heat release fluctuations $\dot{Q}'$ as additional input. The relations were originally derived by Chu [63] and presented in state space formulation by Emmert et al. [35]. The model is closed by a flame transfer function (FTF) model that relates an upstream velocity perturbation u' at the burner mouth to a heat release fluctuation of the flame. This FTF model was retrieved from LES simulation and system identification (SI) techniques and was validated against experimental results by Tay-Wo-Chong et al. [64]. Its impulse response is shown in Figure 4.4.

As illustrated by the boxes in Figure 4.1, the network model elements can be combined into four state space subsystem models for the acoustic boundaries (u,d), the acoustics of the burner (b), and the flame dynamics (f).

4.1.1 Boundary Subsystem

As Figure 4.1 shows, the two boundaries up- and downstream are composite models. The upstream part consists of a closed end, two duct sections of the plenum and the mixing tube and an area contraction in between. Downstream there is just a duct section of the combustion chamber and an open end. The two systems can be appended to form the up- and downstream boundary model (ud):

$$\dot{x}_{ud} = \underbrace{\begin{bmatrix} A_u & 0 \\ 0 & A_d \end{bmatrix}}_{A_{ud}} x_{ud} + B_{ud} \underbrace{\begin{bmatrix} g_u \\ f_d \end{bmatrix}}_{u_{ud}} \tag{4.1}$$

$$\underbrace{\begin{bmatrix} f_u \\ g_d \end{bmatrix}}_{y_{ud}} = C_{ud} x_{ud} \tag{4.2}$$

There is no feed through $D_{ud} = 0$ because the incident waves are propagating in duct sections before they are reflected.

4.1.2 Flame Subsystem

The combustion dynamics of turbulent premixed swirl stabilized flames are modeled by a flame transfer function. The single input of the flame model are velocity fluctuations u' at a reference position at the burner mouth and the output are global heat release fluctuations of the flame $\dot{Q}'$:

$$\dot{x}_f = A_f x_f + B_f \underbrace{\left[u'\right]}_{u_f} \tag{4.3}$$

$$\underbrace{\left[\dot{Q}'\right]}_{y_f} = C_f x_f \tag{4.4}$$

It is assumed that the flame does not have a feed through $D_f = 0$ either. The state space system can be solved for the flame transfer function (FTF) by Laplace transform:

$$\dot{Q}' = \underbrace{C_f (sI - A_f)^{-1} B_f}_{FTF(s)} u' . \tag{4.5}$$

The impulse response of the flame model is depicted in Figure 4.4.

4.1.3 Burner Subsystem

It is assumed that the burner subsystem, which consists of the area expansion into the combustion chamber and the temperature jump, is acoustically compact. This assumption is valid because the length of the burner $l_B \approx 0.074\,\mathrm{m}$ is much smaller than the wavelength at $500\,\mathrm{Hz}$: $\lambda = c/f \approx 0.7\,\mathrm{m}$. It is possible to carry out this investigation under consideration of finite length of the burner, but doing so does not change the fundamental results and merely adds complexity to the derivations. Due to the compactness and lack of losses, the burner itself does not possess any dynamics. Subscript b stands for the burner subsystem, f indicates connections to the flame and subscript ud refers to connections of the up- and downstream boundary subsystem.

$$\begin{bmatrix} y_{b,ud} \\ y_{b,f} \end{bmatrix} = \underbrace{\begin{bmatrix} D_{b,ud,ud} & D_{b,ud,f} \\ D_{b,f,ud} & D_{b,f,f} \end{bmatrix}}_{D_b} \begin{bmatrix} u_{b,ud} \\ u_{b,f} \end{bmatrix}, \tag{4.6}$$

where the input and output vectors are

$$\left[\begin{array}{c} y_{b,ud} \\ \hline y_{b,f} \end{array}\right] = \left[\begin{array}{c} g_u \\ f_d \\ \hline u' \end{array}\right], \quad \left[\begin{array}{c} u_{b,ud} \\ \hline u_{b,f} \end{array}\right] = \left[\begin{array}{c} f_u \\ g_d \\ \hline \dot{Q}' \end{array}\right]. \tag{4.7}$$

4.1.4 Full BRS System

In order to solve for the dynamics of the full composite network model, the three subsystems are appended:

$$\begin{bmatrix} \dot{x}_{ud} \\ \dot{x}_f \end{bmatrix} = \begin{bmatrix} A_{ud} & 0 \\ 0 & A_f \end{bmatrix} \begin{bmatrix} x_{ud} \\ x_f \end{bmatrix} + \begin{bmatrix} B_{ud} & 0 & 0 & 0 \\ 0 & 0 & 0 & B_f \end{bmatrix} \begin{bmatrix} u_{ud} \\ u_{b,ud} \\ u_{b,f} \\ u_f \end{bmatrix} \tag{4.8}$$

$$\begin{bmatrix} y_{ud} \\ y_{b,ud} \\ y_{b,f} \\ y_f \end{bmatrix} = \begin{bmatrix} C_{ud} & 0 \\ 0 & 0 \\ 0 & 0 \\ 0 & C_f \end{bmatrix} \begin{bmatrix} x_{ud} \\ x_f \end{bmatrix} + \begin{bmatrix} 0 & 0 & 0 & 0 \\ 0 & D_{b,ud,ud} & D_{b,ud,f} & 0 \\ 0 & D_{b,f,ud} & D_{b,f,f} & 0 \\ 0 & 0 & 0 & 0 \end{bmatrix} \begin{bmatrix} u_{ud} \\ u_{b,ud} \\ u_{b,f} \\ u_f \end{bmatrix} \tag{4.9}$$

and the feedback by interconnections of the system is evaluated:

$$\begin{bmatrix} u_{ud} \\ u_{b,ud} \\ u_{b,f} \\ u_f \end{bmatrix} = \begin{bmatrix} 0 & 1 & 0 & 0 \\ 1 & 0 & 0 & 0 \\ 0 & 0 & 0 & 1 \\ 0 & 0 & 1 & 0 \end{bmatrix} \begin{bmatrix} y_{ud} \\ y_{b,ud} \\ y_{b,f} \\ y_f \end{bmatrix}. \tag{4.10}$$

Now the output equation (4.9) is plugged into the feedback equation (4.10) and solved for the inputs:

$$\begin{bmatrix} u_{ud} \\ u_{b,ud} \\ u_{b,f} \\ u_f \end{bmatrix} = \begin{bmatrix} 1 & -D_{b,ud,ud} & -D_{b,ud,f} & 0 \\ 0 & 1 & 0 & 0 \\ 0 & 0 & 1 & 0 \\ 0 & -D_{b,f,ud} & -D_{b,f,f} & 1 \end{bmatrix}^{-1} \begin{bmatrix} 0 & 0 \\ C_{ud} & 0 \\ 0 & C_f \\ 0 & 0 \end{bmatrix} \begin{bmatrix} x_{ud} \\ x_f \end{bmatrix} \tag{4.11}$$

Substituting the input vector in the state equation 4.8 using the previous result from equation 4.11 results in the system matrix of the full model:

$$\begin{bmatrix} \dot{x}_{ud} \\ \dot{x}_f \end{bmatrix} = \underbrace{\begin{bmatrix} A_{ud} + B_{ud} C_{ud} D_{b,udud} & B_{ud} C_f D_{b,udf} \\ B_f C_{ud} D_{b,fud} & A_f + B_f C_f D_{b,ff} \end{bmatrix}}_{A} \begin{bmatrix} x_{ud} \\ x_f \end{bmatrix} \tag{4.12}$$

It is an autonomous system and therefore has no physical in- and outputs.

In order to provide validation of the network model, the eigenvalues of the full system are computed and plotted as crosses in Figure 4.2. In agreement with [27], three dominant -least decaying- modes exist at approximately 42 Hz, 111 Hz and 315 Hz. The growth rates of all eigenfrequencies are negative, thus the full system is stable. Tay mentions that the eigenvalue close to 100 Hz is unstable in the expermimental BRS test rig. This is in agreement with the predictions of the model, where although the mode is predicted to be stable, it is the least decaying of the three.

According to a preliminary estimation of Tay-Wo-Chong et al. [27], there are only two acoustic modes expected in the frequency range under investigation. Thus he contributed one of the three dominant modes to flame dynamics. In the following sections we will show that this assumption is actually true and how the eigenmodes of the full BRS model relate to its acoustic eigenmodes and its intrinsic thermoacoustic (ITA) eigenmodes.

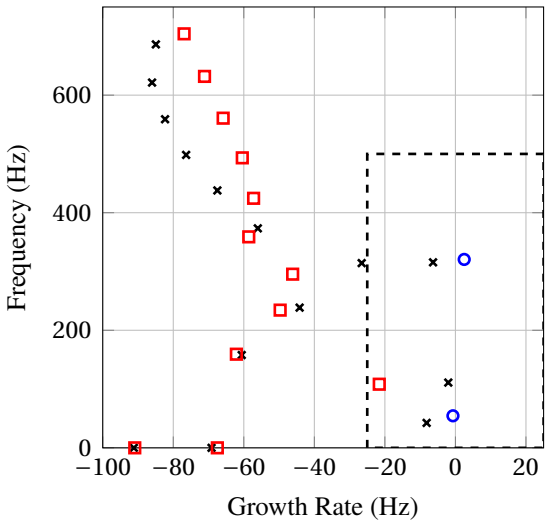

Figure 4.2: Eigenfrequencies of full (×), acoustic (○) and Burner & Flame ITA (□) system of the test rig model are corresponding but distinct.

4.2 BRS Model Disassembly and Reassembly

Subsequently we will exploit the state space representation of the BRS system model in order to find out more about the physical mechanisms involved in the resonant processes that cause the eigenmodes of the system. This is achieved by at first disassembling the BRS model into an Acoustic and an intrinsic Burner & Flame system. Subsequently the system is re-assemblied with a modulation parameter that will establish a link between the full BRS system and the Acoustic and the ITA Burner & Flame systems.

4.2.1 Acoustic System

The pure acoustic eigenmodes of the system are retrieved by connecting just the burner model and the boundaries, see Figures 4.1, 4.3(a). Thus the flame transfer function and therefore the flame dynamics are omitted, but the mean temperature jump due to the combustion is retained in the model. This implies that all links to and from the flame can be omitted and the reduced burner system (equation 4.6) is:

$$y_{b,ud} = D_{b,ud,ud}\, u_{b,ud} \tag{4.13}$$

The state space model of the appended boundary and burner system is:

$$\dot{x} = A_{ud}\, x + \begin{bmatrix} B_{ud} & 0 \end{bmatrix} \begin{bmatrix} u_{ud} \\ u_{b,ud} \end{bmatrix} \tag{4.14}$$

$$\begin{bmatrix} y_{ud} \\ y_{b,ud} \end{bmatrix} = \begin{bmatrix} C_{ud} \\ 0 \end{bmatrix} x + \begin{bmatrix} 0 & 0 \\ 0 & D_{b,ud,ud} \end{bmatrix} \begin{bmatrix} u_{ud} \\ u_{b,ud} \end{bmatrix} \tag{4.15}$$

with feedback:

$$\begin{bmatrix} u_{ud} \\ u_{b,ud} \end{bmatrix} = \begin{bmatrix} 0 & 1 \\ 1 & 0 \end{bmatrix} \begin{bmatrix} y_{ud} \\ y_{b,ud} \end{bmatrix}. \tag{4.16}$$

The system matrix A_A resulting from the interconnection is:

$$A_A = \left[A_{ud} + B_{ud} C_{ud} D_{b,ud,ud} \right] . \tag{4.17}$$

Figure 4.2 shows the eigenvalues of the acoustic modes as blue circles. It is not possible to determine which mode of the full system (black crosses) corresponds to an acoustic mode. As can be seen, the full system overall exhibits more than just the acoustic eigenmodes. Particularly amongst the most dominant low frequency eigenvalues in the range above $-20\,\mathrm{Hz}$ growth rate and below $500\,\mathrm{Hz}$ frequency, there are three modes of the full system, but just two acoustic modes.

4.2.2 Intrinsic Thermoacoustic Burner & Flame System

Previous investigations by Emmert et al. [35] have shown that there may be very strong amplification of acoustic waves, as they are scattered by the Burner & Flame (BF) of a combustion system. This amplification was contributed to intrinsic thermoacoustic eigenmodes of the Burner & Flame resulting from an acoustic-flow-flame-acoustic feedback described by Bomberg et al. [55]. Figure 4.3(b) illustrates the Burner & Flame model that exhibits the intrinsic eigenmodes. For investigating the Burner & Flame system, the burner is disconnected from the boundaries and can be reduced to:

$$y_{b,f} = D_{b,f,f}\, u_{b,f} \tag{4.18}$$

Aggregating the burner and flame systems

$$\dot{x} = A_f x + \begin{bmatrix} B_f & 0 \end{bmatrix} \begin{bmatrix} u_f \\ u_{b,f} \end{bmatrix} \tag{4.19}$$

$$\begin{bmatrix} y_f \\ y_{b,f} \end{bmatrix} = \begin{bmatrix} C_f \\ 0 \end{bmatrix} x + \begin{bmatrix} 0 & 0 \\ 0 & D_{b,f,f} \end{bmatrix} \begin{bmatrix} u_f \\ u_{b,f} \end{bmatrix} \tag{4.20}$$

with feedback:

$$\begin{bmatrix} u_f \\ u_{b,f} \end{bmatrix} = \begin{bmatrix} 0 & 1 \\ 1 & 0 \end{bmatrix} \begin{bmatrix} y_f \\ y_{b,f} \end{bmatrix} \tag{4.21}$$

leads to the system matrix A_{BF} of the intrinsic Burner & Flame system:

$$A_{BF} = \left[A_f + B_f C_f D_{b,f,f} \right] . \tag{4.22}$$

Eigenvalues of the pure intrinsic Burner & Flame system are ploted in Figure 4.2 as red boxes. Due to the high order of the LES system identification FTF heat release model, there are many intrinsic eigenvalues in the frequency range of interest. All of the intrinsic eigenvalues are stable and there is one least decaying and therefore most dominant eigenmode at $\approx 100\,\mathrm{Hz}$. The frequency of this eigenmode is corresponding to a characteristic time scale of the resonant process $\tau_{BF} = 1/100\,\mathrm{Hz} = 0.01\,\mathrm{s}$. As the Burner & Flame domain is acoustically almost compact ($\tau \gg l/c$), this delay is mostly governed by the flow-flame dynamics modeled by the flame transfer function. Due to the negative relation between the velocity perturbation and the upstream traveling acoustic wave $u' \propto -g_u$, the characteristic time of the burner & flame feedback is expected to be about twice the characteristic time delay of the FTF respectively

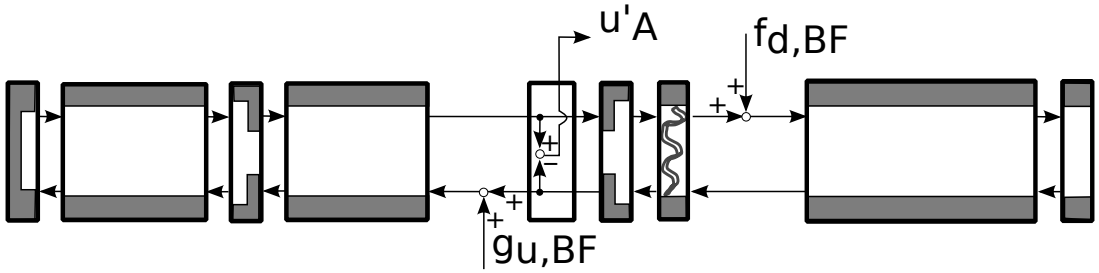

(a) Acoustic system.

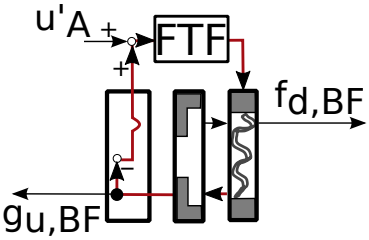

(b) Intrinsic burner & flame system.

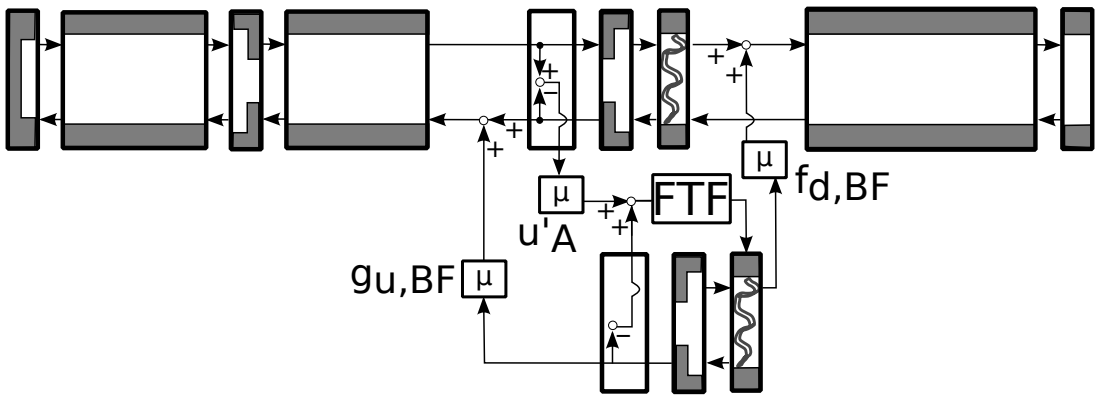

(c) Coupled, modulated system.

Figure 4.3: Decomposition and recomposition of the BRS model.

$\tau_{BF}/2 = \tau_{FTF}$. Estimating τ_{FTF} from Figure 4.4 is showing agreement with this assumption: $\tau_{BF}/2 = 0.005\,\mathrm{s} \approx 0.0048\,\mathrm{s} = \tau_{FTF}$.

At this point, we can draw the conclusion, that it is very likely, that the three dominant modes of the BRS model are related to two acoustic modes and one intrinsic mode of the system. However it is not clear which of the modes of the full system is associated with which resonant process.

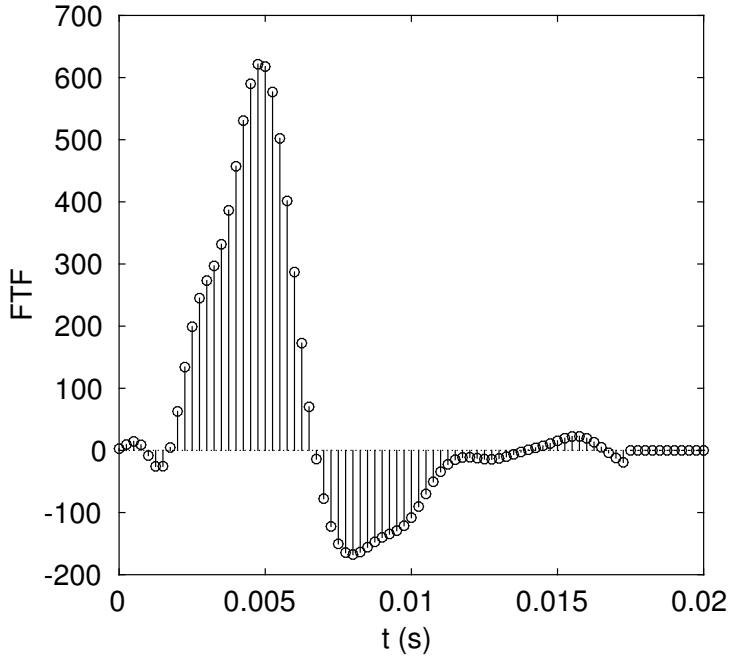

Figure 4.4: Impulse response of the BRS flame transfer function.

4.2.3 Modulated Coupling of Burner & Flame and Acoustic System

In order to discriminate between modes of the full system originating from acoustic modes and such from Burner & Flame modes, the coupling between them is modulated. The waves $g_{u,BF}$ and $f_{d,BF}$ generated by the intrinsic BF subsystem are injected into the acoustic system by the off diagonal coupling term $D_{b,f,ud}$ from the burner system equation 4.6. In the other direction, velocity perturbations u'_A originating from the acoustic subsystem are linked back into the intrinsic system by the term $D_{b,ud,f}$. We will modulate the cross talking terms with an artificial paramter μ as shown schematically in Figure 4.3(c). The modulated burner system is:

$$\begin{bmatrix} y_{b,ud} \\ y_{b,f} \end{bmatrix} = \begin{bmatrix} D_{b,ud,ud} & \boldsymbol{\mu} D_{b,ud,f} \\ \boldsymbol{\mu} D_{b,f,ud} & D_{b,f,f} \end{bmatrix} \begin{bmatrix} u_{b,ud} \\ u_{b,f} \end{bmatrix}. \tag{4.23}$$

The full coupled system with modulation parameter (M) is evaluated the same way as the full system and this results in:

$$\begin{bmatrix} \dot{x}_{ud} \\ \dot{x}_f \end{bmatrix} = \underbrace{\begin{bmatrix} A_{ud} + B_{ud} C_{ud} D_{b,udud} & \boldsymbol{\mu} B_{ud} C_f D_{b,udf} \\ \boldsymbol{\mu} B_f C_{ud} D_{b,fud} & A_f + B_f C_f D_{b,ff} \end{bmatrix}}_{A_M} \begin{bmatrix} x_{ud} \\ x_f \end{bmatrix} \tag{4.24}$$

where the parameter μ is modulating the coupling.

For $\mu = 1$, the system matrix of the modulated system is equivalent to the one of the full system (equation 4.12). Therefore, the systems have the same eigenvalues.

Considering $\mu = 0$ instead, the system matrix is a Block diagonal matrix containing the acoustic and the intrinsic system matrices (see equations 4.17,4.22):

$$\begin{bmatrix} \dot{x}_{ud} \\ \dot{x}_f \end{bmatrix} = \begin{bmatrix} A_A & 0 \\ 0 & A_{BF} \end{bmatrix} \begin{bmatrix} x_{ud} \\ x_f \end{bmatrix} \tag{4.25}$$

The characteristic polynomial factors into:

$$0 = \det(sI - A_A) \det(sI - A_{BF}) . \tag{4.26}$$

Thus, the system exactly has the sum of the acoustic and the Burner & Flame system's eigenmodes.

4.3 Numerical Results

Using the derivations from the previous sections, the BRS system is now examined numerically. For this purpose, the eigenvalues and eigenvectors of the systems under investigation are computed. At first the modulation parameter is used to discriminate between acoustic and Burner & Flame eigenmodes of the full system. Subsequently, the eigenvectors of the most dominant eigenmodes are analyzed. Eventually the influence of the downstream reflection coefficient on the eigenvalues of the system is investigated. Overall, special attention is drawn to the differences between acoustic and Burner & Flame ITA eigenmodes.

4.3.1 Correspondence of Eigenvalues

In the previous sections, we have shown that for $\mu = 1$, the full system dynamics are recovered from the system with modulation parameter. For $\mu = 0$ the dynamics of the acoustic and Burner & Flame systems emerges. By sweeping the parameter μ continuously from 0 to 1, we can track how the eigenmodes evolve from acoustic and Burner & Flame ITA to full system eigenmodes as shown in Figure 4.5.

The sweep establishes a clear relation between the eigenmodes of the full system and the acoustic and intrinsic systems. We observe, that the three most dominant - highest growth rate - eigenmodes of the full system are in fact due to two acoustic cavity and one ITA mode. Furthermore, all eigenvalues get shifted and the shifting is not linear.

Both acoustic eigenmodes are stabilized by the coupling with the flame dynamics. Opposed to that the most dominant Burner & Flame mode becomes more unstable.

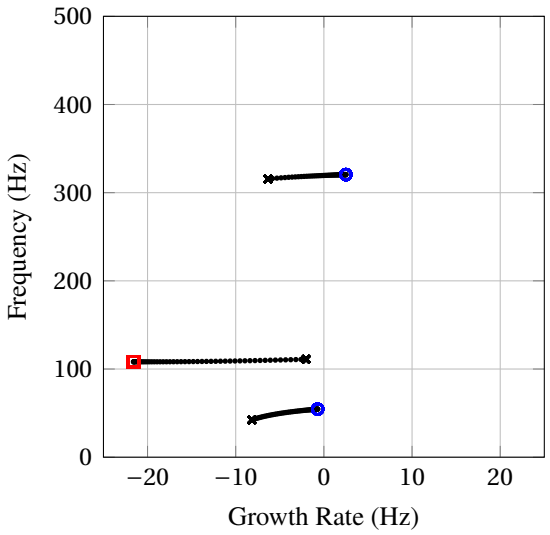

Figure 4.5: Correspondence of acoustic (○) and Burner & Flame ITA (□) to full system (×) eigenmodes. Modulation parameter μ is varied from 0 to 1 (·).

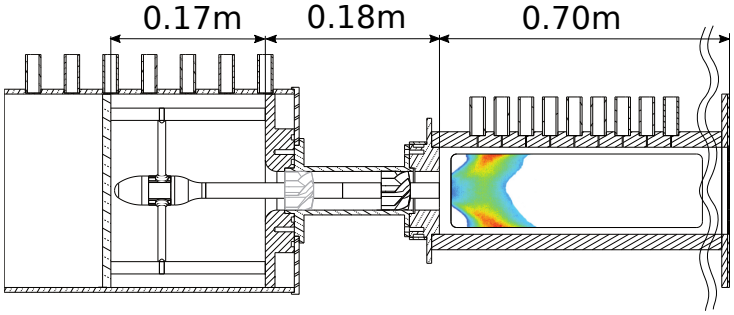

Figure 4.6: Geometry of the thermoacoustic test rig.

4.3.2 Comparison of Mode Shapes

Figure 4.6 is adapted from Komarek and shows the geometry of the test rig in order to facilitate the analysis of the mode shapes. The first (blue) and second (black) acoustic and intrinsic (red) eigenmodes are shown in Figure 4.7. The mode shapes of the pure acoustic system are drawn as dashed lines, wheres the full system modes are full lines.

The first acoustic mode -●- has almost constant phase for both pressure and velocity throughout the system. In the plenum, there is a high pressure and in the mixing tube, there is high velocity, whereas in the combustion chamber, there are overall low amplitudes. Therefore the first acoustic mode is a Helmholtz mode of the plenum and mixing tube. Due to the coupling with the flame, it is shifted towards higher pressures and velocities in the combustion chamber and comparatively lower velocities in the mixing section —●—. This is what is to be expected as the flame is mainly acting as a volume source.

We observe that for the second acoustic mode -○- velocity fluctuations follow pressure fluctuations by $\pi/2$. Also the comparably large amplitudes of velocity and pressure and the combustion chamber indicate that it is a quarter wave resonance of the combustion chamber. Due to the large

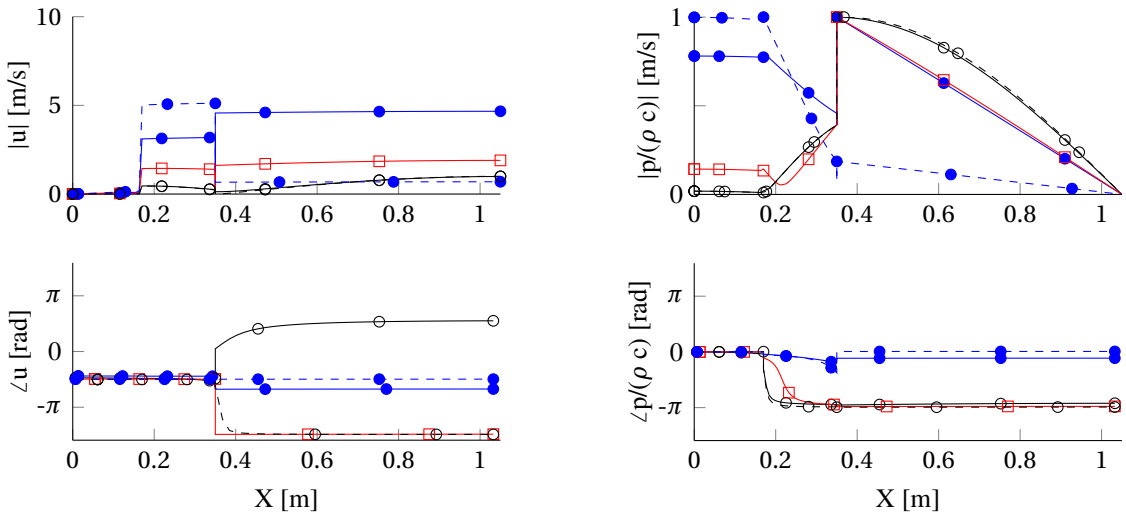

Figure 4.7: Velocity and pressure mode shapes of the first acoustic (plenum Helmholtz; full: —●—, pure: - -●- -), second acoustic (1/4 wave combustion chamber; full: —○—, pure: - -○- -) and ITA mode (full: —□—).

area change at the burner exit, it acts similar to a close end on the mode. Overall, the second acoustic mode shape is not much affected by the coupling with the flame —○—. The pure - -○- - and the full —○— system mode shapes are very similar.

The intrinsic mode shape can only be visualized for the full system, because the pure intrinsic mode is just due to flame dynamics and per definition prohibits a resonating acoustic field. The ITA mode of the full system —□— has features similar to both acoustic modes. The pressure profile looks a lot like the second acoustic mode, including the phase jump at the end of the plenum, whereas the velocity profile seems closer to the one of the first acoustic mode. Thus it is difficult to distinguish the intrinsic mode from acoustic modes by comparing mode shapes.

4.3.3 Sensitivity of Eigenvalues to Downstream Reflection Coefficient

As mentioned by Tay-Wo-Chong et al. [27], the downstream reflection coefficient of the BRS test rig is not known precisely. Therefore, a parameter study of the changes in eigenvalue due to changes in the reflection coefficient is carried out. It is varied between -1, which is a fully reflective open end and 0, a non reflective boundary condition. The level in the experiment is bounded by those values.

Figure 4.8 shows that the reduction of reflections has a damping effect on the two acoustic modes of the system, whereas the intrinsic mode becomes even more unstable. As the acoustic modes need the reflections at boundaries to exist, the higher damping is to be expected. The first acoustic mode, which is a Helmholtz mode of the plenum, degenerates for a non reflective downstream boundary to a frequency of 0 Hz. The second acoustic mode remains resonating, but gets heavily damped. It is interesting that the intrinsic mode is getting more amplified and even becomes unstable as the reflections are reduced. This is a counter intuitive result, as one would assume that less reflections relate to more acoustic losses and therefore increased overall

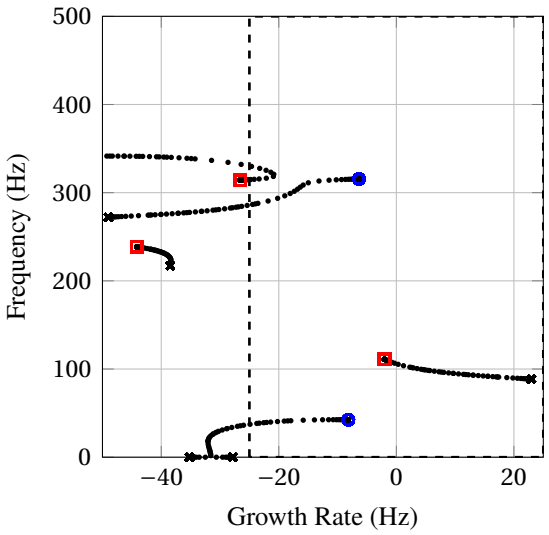

Figure 4.8: Eigenvalue shift due to changes in downstream reflection factor. Fully reflective ($R_x = -1$) open end: acoustic modes (○), ITA modes (□); Gradually lower reflections (·) until non reflective (×).

thermoacoustic stability. But the finding is in agreement with the assertion of Tay-Wo-Chong et al. [27] that in the experiment this mode is unstable.

4.4 Conclusion

Thermoacoustic systems exhibit acoustic and intrinsic thermoacoustic eigenmodes. The total number of eigenmodes is greater than just the number of acoustic cavity modes. Intrinsic thermoacoustic eigenmodes of velocity sensitive premixed flames are due to an acoustic-flow-flame-acoustic feedback. The concept of intrinsic feedback is fairly general and can be expected to take place in different combustion regimes as well as for different sound generation and amplification phenomena. Heat release fluctuations due to technically premixed flames can couple with the mixing process. Even aero-acoustic whistling may be expected to be caused by an intrinsic feedback.

The eigenmodes of the full system are corresponding, but not equivalent to pure intrinsic and acoustic modes. By modulation of the coupling parameter μ between Burner & Flame intrinsic and acoustic dynamics, full system modes can be identified to be caused by either intrinsic feedback or by acoustic resonance. Due to the modulation, all acoustic and intrinsic modes are shifted in frequency and growth rate. The closer the eigenfrequency of the intrinsic and acoustic modes match, the more they interact. It is hard to predict whether the coupling will stabilize or destabilize a mode as the effect is not linear.

It is important that a thermoacoustic model is able to reproduce the intrinsic eigenmodes, as they may lead to instability even if the acoustic modes are stable. This may put into question thermoacoustic models that assume weak coupling of the flame for stability prediction.

Paradoxically increasing acoustic losses by non reflective boundaries such as perforated plates

may render a thermoacoustic system unstable. Even though the acoustic modes get damped, an intrinsic Burner & Flame mode may get amplified.

5 Summary of Achievements

The author has contributed to the modeling, the stability analysis and the fundamental understanding of thermoacoustic systems. These contributions are reflected in four major publications, which are linked by the aim of promoting the advancement of efficient modeling of thermoacoustic systems.

He has developed and implemented a unified thermoacoustic modeling framework based on linear state space models and system theory, as documented by the first paper [29]. It enables us to seamlessly incorporate and connect models from a wide variety of modeling methods: 1D analytical solutions, linearized PDEs of perturbation equations and system identification. The framework provides a method to connect the sets of models that constitute a thermoacoustic network model in such a way that again a state space model is retrieved. Due to the fact that the search for eigenvalues can be expressed by a linear eigenvalue problem, very fast standard algorithms can be used for the computation. This is in sharp contrast to the traditional thermoacoustic network modeling in frequency domain, where a nonlinear eigenvalue problem needs to be solved. But even more importantly, it is clearing up the thermoacoustic nomenclature and modeling paradigms to a point, where fundamental insights become simple and obvious.

The models can be simulated in time domain and may be coupled with compressible and incompressible LES of flames. This has been exploited by Jaensch et al. [65] in order to investigate the nonlinear dynamics of flames.

The third paper [35] establishes a link between sound power amplification of premixed flames and a formal stability criterion for individual parts of a system called the *small gain theorem*. In the thermoacoustic community, the stability criterion is known as *instability potentiality* whereas in the acoustic community it is called *whistling potential*. Intrinsic thermoacoustic feedback has been identified as the most important cause for sound power amplification in premixed flames.

Eventually an algorithm to discriminate between eigenmodes of a full combustion system that originate from acoustic modes versus those that are constituted by burner & flame intrinsic feedback has been developed and published in the third paper [59]. The theory in the paper is presented using a classical frequency domain approach even though the idea was developed by investigating state space systems as shown in section 4. This choice was made in favor of promoting the idea of intrinsic feedback in the thermoacoustic community, where the classical frequency domain methods are more common. The fact that intrinsic thermoacoustic eigenmodes exist in full combustion systems leads to several fundamental insights and a paradigm change in the theory of combustion instabilities. The total number of eigenmodes of a thermoacoustic system is greater than just the number of acoustic cavity modes. Even though most thermoacoustic models contain by design implicitly the effect of intrinsic feedback, the common theories of combustion instability are based on the assumption, that some acoustic eigenmode becomes un-

stable due to the driving by the flame. In fact it may just as well be an intrinsic eigenmode of the burner & flame that becomes unstable and to increase acoustic dissipation may even deteriorate the stability of the combustion system.

5.1 Linear State Space Network Modeling of Acoustic Systems

Abstract: Linear acoustic network models are a state of the art tool to cope with the complexity of large acoustic systems. Such systems are composed by a set of interconnected acoustic subsystems. We introduce a generalized linear modeling framework for acoustic systems that is based on a state space formalism and linear system theory. In order to enable the modeling of large acoustic network systems, the framework is taking into account the sparse structure of acoustic models. It is shown how acoustic models retrieved from 1D low order modeling, 3D linearized perturbation equations as well as computational fluid dynamics or experimental data can be translated into state space models. This translation does not involve any approximations beyond those made by the acoustic modeling in the first place. An algorithm to evaluate the interconnection of state space models is presented, which results in one single state space model for the connected acoustic network system. In order to compute the eigenvalues and vectors of a state space model, a standard or generalized linear eigenvalue problem needs to be solved. For large acoustic systems an efficient iterative eigenvalue solver is required. The methods are validated by the comparison of eigenmodes of a generic annular combustor test case with non trivial topology.

Contribution: I have reverse engineered and implemented the connection methods and developed 1D acoustic models, performed the 1D analysis and lead the process to compose the manuscript.

Status: Published in Acta Acustica united with Acustica.

Reference: T. Emmert et al. “Linear State Space Interconnect Modeling of Acoustic Systems”. In: *Acta Acustica united with Acustica* 102.5 (2016), pp. 824–833. DOI: 10.3813/AAA.918997, reproduced on page 59.

5.2 Hybrid CFD/low-order modeling of nonlinear thermoacoustic oscillations

Abstract: This paper proposes and compares two nonlinear time-domain models of self-excited thermoacoustic oscillations of laminar premixed flames. The flame and its immediate vicinity are resolved with reactive flow simulations. Simultaneously, the acoustic field is modeled with low-order models, which are coupled to the reactive flow simulations. On the one hand a flame model based on the fully compressible Navier-Stokes equations is investigated. Here, the simulation is coupled to the low-order model via the characteristic wave amplitudes at the inlet boundary. The other model resolves the flame with a low Mach number reactive flow simula-

tion. In order to include thermoacoustic feedback, this flame model is coupled with an acoustic network model by the global heat release rate and the fluctuation of the axial velocity at a reference position upstream of the flame. A bifurcation analysis using the plenum length as bifurcation parameter is conducted. Both models exhibit complex nonlinear oscillations and are in good agreement with each other. Therefore, we conclude that the coupling of a linear acoustic model and a nonlinear flame model via reference velocity and global heat release rate is sufficient to accurately capture thermoacoustic oscillations of the configuration investigated. This implies that the most important nonlinearities can be attributed to hydrodynamic effects and the flame kinematics. Additionally, the study provides further evidence that premixed flames respond predominantly to fluctuations of the upstream velocity.

Contribution: I have developed the low-order linear state space thermoacoustic network code and helped proof read the manuscript.

Status: Published in Proceedings of the Combustion Institute.

Reference: S. Jaensch et al. “Hybrid CFD/ Low-Order Modeling of Nonlinear Thermoacoustic Oscillations”. In: *Proceedings of the Combustion Institute* 36 (2016). DOI: 10.1016/j.proci.2016.08.006, reproduced on page 69.

5.3 Intrinsic Thermoacoustic Instability of Premixed Flames

Abstract: The thermoacoustic stability of velocity sensitive premixed flames is investigated. A causal representation of the flow-flame-acoustic interactions reveals a flame-intrinsic feedback mechanism. The feedback loop may be described as follows: An upstream velocity disturbance induces a modulation of the heat release rate, which in turn generates an acoustic wave traveling in the upstream direction, where it influences the acoustic velocity and thus closes the feedback loop. The resonances of this feedback dynamics, which are identified as intrinsic eigenmodes of the flame, have important consequences for the dynamics and stability of the combustion process in general and the flame in particular. It is found that the amplification of acoustic power by flame-acoustic interactions can reach very high levels at frequencies close to the intrinsic eigenvalues due to the flame-internal feedback mechanism. This is shown rigorously by evaluating the ”instability potentiality” from a balance of acoustic energy fluxes across the flame. One obtains factors of maximum (as well as minimum) power amplification. Based on the acoustic energy amplification, the small gain theorem is introduced as a stability criterion for the combustion system. It allows to formulate an optimization criterion for the acoustic characteristics of burners or flames without regard of the boundary conditions offered by combustor or plenum. The concepts and methods are exemplified first with a simplistic n-τ model and then with a flame transfer function that is representative of turbulent swirl burners.

Contribution: I have developed and implemented the methods, constructed the models, performed the analysis and lead the process to compose the manuscript.

Status: Published in Combustion and Flame.

Reference: T. Emmert et al. “Intrinsic Thermoacoustic Instability of Premixed Flames”. In: *Combust. Flame* 162.1 (Jan. 2015), pp. 75–85. ISSN: 0010-2180. DOI: 10.1016/j.combustflame.2014.06.008, reproduced on page 77.

5.4 Acoustic and Intrinsic Thermoacoustic Modes of a Premixed Combustor

Abstract: Premixed flames are velocity sensitive, i.e. they react to a velocity perturbation at the burner mouth, say, with fluctuations in heat release rate. Unsteady heat release generates acoustic waves that travel back from the flame to the burner mouth, where they modulate the velocity and thereby close an intrinsic thermoacoustic (ITA) feedback loop. The present paper demonstrates that corresponding ITA eigenmodes are in general important for the dynamics and stability of premixed combustion systems. It is shown that the complete set of eigenmodes of a combustor test rig should be interpreted as the sum of acoustic and ITA eigenmodes. A procedure is presented which allows to distinguish between eigenmodes that may be considered as acoustic modes driven by the flame, versus those resulting from ITA feedback (but influenced by the acoustic properties of the combustor). This procedure is based on a factorization of the dispersion relation of the thermoacoustic model. Differences between the acoustic and intrinsic eigenmodes of a combustor test rig, in particular the corresponding mode shapes, are discussed. The paradoxical observation that increased acoustic losses at the boundaries may destabilize a combustion system is explained as an instability of the dominant ITA mode.

Contribution: I have developed the theory for the separation of acoustic and ITA modes, implemented the methods, constructed the models, performed the analysis and lead the process to compose the the manuscript.

Status: Published in Proceedings of the Combustion Institute.

Reference: T. Emmert et al. “Acoustic and Intrinsic Thermoacoustic Modes of a Premixed Combustor”. In: *36th Int’l Symposium on Combustion*. Seoul, Korea: Combustion Institute, 2016. DOI: 10.1016/j.proci.2016.08.002, reproduced on page 88.

6 Outlook

Even though there is substantial knowledge about the 1D low frequency dynamics of thermoacoustic systems, it is still subject to ongoing research. In analogy to the intrinsic feedback that was found for perfectly premixed flames, it is to be expected, that there are intrinsic eigenfrequencies associated with technically premixed flames and a feedback with the injection system. Further extending the scope, even more complex network interactions and feedbacks such as swirl fluctuations and acoustic scattering from entropy waves will need to be considered.

As the intrinsic feedback is independent of the combustion chamber geometry, there should exist similar interactions in 3D annular and canned combustors. The assumption of compact flames and velocity sensitivity is valid even for moderately low frequency azimuthal eigenmodes in annular geometries. Then the propagation of acoustic waves inside the burner tubes is still expected to be plane.

Models retrieved from FEM of 3D linearized PDEs of perturbations equations are very large but sparse. In this case, it is possible to reduce them using standard (modal) or advanced (Krylov subspace) model order reduction techniques. This is particularly useful for the computation of parameter studies, where different flame models shall be compared with respect to the same acoustic system.

It is possible to couple a 3D linear acoustic model of an annular combustor with nonlinear flame simulations. The flames may be incompressible LES simulations, whereas the acoustic model may be a model order reduced FEM model. By doing so, it could be possible to simulate the nonlinear dynamics of such systems with unprecedented numerical efficiency.

In order to further increase the computational efficiency of nonlinear flame simulations, reduced order flame models need to be constructed. One possible path would be to optimize the parameters of an under resolved LES simulation in order to match an expensive high fidelity LES. Advanced machine learning techniques like boosting and bagging [66] with multiple LES (e.g. differently anchored flames) and support vector machines, kernel PCA or neuronal networks can be applied to optimize the residuals of the low order nonlinear Flame model.

Bibliography

[1] E. Schneider et al. “Model Based Active Combustion Control Concept for Reduction of Pulsations and NOx Emissions in Lean Premixed Gas Turbine Combustors”. In: *ASME Turbo Expo 2008*. Berlin, Germany: American Society of Mechanical Engineers, 2008.

[2] S. Jaensch, C. Sovardi, and W. Polifke. “On the Robust, Flexible and Consistent Implementation of Time Domain Impedance Boundary Conditions for Compressible Flow Simulations”. In: *J. Comp. Phys.* 314 (2016), pp. 145–159. DOI: 10.1016/j.jcp.2016.03.010.

[3] M. L. Munjal. *Acoustics of Ducts and Mufflers*. Second edition. Chichester, West Sussex, United Kingdom: Wiley, 2014. 399 pp. ISBN: 978-1-118-44312-5.

[4] B. Schuermans, V. Bellucci, and C. O. Paschereit. “Thermoacoustic Modeling and Control of Multi-Burner Combustion Systems”. In: *Int’l Gas Turbine and Aeroengine Congress & Exposition*. GT2003-38688. Atlanta, GA, U.S.A.: ASME, 2003, pp. 509–519. DOI: 10.1115/GT2003-38688.

[5] M. Bothien et al. “Time Domain Modelling and Stability Analysis of Complex Thermoacoustic Systems”. In: *Proceedings of the Institution of Mechanical Engineers, Part A: Journal of Power and Energy* 221.5 (Jan. 2007), pp. 657–668. DOI: 10.1243/09576509JPE384.

[6] T. Emmert et al. “taX - a Flexible Tool for Low-Order Duct Acoustic Simulation in Time and Frequency Domain”. In: *7th Forum Acusticum*. Krakow: DEGA, Sept. 2014.

[7] A. P. Dowling. “The Calculation of Thermoacoustic Oscillation”. In: *J. of Sound and Vibration* 180 (1995), pp. 557–581.

[8] B. B. H. Schuermans, W. Polifke, and C. O. Paschereit. “Prediction of Acoustic Pressure Spectra in Combustion Systems Using Swirl Stabilized Gas Turbine Burners”. In: *Int’l Gas Turbine and Aeroengine Congress & Exposition*. ASME 2000-GT-105. Munich, Germany, 2000.

[9] S. Evesque and W. Polifke. “Low-Order Acoustic Modelling for Annular Combustors: Validation and Inclusion of Modal Coupling”. In: *Int’l Gas Turbine and Aeroengine Congress & Exposition*. ASME GT-2002-30064. Amsterdam, NL, 2002. DOI: 10.1115/GT2002-30064.

[10] M. Bauerheim et al. “An Analytical Model for Azimuthal Thermoacoustic Modes in an Annular Chamber Fed by an Annular Plenum”. In: *Combustion and Flame* 161.5 (May 2014), pp. 1374–1389. ISSN: 0010-2180. DOI: 10.1016/j.combustflame.2013.11.014.

[11] W. Polifke, J. van der Hoek, and B. Verhaar. *Everything You Always Wanted to Know about F and G*. Baden, Switzerland: Technical Report of ABB Corporate Research, 1997, p. 85.

[12] J. Lunze. *Regelungstechnik 1*. Berlin: Springer Vieweg, 2014. ISBN: 978-3-642-53908-4.

[13] R. I. Sujith. "Thermoacoustic Instabilities". In: 21st CISM-IUTAM International Summer School on Measurement, Analysis and Passive Control of Thermoacoustic Oscillations. Udine, Italy: CISM, June 29–July 3, 2015.

[14] H. Mangesius and W. Polifke. "A Discrete-Time, State-Space Approach for the Investigation of Non-Normal Effects in Thermoacoustic Systems". In: *Int. J. Spray Comb. Dynamics* 3.4 (2011), pp. 331–350.

[15] R. S. Blumenthal. "A Systems View on Non-Normal Transient Growth in Thermoacoustics". Ph.D. Thesis. Technische Universität München, 2015.

[16] C. Pankiewitz. "Hybrides Berechnungsverfahren Für Thermoakustische Instabilitäten von Mehrbrennersystemen". PhD Thesis. TU München, 2004.

[17] L. Benoit. "Prediction Des Instabilites Thermoacoustiques Dans Les Turbines a Gaz". 2005.

[18] F. Nicoud et al. "Acoustic Modes in Combustors with Complex Impedances and Multidimensional Active Flames". In: *AIAA Journal* 45.2 (2007), pp. 426–441.

[19] J. Gikadi. "Prediction of Acoustic Modes in Combustors Using Linearized Navier-Stokes Equations in Frequency Space". PhD Thesis. Garching, Germany: Technische Universität München, Nov. 8, 2013. 156 pp.

[20] M. Schulze and T. Sattelmayer. "Frequency Domain Simulations for the Determination of Liner Effects on Longitudinal Wave Propagation". In: *International Journal of Aeroacoustics* 14 (7-8 2015), pp. 1025–1047.

[21] T. Hummel et al. "Reduced-Order Modeling of Transversal and Non-Compact Combustion Dynamics". In: *ICSV 22*. International Congress of Sound and Vibration 22. July 2015.

[22] M. Meindl, T. Emmert, and W. Polifke. "Efficient Calculation of Thermoacoustic Modes Utilizing State-Space Models". In: *23nd Int. Congress on Sound and Vibration (ICSV23)*. Athens, Greece, 2016.

[23] A. Castagnotto et al. "Analyse und Reduktion dynamischer Systeme sehr hoher Ordnung". Poster. Matlab Expo 2016. München, 5/10/16.

[24] A. Huber and W. Polifke. "Dynamics of Practical Premix Flames, Part II: Identification and Interpretation of CFD Data". In: *Int. J. Spray Comb. Dynamics*. 2nd ser. 1 (2009), pp. 229–250. DOI: 10.1260/175682709788707440.

[25] A. Huber and W. Polifke. "Dynamics of Practical Premix Flames, Part I: Model Structure and Identification". In: *Int. J. Spray Comb. Dynamics*. 2nd ser. 1 (2009), pp. 199–229. DOI: 10.1260/175682709788707431.

[26] S. Föller and W. Polifke. "Identification of Aero-Acoustic Scattering Matrices from Large Eddy Simulation: Application to a Sudden Area Expansion of a Duct". In: *Journal of Sound and Vibration* 331.13 (June 2012), pp. 3096–3113. ISSN: 8928916216. DOI: http://dx.doi.org/10.1016/j.jsv.2012.01.004.

[27] L. Tay-Wo-Chong et al. “Comparative Validation Study on Identification of Premixed Flame Transfer Function”. In: *Journal of Engineering for Gas Turbines and Power* 134.2 (2012), pp. 021502–1–8. DOI: 10.1115/1.4004183.

[28] W. Polifke. “Black-Box System Identification for Reduced Order Model Construction”. In: *Annals of Nuclear Energy*. Advanced stability analysis for nuclear reactors 67C (May 2014), pp. 109–128. ISSN: 0306-4549. DOI: 10.1016/j.anucene.2013.10.037.

[29] T. Emmert et al. “Linear State Space Interconnect Modeling of Acoustic Systems”. In: *Acta Acustica united with Acustica* 102.5 (2016), pp. 824–833. DOI: 10.3813/AAA.918997.

[30] I. The MathWorks. *Control System Toolbox - MATLAB - MathWorks Deutschland*. 2016. URL: http://de.mathworks.com/products/control/ (visited on 05/19/2016).

[31] J. W. Eaton et al. *GNU Octave*. 2015. URL: http://www.octave.org (visited on 05/19/2016).

[32] R. Lehoucq, D. Sorensen, and C. Yang. *ARPACK Users' Guide*. Software, Environments and Tools. Society for Industrial and Applied Mathematics, Jan. 1, 1998. 150 pp. ISBN: 978-0-89871-407-4.

[33] P. R. Amestoy et al. “MUMPS: A General Purpose Distributed Memory Sparse Solver”. In: *Applied Parallel Computing. New Paradigms for HPC in Industry and Academia*. Ed. by T. Sørevik et al. Lecture Notes in Computer Science 1947. Springer Berlin Heidelberg, June 18, 2000, pp. 121–130. ISBN: 978-3-540-41729-3 978-3-540-70734-9. DOI: 10.1007/3-540-70734-4_16.

[34] A. M. Lyapunov. *General Problem of the Stability Of Motion*. In collab. with A. T. Fuller. London ; Washington, DC: Tayor & Francis, Aug. 28, 1992. 270 pp. ISBN: 0-7484-0062-1 978-0-7484-0062-1.

[35] T. Emmert, S. Bomberg, and W. Polifke. “Intrinsic Thermoacoustic Instability of Premixed Flames”. In: *Combust. Flame* 162.1 (Jan. 2015), pp. 75–85. ISSN: 0010-2180. DOI: 10.1016/j.combustflame.2014.06.008.

[36] L. N. Trefethen et al. “Hydrodynamic Stability Without Eigenvalues”. In: *Science* 261 (July 1993), pp. 578–584.

[37] P. J. Schmid. “Nonmodal Stability Theory”. In: *Annu. Rev. Fluid Mech.* 39 (2007), pp. 129–62.

[38] T. Gebhardt and S. Grossmann. “Chaos Transition despite Linear Stability”. In: *J. Fluid Mech Phys Rev E* 50 (1993), p. 3705.

[39] K. Takaba, N. Morihira, and T. Katayama. “A Generalized Lyapunov Theorem for Descriptor System”. In: *Systems & Control Letters* 24.1 (Jan. 9, 1995), pp. 49–51. ISSN: 0167-6911. DOI: 10.1016/0167-6911(94)00041-S.

[40] B. T. Chu. “On the Energy Transfer to Small Disturbances in Fluid Flow (Part 1)”. In: *Acta Mechanica* 1.3 (1965), pp. 215–234.

[41] R. H. Cantrell and R. W. Hart. “Interaction between Sound and Flow in Acoustic Cavities: Mass, Momentum, and Energy Considerations”. In: *The Journal of the Acoustical Society of America* 36.4 (Apr. 1, 1964), pp. 697–706. ISSN: 0001-4966. DOI: 10.1121/1.1919047.

[42] C. L. Morfey. “Acoustic Energy in Non-Uniform Flows”. In: *J. Sound Vib.* 14.2 (Jan. 1971), pp. 159–170. ISSN: 0022460X. DOI: 10.1016/0022-460X(71)90381-6.

[43] M. Myers. “Transport of Energy by Disturbances in Arbitrary Steady Flows”. In: *Journal of Fluid Mechanics* 226 (1991), pp. 383–400.

[44] A. Giauque et al. “Budget of Disturbance Energy in Gaseous Reacting Flows”. In: *Proc of the Summer Program*. Stanford, CA, USA: Center for Turbulence Research, NASA Ames/Stanford Univ., 2006, pp. 285–297.

[45] M. J. Brear et al. “Disturbance Energy Transport and Sound Production in Gaseous Combustion”. In: *Journal of Fluid Mechanics* 707 (July 12, 2012), pp. 53–73. ISSN: 0022-1120, 1469-7645. DOI: 10.1017/jfm.2012.264.

[46] K. J. George and R. Sujith. “Disturbance Energy Norms: A Critical Analysis”. In: *Journal of Sound and Vibration* 331.7 (2012), pp. 1552–1566. ISSN: 0022-460X. DOI: 10.1016/j.jsv.2011.11.027.

[47] R. S. Blumenthal et al. “A Systems Perspective on Non-Normality in Low-Order Thermoacoustic Models: Full Norms, Semi-Norms and Transient Growth”. In: *Int. J. Spray Combust. Dyn.* (Aug. 2016). Published online Aug 5th 2016. DOI: 10.1177/1756827716652474.

[48] R. Ortega et al. *Passivity-Based Control of Euler-Lagrange Systems: Mechanical, Electrical and Electromechanical Applications*. Springer Science & Business Media, June 29, 2013. 560 pp. ISBN: 978-1-4471-3603-3.

[49] G. Zames. “On the Input-Output Stability of Time-Varying Nonlinear Feedback Systems Part One: Conditions Derived Using Concepts of Loop Gain, Conicity, and Positivity”. In: *Automatic Control, IEEE Transactions on* 11.2 (1966), pp. 228–238. DOI: 10.1109/TAC.1966.1098316.

[50] H. Nyquist. “Regeneration Theory”. In: *Bell System Technical Journal* (1932), pp. 1–24.

[51] Y. Aurégan and R. Starobinski. “Determination of Acoustical Energy Dissipation/Production Potentiality from the Acoustical Transfer Functions of a Multiport”. In: *Acta Acustica united with Acustica* 85.6 (1999), pp. 788–792.

[52] W. Polifke. “Thermo-Acoustic Instability Potentiality of a Premix Burner”. In: *European Combustion Meeting, ECM2011*. ECM2011. Cardiff, UK: British Section of the Comb. Inst., July 2011.

[53] M. Hoeijmakers et al. “Flames in Context of Thermo-Acoustic Stability Bounds”. In: *Proc. Combust. Inst.* 35.1 (2015), pp. 1073–1078. ISSN: 1540-7489. DOI: 10.1016/j.proci.2014.06.059.

[54] A. Gentemann and W. Polifke. “Scattering and Generation of Acoustic Energy by a Premix Swirl Burner”. In: *Int’l Gas Turbine and Aeroengine Congress & Exposition*. ASME GT2007-27238. Montreal, Quebec, Canada, 2007.

[55] S. Bomberg, T. Emmert, and W. Polifke. “Thermal Versus Acoustic Response of Velocity Sensitive Premixed Flames”. In: *Proc. Comb. Inst.* 35 (3) (2015), pp. 3185–3192. DOI: 10.1016/j.proci.2014.07.032.

[56] E. Courtine, L. Selle, and T. Poinsot. “DNS of Intrinsic Thermoacoustic Modes in Laminar Premixed Flames”. In: *Combust. Flame* 162.11 (2015), pp. 4331–4341. DOI: 10.1016/j.combustflame.2015.07.002.

[57] M. Hoeijmakers et al. “Intrinsic Instability of Flame-Acoustic Coupling”. In: *Combust. Flame* 161.11 (Nov. 2014), pp. 2860–2867. DOI: 10.1016/j.combustflame.2014.05.009.

[58] C. F. Silva et al. “Numerical Study on Intrinsic Thermoacoustic Instability of a Laminar Premixed Flame”. In: *Combust. Flame* 162.9 (2015), pp. 3370–3378. ISSN: 0010-2180. DOI: 10.1016/j.combustflame.2015.06.003.

[59] T. Emmert et al. “Acoustic and Intrinsic Thermoacoustic Modes of a Premixed Combustor”. In: *36th Int’l Symposium on Combustion*. Seoul, Korea: Combustion Institute, 2016. DOI: 10.1016/j.proci.2016.08.002.

[60] R. Kaess et al. “CFD-Based Mapping of the Thermo-Acoustic Stability of a Laminar Premix Burner”. In: *Proceedings of the 2008 Summer Program*. Stanford, USA: Stanford Univ., Center for Turbulence Research, 2008, pp. 289–302.

[61] T. Komarek and W. Polifke. “Impact of Swirl Fluctuations on the Flame Response of a Perfectly Premixed Swirl Burner”. In: *Journal of Engineering for Gas Turbines and Power* 132.6 (June 2010), pp. 061503–1, 7. DOI: 10.1115/1.4000127.

[62] P. R. Alemela et al. “Flame Transfer Matrices of a Premixed Flame and a Global Check with Modelling and Experiments”. In: Proc. of ASME Turbo Expo 2008 Power for Land, Sea and Air. ASME, 2008, pp. 9–9.

[63] B. T. Chu. “On the Generation of Pressure Waves at a Plane Flame Front”. In: *4th Symposium (International) on Combustion*. Vol. 4. Cambridge, Massachusetts, USA: Combustion Institute, 1953, pp. 603–612. DOI: 10.1016/S0082-0784(53)80081-0.

[64] L. Tay-Wo-Chong et al. “LES-Based Identification of the Dependence of Premix Flame Dynamics on Swirler Position”. In: *EFMC-8 (8th European Fluid Mechanics Conference)*. Bad Reichenhall, Germany, Sept. 13–16, 2010.

[65] S. Jaensch et al. “Hybrid CFD/ Low-Order Modeling of Nonlinear Thermoacoustic Oscillations”. In: *Proceedings of the Combustion Institute* 36 (2016). DOI: 10.1016/j.proci.2016.08.006.

[66] K. P. Murphy. *Machine Learning: A Probabilistic Perspective*. MIT Press, Aug. 24, 2012. 1098 pp. ISBN: 978-0-262-01802-9.

List of Figures

List of Tables

Reproduction of Papers

Acta Acustica united with Acustica
Vol. 98 (2016)

Linear State Space Network Modeling of Acoustic Systems

Thomas Emmert, Max Meindl, Stefan Jaensch, Wolfgang Polifke
Professur für Thermofluiddynamik, Technische Universität München, D-85747, Garching, Germany
emmert@tfd.mw.tum.de

Summary
Linear acoustic network models are a state of the art tool to cope with the complexity of large acoustic systems. Such systems are composed by a set of interconnected acoustic subsystems. We introduce a generalized linear modeling framework for acoustic systems that is based on a state space formalism and linear system theory. In order to enable the modeling of large acoustic network systems, the framework is taking into account the sparse structure of acoustic models. It is shown how acoustic models retrieved from 1D low order modeling, 3D linearized perturbation equations as well as computational fluid dynamics or experimental data can be translated into state space models. This translation does not involve any approximations beyond those made by the acoustic modeling in the first place. An algorithm to evaluate the interconnection of state space models is presented, which results in one single state space model for the connected acoustic network system. In order to compute the eigenvalues and vectors of a state space model, a standard or generalized linear eigenvalue problem needs to be solved. For large acoustic systems an efficient iterative eigenvalue solver is required. The methods are validated by the comparison of eigenmodes of a generic annular combustor test case with non trivial topology.

PACS no. 43 ...

Nomenclature

PDE	Partial differential equation	
CWA	Characteristic wave amplitude	
f	Downstream traveling CWA	$\mathrm{m\,s^{-1}}$
g	Upstream traveling CWA	$\mathrm{m\,s^{-1}}$
p'	Acoustic pressure fluctuation	$\mathrm{m\,s^{-1}}$
u'	Acoustic velocity fluctuation	$\mathrm{m\,s^{-1}}$
s	Laplace variable $(= j\omega + \sigma)$	$\mathrm{rad\,s^{-1}}$
ω	Frequency	$\mathrm{rad\,s^{-1}}$
σ	Growth rate	$\mathrm{rad\,s^{-1}}$
A	System matrix	
B	Input matrix	
C	Output matrix	
D	Feed through matrix	
E	Mass/Descriptor matrix	
F	Feedback matrix	
x	State vector	
u	Input vector	
y	Output vector	

Received 31 January 2016,
accepted 31 January 2016.

1. Introduction

Prediction and optimization of generation, propagation and attenuation of sound and aero- and thermoacoustic stability, is an important objective in the development of many applications like gas turbines or HVAC systems. Typically such systems are of considerable spatial extent but involve small scale phenomena like turbulence or combustion. This causes a need for very detailed models with complex physics in large domains. Therefore the simulation of models derived from first principles is very expensive even though the propagation of acoustic waves may still be modeled linear.

A strategy to cope with this modeling complexity is to divide the entire system into several interconnected parts. Linear models of the acoustic dynamics of the different parts of the system are retrieved using suitable methods according to complexity and physical phenomena involved. In the simplest case, there are low order models assuming 1D plane wave propagation, which may be solved analytically. Such models are either algebraic relations due to acoustically compact discontinuities in area and temperature or (linear) Green's functions of ducts [1, 2]. If the propagation of acoustic waves is not one dimensional, but

Acta Acustica united with Acustica
Vol. 98 (2016)

the mean flow is still unaffected by acoustic perturbations, CAA tools can be used to retrieve acoustic models of the domain. Such tools model the acoustic dynamics by 2D or 3D linearized partial differential equations (e.g. Helmholtz, LEE, APE, LNSE) against the background of a given mean field [3, 4]. In case of two way interactions between mean flow and acoustic perturbations, a full LES computation or an experiment are needed. Linearized models of the acoustic dynamics are then inferred from time series data by system identification [5] or fitting polynomials to the frequency responses of the system.

The resulting set of interconnected linear models may be called a linear acoustic network model. Such network models are state of the art and have proven to predict the dynamics of acoustic systems. Typically those models are either coupled in time domain and simultaneously but segregatedly simulated [6] or in frequency domain by individual evaluation and multiplicative coupling [7–11].

Here we present the application of linear system theory and unified state space modeling to acoustic network systems. The generic state space structure enables us to incorporate models of varying modeling depth. This comprises 1D low order models as well as models retrieved from linearized PDEs on complex geometries or even data driven models from LES or experiments. In addition, multi physics modeling is easily incorporated in the framework by means of for example flame transfer functions for combustion processes or active control. As we will show, the state space modeling is numerically very efficient as it is based on matrices with constant, frequency independent coefficients. Therefore the search for eigenvalues is a standard or generalized linear eigenvalue problem. For small models, it is possible to directly solve for all eigenvalues. The efficient computation of eigenvalues of large models requires an iterative algorithm.

The concept is introduced using a minimal example of the 1D scattering matrix of a duct section. Subsequently we show how all kinds of linear acoustic models can be translated into state space formulation. This translation does not involve any approximation beyond those already made by the linear acoustic modeling. All methods and algorithms are publicly available by a (thermo-) acoustic network modeling framework called taX [12].

Based on the unified modeling, we demonstrate an algorithm for the interconnection of state space models, which results in a single joint state space model. Similar algorithms are implemented by Matlab and Octave control toolboxes. In contrast to those, our implementation takes advantage of the sparse structure of acoustic models, which makes possible the solution of very large acoustic network systems. The concept is illustrated using a minimal example of two duct sections. Subsequently, a generalized state space model interconnection algorithm is presented.

As the resulting interconnected network model is again a state space model, the eigenvalues and vectors can be determined by solving a standard or generalized linear eigenvalue problem. We present a memory and time efficient iterative eigenvalue solver based on a direct method for the LU decomposition [13] and an Arnoldi algorithm [14].

Eventually the modeling strategy developed is applied to a cavity problem, where two cylinders are connected by multiple tubes. The cylinders are modeled using 3D linearized PDEs, whereas the ducts are modeled by a low order 1D model. Results are validated with a CAA model where the entire system including the ducts is modeled by linearized PDEs.

2. State Space Modeling

Acoustic network systems are composed of interconnected subsystems called elements. These individual subsystems are modeling internal sources of acoustic waves and how incident waves are transmitted and reflected in between its interfaces. Sources of acoustic waves are for example aero- acoustic noise due to turbulence or actuators like loudspeakers.

We are assuming that on the interfaces between the subsystems only plane waves are propagating, whereas inside of the subsystems arbitrary e.g. 3D wave propagation is possible. This assumption is valid if the wave length of the highest frequency of interest is large compared to the diameter of the interface.

The models that describe the scattering of acoustic waves are typically characterized by frequency responses of the scattering matrix or transfer matrix. The scattering matrix is relating incident and emitted characteristic wave amplitudes, whereas the transfer matrix is relating pressure and velocity perturbation amplitudes at the different interfaces of the system. It is important to note that in system theory one distinguishes the frequency responses from the subsystem models. Frequency responses are not models but rather the results of the models evaluated at discrete frequencies. Linear dynamic models are described by a set of ordinary differential equations relating inputs u (e.g. incident acoustic waves) and outputs y (emitted acoustic waves). They are given either by high order one dimensional transfer functions:

$$b_0 y(t) + b_1 \dot{y}(t) + b_2 \ddot{y}(t) + \ldots + b_m \frac{\partial^m y(t)}{\partial t^m} = a_0 u(t) + a_1 \dot{u}(t) + a_2 \ddot{u}(t) + \ldots + a_n \frac{\partial^n u(t)}{\partial t^n}\,, \tag{1}$$

or as a generic high dimensional first order state space system:

$$\dot{x} = Ax + Bu \tag{2}$$

$$y = Cx + Du\,. \tag{3}$$

In the following sections we show how linear acoustic subsystem models ("elements") from different

ACTA ACUSTICA UNITED WITH ACUSTICA
Vol. 98 (2016)

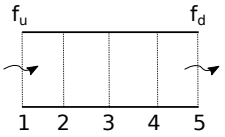

Figure 1. Discretized duct section.

sources can be translated into a state space formulation. At first, a minimal example of a 1D duct is provided in order to motivate and introduce the state space models. Following this, we generalize the result to models retrieved from linearized PDEs. Subsequently, we indicate how state space models are retrieved from experimental or LES data.

Eventually, an algorithm to compute the eigenvalues of large sparse state space systems is presented.

2.1. Minimal Example 1D SS Duct Model

Acoustic wave propagation in a duct is in the simplest case governed by a 1D Helmholtz equation

$$\frac{1}{c^2}\frac{\partial^2 p'}{\partial t^2} = \frac{\partial^2 p'}{\partial x^2}\,. \tag{4}$$

The solution can be written as the superposition of characteristic waves

$$\frac{p'(x,t)}{\rho c} = f\left(t-\frac{x}{c}\right)+g\left(t+\frac{x}{c}\right)\;;\; u' = f-g\,. \tag{5}$$

The propagation of the characterisic wave amplitudes f and g is described by an advection equation

$$\frac{\partial f}{\partial t} = \frac{1}{c}\frac{\partial f}{\partial x} \quad ; \quad \frac{\partial g}{\partial t} = -\frac{1}{c}\frac{\partial g}{\partial x} \tag{6}$$

The Laplace transform of the analytic solution of the spatial integral over a duct of length L with non-reflecting boundary conditions is known as the scattering matrix

$$\begin{bmatrix} g_u(s) \\ f_d(s) \end{bmatrix} = \underbrace{\begin{bmatrix} 0 & e^{-s\tau} \\ e^{-s\tau} & 0 \end{bmatrix}}_{\text{Scattering matrix } S(s)} \begin{bmatrix} f_u(s) \\ g_d(s) \end{bmatrix}. \tag{7}$$

During time $\tau = L/c$, the waves travel through the duct. The formulation is using the Laplace variable $s = j\omega + \sigma$ with the angular frequency ω and growth rate σ.

Instead of analytically integrating the propagation of the characteristic waves, we can spatially discretize the PDE with a first order upwind scheme to obtain an ordinary differential equation (ODE)

$$\frac{df_j}{dt} = c\frac{f_j - f_{j-1}}{\Delta x}\,. \tag{8}$$

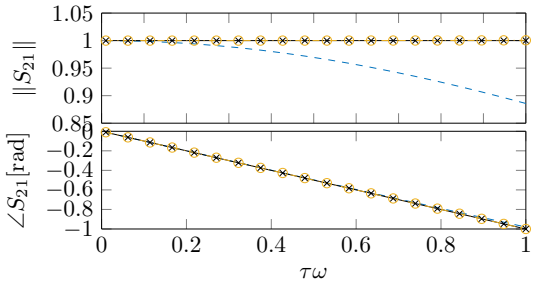

Figure 2. Frequency response of f_u to f_d: First order upwind (- - -), third order upwind (-⊖-) and analytic solution (—×—) .

For simplicity, we choose $\Delta x = L/4$. With $a \equiv c/\Delta x$ the propagation of f waves in the duct section is described by a system of ODEs

$$\frac{d}{dt}\begin{bmatrix} f_2 \\ f_3 \\ f_4 \\ f_5 \end{bmatrix} = \begin{bmatrix} a & 0 & 0 & 0 \\ -a & a & 0 & 0 \\ 0 & -a & a & 0 \\ 0 & 0 & -a & a \end{bmatrix}\begin{bmatrix} f_2 \\ f_3 \\ f_4 \\ f_5 \end{bmatrix} + \begin{bmatrix} -a \\ 0 \\ 0 \\ 0 \end{bmatrix}\begin{bmatrix} f_u \end{bmatrix} \tag{9}$$
$$\begin{bmatrix} f_d \end{bmatrix} = \begin{bmatrix} 0 & 0 & 0 & 1 \end{bmatrix} x + \begin{bmatrix} 0 \end{bmatrix} f_u\,.$$

The wave amplitudes f_j at the positions j inside the duct and on its interfaces are collected in a state vector $x = \begin{bmatrix} f_2 & f_3 & f_4 & f_5 \end{bmatrix}^T$. The wave at the left boundary is an input $u = f_u = f_1$ to the system and is not part of the acoustic state, whereas the wave leaving on the right boundary is an output $y = f_d = f_5$ and a state. The same derivation can be done for the g waves and block diagonal appending leads to a generalized state space model

$$\dot{x} = Ax + Bu \tag{10}$$
$$y = Cx + Du \tag{11}$$

with inputs $u = \begin{bmatrix} f_u & g_d \end{bmatrix}^T$, outputs $y = \begin{bmatrix} g_u & f_d \end{bmatrix}^T$ and without feed through $D = 0$. Laplace transform is used to solve the model for its scattering matrix $S(s)$

$$y = \underbrace{C(sI - A)^{-1}B}_{S(s)}\, u \tag{12}$$

with I the identity matrix.

Figure 2 shows the frequency responses of the analytical (—×—) and the first order upwind (- - -) state space models. In addition, a state space duct model resulting from third order upwind discretization with the same resolution $\Delta x = L/4$ is displayed (-⊖-). We observe that all three models have the same low frequency properties. The damping of the first order upwind model increases for high frequencies, whereas the third order model is matching the analytical model very well within the given frequency range. By increasing the spatial resolution, the discretized models approach the analytical solution for yet higher frequencies.

Acta Acustica united with Acustica
Vol. 98 (2016)

2.2. Generalization to Linearized Fields of Perturbation Equations

Instead of modeling acoustic propagation by 1D Helmholtz equations as in the previous section, various 2D or 3D linearized PDEs (LEE, LNSE, APE, reactive LNSE) may be considered. This gives the opportunity to incorporate complex geometry, the effects of mean flow, dissipation and even acoustic-vortex interaction with all its advantages and issues [15]. As demonstrated above, the partial differential equation may be spatially discretized using a finite volume or finite element method, which results in a system of ordinary differential equations. On the interfaces, boundary conditions need to be implemented, which excite and receive plane waves. This is achieved by averaging across the surface of the interface and to excite for instance either p' or the incident wave and to measure the remaining free variable u' or the outgoing wave. Depending on the discretization scheme, the translation to state space formulation may require a so called mass or descriptor matrix E:

$$\begin{aligned} E\dot{x} &= Ax + Bu \\ y &= Cx + Du\,. \end{aligned} \tag{13}$$

However this translation to state space formulation is achieved just by a rearrangement of the system of equations. Most notably it does not introduce any approximation other than the ones made by choosing the type of PDE and the discretization scheme.

As the relation between the states x and the field variables on the computational grid are known, the state vector of such models may be interpreted physically and visualized.

The procedure of defining the perturbation equations, geometry, boundary conditions, grid and discretization scheme may be supported by tools like freeFEM or COMSOL Multiphysics. COMSOL is facilitating the process by providing a default set of LEE and LNSE equations, as well as an export interface to directly obtain the state space matrices A, B, C, D, E.

Note that there are alternative methods to create state space systems from the eigenmodes of a linearized field system [16, 17]. However this method is a reduced order approximation of the original field based system, whereas the direct method presented above is not.

2.3. Application to Experimental and LES Data

Instead of deriving acoustic models directly from linearized PDEs, they may be given in form of scattering or transfer matrices. Such models may for instance be derived from experiment using the multi-microphone method. Typically harmonic excitation is used and the time series of acoustic waves up- and downstream of the system are measured. Subsequently, polynomials are fitted to the measured frequency response [11].

When carrying out LES computations, it is more convenient to excite the system with broadband acoustic perturbations, as this reduces the necessary computational time compared to harmonic forcing [5]. Discrete time models are inferred by system identification from the input and output time series of the system. Eventually, the discrete time models can be transformed to continuous time.

For a system with two interfaces (upstream, downstream) this is expressed by either the scattering matrix S or the transfer matrix T

$$\begin{bmatrix} g_u(s) \\ f_d(s) \end{bmatrix} = \begin{bmatrix} S_{11}(s) & S_{12}(s) \\ S_{21}(s) & S_{22}(s) \end{bmatrix} \begin{bmatrix} f_u(s) \\ g_d(s) \end{bmatrix} \tag{14}$$

$$\begin{bmatrix} p'_u(s) \\ u'_u(s) \end{bmatrix} = \begin{bmatrix} T_{11}(s) & T_{12}(s) \\ T_{21}(s) & T_{22}(s) \end{bmatrix} \begin{bmatrix} p'_d(s) \\ u'_d(s) \end{bmatrix}\,. \tag{15}$$

In this case, the transfer functions $G = S_{ij}, T_{ij}$ between either incident, emitted waves or pressure, velocity perturbations at the interfaces of the system are known. In general, each transfer function $G(s)$ may be represented as a rational polynomial in s, which relates the corresponding input variable u and the output y:

$$y(s) = G(s)u(s)\,; \tag{16}$$

$$G(s) = \frac{b_n s^n + \ldots + b_1 s + b_0}{s^m + a_{m-1}s^{m-1} + \ldots + a_1 s + a_0}\,, \tag{17}$$

and corresponds to a linear differential equation in time:

$$\begin{aligned} \frac{d^m y(t)}{dt^m} + a_{m-1}\frac{d^{m-1}y(t)}{dt^{m-1}} + \ldots + a_1\dot{y}(t) + a_0 y(t) = \\ b_n\frac{d^n u(t)}{dt^n} + \ldots + b_1\dot{u}(t) + b_0 u(t)\,. \end{aligned} \tag{18}$$

All transfer functions $G(s)$ can be translated into state space models (Eq. (25) in [18], [19]):

$$\dot{x} = \begin{bmatrix} 0 & 1 & & \\ & \ddots & \ddots & \\ & & 0 & 1 \\ -a_0 & -a_1 & \ldots & -a_{m-1} \end{bmatrix} x + \begin{bmatrix} 0 \\ \vdots \\ 0 \\ 1 \end{bmatrix} u \tag{19}$$

$$y = \begin{bmatrix} b_0 - b_n a_0,\ b_1 - b_n a_1,\ \ldots,\ b_{n-1} - b_n a_{m-1} \end{bmatrix} x + b_n u\,.$$

However, compared with the linearized PDE based models, these state space models do not establish a direct relation between acoustic perturbations inside the domain and the state x of the model. Therefore the state vector of such models cannot be physically interpreted or visualized.

2.4. Computation of Eigenvalues

The eigenvalues and vectors of a state space system are computed by Laplace transformation of the system equation (13). Depending on whether $E = I$ or not, a standard or generalized eigenvalue problem

$$sEx = Ax \tag{20}$$

ACTA ACUSTICA UNITED WITH ACUSTICA
Vol. 98 (2016)

needs to be solved. The procedure to do so for large, sparse systems is the shift and invert method in combination with an Arnoldi algorithm. It involves an LU decomposition of the matrix pencil $A - s_o E$ at a shift frequency s_o. As this decomposition involves just constant coefficients, it needs to be performed only once. This is a fundamental difference compared to other acoustic network codes, where the system matrices are functions of the frequency. Subsequently the implicitly restarted Arnoldi method (IRAM) is executed using arpack [14] in order to retrieve eigenvalues and vectors close the the shift frequency. The LU decomposition is the bottleneck of the computation. Therefore we perform this decomposition using the MUMPS algorithm [13], which is very efficient for large sparse systems resulting from the FEM discretization of linearized PDEs.

The computation of five eigenvalues around one shift frequency for the model in section 4 of order 10×10^5 takes about 38 s and 1.5 GB of RAM on a workstation. For comparison, the Matlab eigs() command is more than 6.5 times slower (248 s) and needs 4.3 times more ram (6.5 GB). The same computation for the full model in section 4 of order 15×10^5 takes about 180 s and 4.2 GB of RAM whereas the Matlab eigs() command takes more than 28 GB and runs out of memory after 15 min.

3. Interconnection of Acoustic Network Models

As shown in the previous section, duct acoustic systems can be modeled by a set of interconnected state space models. In this section we will demonstrate how the interconnections of the state space models can be evaluated to retrieve one joint state space model. Such algorithms are provided by the control toolboxes of Matlab and Octave. Both are based on full matrices, which restricts them to small systems due to memory restrictions. Therefore we have re-implemented the functionality in a sparse state space toolbox, which is able to exploit the sparse structure of acoustic network systems and is part of tax [12].

3.1. Minimal Example Connection of Two Duct Sections

In order to motivate and illustrate the algorithm to connect two state space models, the previous minimal example is revisited. We demonstrate the interconnection of two identical duct sections of half the length $L' = L/2$ of the minimal example as depicted in Fig. 3. At first, the analytical solution and then the state space connection are shown.

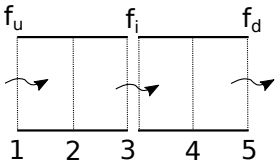

Figure 3. Connected duct sections.

The analytic solution for the scattering matrices of the two duct sections are according to Eq. (7)

$$\begin{bmatrix} g_u(s) \\ f_i(s) \end{bmatrix} = \begin{bmatrix} 0 & e^{-s\tau/2} \\ e^{-s\tau/2} & 0 \end{bmatrix} \begin{bmatrix} f_u(s) \\ g_i(s) \end{bmatrix}; \tag{21}$$

$$\begin{bmatrix} g_i(s) \\ f_d(s) \end{bmatrix} = \begin{bmatrix} 0 & e^{-s\tau/2} \\ e^{-s\tau/2} & 0 \end{bmatrix} \begin{bmatrix} f_i(s) \\ g_d(s) \end{bmatrix} \tag{22}$$

with the intermediate state i. The system of equations needs to be solved for the input output dynamics between upstream and downstream position, by eliminating the internal state. This is achieved by a linear fractional transformation called the Redheffer star product [20]:

$$S = S_u \star S_d \,. \tag{23}$$

The resulting scattering matrix in the special case of connected ducts with zeros on the diagonal entries

$$\begin{bmatrix} g_u(s) \\ f_d(s) \end{bmatrix} = \begin{bmatrix} 0 & e^{-s\tau} \\ e^{-s\tau} & 0 \end{bmatrix} \begin{bmatrix} f_u(s) \\ g_d(s) \end{bmatrix} \tag{24}$$

is exactly the same as the one for the original minimal example in Eq. (7).

Now the interconnection of state space models is considered. The coefficients of the f-wave propagation of the two discretized duct section state space models are identical:

$$\frac{\partial}{\partial t} \begin{bmatrix} f_2 \\ f_3 \end{bmatrix} = \begin{bmatrix} a & 0 \\ -a & a \end{bmatrix} \begin{bmatrix} f_2 \\ f_3 \end{bmatrix} + \begin{bmatrix} -a \\ 0 \end{bmatrix} \begin{bmatrix} f_u \end{bmatrix} \tag{25}$$

$$\begin{bmatrix} f_i \end{bmatrix} = \begin{bmatrix} 0 & 1 \end{bmatrix} \begin{bmatrix} f_2 \\ f_3 \end{bmatrix} + \begin{bmatrix} 0 \end{bmatrix} f_u \tag{26}$$

$$\frac{\partial}{\partial t} \begin{bmatrix} f_4 \\ f_5 \end{bmatrix} = \begin{bmatrix} a & 0 \\ -a & a \end{bmatrix} \begin{bmatrix} f_4 \\ f_5 \end{bmatrix} + \begin{bmatrix} -a \\ 0 \end{bmatrix} \begin{bmatrix} f_i \end{bmatrix} \tag{27}$$

$$\begin{bmatrix} f_d \end{bmatrix} = \begin{bmatrix} 0 & 1 \end{bmatrix} \begin{bmatrix} f_4 \\ f_5 \end{bmatrix} + \begin{bmatrix} 0 \end{bmatrix} f_i \,. \tag{28}$$

We can block diagonally append the two systems

$$\frac{\partial}{\partial t} \begin{bmatrix} f_2 \\ f_3 \\ f_4 \\ f_5 \end{bmatrix} = \begin{bmatrix} a & 0 & 0 & 0 \\ -a & a & 0 & 0 \\ 0 & 0 & a & 0 \\ 0 & 0 & -a & a \end{bmatrix} \begin{bmatrix} f_2 \\ f_3 \\ f_4 \\ f_5 \end{bmatrix} + \begin{bmatrix} -a & 0 \\ 0 & 0 \\ 0 & -a \\ 0 & 0 \end{bmatrix} \begin{bmatrix} f_u \\ f_i \end{bmatrix} \tag{29}$$

$$\begin{bmatrix} f_i \\ f_d \end{bmatrix} = \begin{bmatrix} 0 & 1 & 0 & 0 \\ 0 & 0 & 0 & 1 \end{bmatrix} \begin{bmatrix} f_2 \\ f_3 \\ f_4 \\ f_5 \end{bmatrix} + \begin{bmatrix} 0 \end{bmatrix} f_u \tag{30}$$

ACTA ACUSTICA UNITED WITH ACUSTICA
Vol. 98 (2016)

and the intermediate f_i wave appears as an input and as well as an output of the appended system. This feedback can be eliminated by substituting f_i by the output equation in the input vector:

$$\begin{bmatrix} -a & 0 \\ 0 & 0 \\ 0 & -a \\ 0 & 0 \end{bmatrix} \begin{bmatrix} f_u \\ f_i \end{bmatrix} = \begin{bmatrix} -a \\ 0 \\ 0 \\ 0 \end{bmatrix} \begin{bmatrix} f_u \end{bmatrix} + \begin{bmatrix} 0 \\ 0 \\ -a \\ 0 \end{bmatrix} \begin{bmatrix} 0 & 1 & 0 & 0 \end{bmatrix} \begin{bmatrix} f_2 \\ f_3 \\ f_4 \\ f_5 \end{bmatrix} \quad (31)$$

Eventually, by dropping the internal output f_i and merging the system matrix A with the result of the feedback, the exactly same state space system as for the minimal example in Eq. (10) is obtained:

$$\frac{\partial}{\partial t} \begin{bmatrix} f_2 \\ f_3 \\ f_4 \\ f_5 \end{bmatrix} = \begin{bmatrix} a & 0 & 0 & 0 \\ -a & a & 0 & 0 \\ 0 & -a & a & 0 \\ 0 & 0 & -a & a \end{bmatrix} \begin{bmatrix} f_2 \\ f_3 \\ f_4 \\ f_5 \end{bmatrix} + \begin{bmatrix} -a \\ 0 \\ 0 \\ 0 \end{bmatrix} \begin{bmatrix} f_u \end{bmatrix} \quad (32)$$

$$\begin{bmatrix} f_d \end{bmatrix} = \begin{bmatrix} 0 & 0 & 0 & 1 \end{bmatrix} \begin{bmatrix} f_2 \\ f_3 \\ f_4 \\ f_5 \end{bmatrix} + \begin{bmatrix} 0 \end{bmatrix} f_u$$

This way to solve for the interconnected state space model can be generalized to arbitrary interconnections of state space systems, which is the subject of the following section.

3.2. Interconnection of SS Models

The connection of multiple state space systems can be achieved by a three step procedure. At first all subsystems are appended. Then the interconnections are evaluated and a feedback equation is formulated. Finally the feedback equation is eliminated and the state space model of the interconnected system is retrieved.

3.2.1. Appending of SS Models

State space systems are appended by the block diagonal collection of the system matrices A_i, B_i, C_i, D_i, E_i of each of the state space models $i = 1, 2, \ldots, n$. Exemplary for $\tilde{A}$:

$$\tilde{A} = \begin{bmatrix} A_1 & 0 & 0 & 0 \\ 0 & A_2 & 0 & 0 \\ 0 & 0 & \ddots & 0 \\ 0 & 0 & 0 & A_n \end{bmatrix}; \quad (33)$$

This implies that the state vectors and the input and output vectors of the systems are stacked as well

$$x = \begin{bmatrix} x_1 \\ x_2 \\ \vdots \\ x_n \end{bmatrix}; \quad \tilde{u} = \begin{bmatrix} u_1 \\ u_2 \\ \vdots \\ u_n \end{bmatrix}; \quad \tilde{y} = \begin{bmatrix} y_1 \\ y_2 \\ \vdots \\ y_n \end{bmatrix}. \quad (34)$$

3.2.2. Evaluation of Feedback

The input of the appended system $\tilde{u}$ consists of true external inputs u and internal feedbacks $\tilde{y}$. External inputs of the connected system are for example noise sources or perturbations at plane wave interfaces that are not connected internally like f_u in Eq. (32) of the previous example. The internal feedbacks are due to the plane wave connections between the appended models. For example waves that are leaving one element model $\tilde{y}_j$ enter another element model $\tilde{u}_k$. This is expressed by a feedback matrix F that contains binary $(0, 1)$ entries corresponding to the topology of the network.

$$\tilde{u} = F\tilde{y} + u \quad (35)$$

The feedback matrix is retrieved by evaluating the names which are assigned to the inputs and outputs of the appended system.

3.2.3. Solve for the Connected SS Model

Using the feedback equation (35), the connected system is expressed by

$$\tilde{E}\dot{x} = \tilde{A}x + \tilde{B}\tilde{u} \quad (36)$$

$$\tilde{y} = \tilde{C}x + \tilde{D}\tilde{u} \quad (37)$$

$$\tilde{u} = F\tilde{y} + u\,. \quad (38)$$

In order to obtain a state space model with the generic structure as in Eq. (13), the feedback equation needs to be eliminated. This is achieved by replacing $\tilde{y}$ in the feedback equation (38) using the output equation (37) and then solve for $\tilde{u}$

$$\tilde{u} = (1 - F\tilde{D})^{-1}F\tilde{C}x + (1 - F\tilde{D})^{-1}u\,. \quad (39)$$

Subsequently $\tilde{u}$ can be eliminated in the system equation (36) and the output equation (37) and the state space system matrices of the connected system are:

$$A = \tilde{A} + \tilde{B}(1 - F\tilde{D})^{-1}F\tilde{C}\,;$$
$$B = \tilde{B}(1 - F\tilde{D})^{-1}\,;$$
$$C = \tilde{C} + \tilde{D}(1 - F\tilde{D})^{-1}F\tilde{C}\,;$$
$$D = \tilde{D}(1 - F\tilde{D})^{-1}\,; \qquad E = \tilde{E}\,.$$

Eventually, the internally connected outputs in $\tilde{y}$ can be dropped, such that only the relevant outputs y remain. Thus the connected state space model has the generic form

$$E\dot{x} = Ax + Bu$$
$$y = Cx + Du$$

ACTA ACUSTICA UNITED WITH ACUSTICA
Vol. 98 (2016)

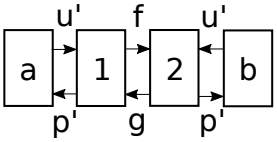

Figure 4. Interconnection of incompatible system interfaces (a,b) by Connectors (1,2).

3.2.4. Invertibility of Feedback

Evaluating the feedback needs an inversion of $1-F\tilde{D}$. This operation is typically very cheap as both F and $\tilde{D}$ are very sparse. In fact $F\tilde{D}$ only has non zero entries, where a feed through ($\tilde{D}$) is internally connected. Such a feed through occurs in low order models of acoustically compact elements, like duct singularities such as discontinuities in area or temperature, and at plane wave boundary interfaces which are defined in primitive variables u', p'.

There are rare cases when the inversion is not possible. This happens when there is a connection between two interfaces, which implicitly connect two inputs. If both systems (a,b) have for example u' as an output and p' as an input, it is not possible to connect them directly. However, it is possible to convert the interface to wave amplitudes f, g on both sides, and subsequently connect the two systems as shown in Fig. 4. The connectors (1,2) represent algebraic relations, so-called "feed through" between inputs and outputs:

$$\begin{bmatrix} f \\ p' \end{bmatrix} = \begin{bmatrix} 1 & 1 \\ 2 & 1 \end{bmatrix} \begin{bmatrix} g \\ u' \end{bmatrix} \; ; \; \begin{bmatrix} g \\ p' \end{bmatrix} = \begin{bmatrix} 1 & -1 \\ 2 & -1 \end{bmatrix} \begin{bmatrix} f \\ u' \end{bmatrix} . \quad (40)$$

The connection of the converted interfaces leads to an algebraic equation linking two inputs ($p'_a = p'_b$), which results in a rank deficiency of $1 - F\tilde{D}$. The solution to this is to append the feed back equation (39) to the system equation (36), instead of inverting it. Then the state vector becomes $\tilde{x} = \begin{bmatrix} x & \tilde{u} \end{bmatrix}^T$ and the resulting system matrices are:

$$A = \begin{bmatrix} \tilde{A} & \tilde{B} \\ F\tilde{C} & F\tilde{D} - I \end{bmatrix} \; ; \quad B = \begin{bmatrix} 0 \\ I \end{bmatrix}$$
$$C = \begin{bmatrix} \tilde{C} & \tilde{D} \end{bmatrix} \; ; \quad D = \begin{bmatrix} 0 \end{bmatrix} \; ; \quad E = \begin{bmatrix} \tilde{E} & 0 \\ 0 & 0 \end{bmatrix} \quad (41)$$

4. Acoustic Eigenmodes of an Annular Combustor

In order to demonstrate the functionality and effectiveness of the connection algorithm, we consider an annular combustor geometry which was investigated by Evesque et.al [21]. The system is shown in Fig. 5 and consists of an annular plenum (P) and combustion chamber (C), which are connected by 12 burner tubes (B). The geometrical parameters of the system are listed in Table I. The plenum and combustion chamber have equal middle radii R and widths δ. We consider a cold case of the combustion system, where there is no reaction or temperature gradients in the field. Furthermore, low Mach number is assumed and mean flow is neglected.

Table I. Geometrical parameters of the combustor in [m].

l_P	l_B	l_C	$R_{P,C}$	$\delta_{P,C}$	r_B
0.1	0.13	0.35	0.22	0.12	0.03

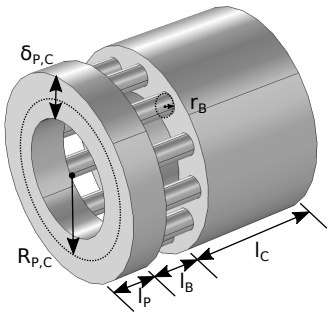

Figure 5. Geometry of the annular combustion system.

We will investigate the system with two different models. The first model discretizes the entire system using linearized Navier-Stokes equations (LNSE) and an FEM scheme with the commercial tool Comsol[1]. Especially the duct sections need to be highly refined in order to avoid numerical issues in this area. The total order of the full system is 152547. The second model discretizes just the plenum and combustion chamber in Comsol and uses a 1D third order upwind scheme as introduced in the minimal example for the tubes. The length of the tubes is $L = 0.13\,\mathrm{m}$, speed of sound $c = 350\,\mathrm{m\,s^{-1}}$ and the maximum frequency of interest is up to $f = 400\,\mathrm{Hz}$. Therefore, the non-dimensionalized frequency $\tau\omega = 2\pi fL/c = 0.93$ is within the range where the model is performing well (Fig. 2, - ⊖ -). The state space system matrices (A,B,C,D,E) of the plenum and combustion chamber submodels are exported from Comsol. Subsequently input and output names of the subsystems may either be manually assigned or the system is assembled using the graphical interface of taX as shown in Fig. 6. Finally all 12 duct models of the tubes and the plenum and combustion chamber models are connected with the algorithm presented in the previous section. The total order of the connected system is 136702, which is approximately 90% of the full model.

Table II shows the first four physical eigenvalues of the full model, which was entirely computed in Comsol (column "Full"), the eigenvalues computed by the connected system (column "Connected") and the eigenvalues reported by [21] (column "Evesque"). We can see that there is very good agreement between the three computational models. The modeshapes of the second mode of the full and connected model are

[1] https://www.comsol.de/

Acta Acustica united with Acustica
Vol. 98 (2016)

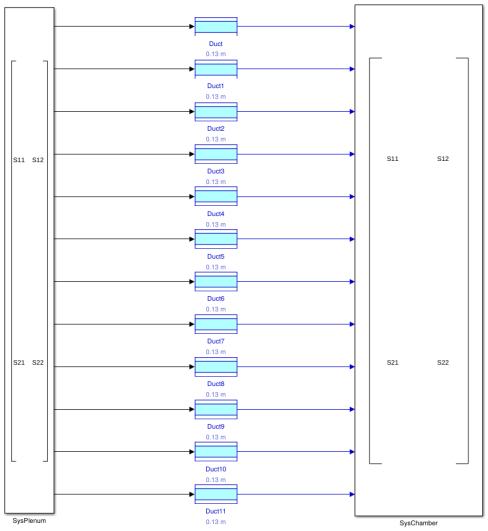

Figure 6. Screenshot of the taX Simulink gui.

Table II. Eigenfrequency of the first four eigenmodes.

	Full	Connected	Evesque [21]
1. Mode	139.3	144.6	≈ 143
2. Mode	274.8	276.7	≈ 278
3. Mode	274.8	277.0	≈ 278
4. Mode	293.2	305.6	≈ 305

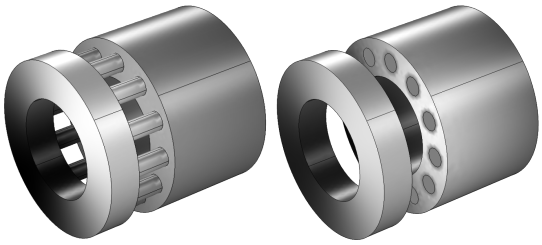

Figure 7. Pressure fields of the second acoustic eigenmode of the full system (left) and connected system (right).

shown in Fig. 7. As the tube sections are not part of the Comsol mesh in the connected model, only the plenum and combustion chamber are shown there. The visualization of the pressures on the tube interfaces of the connected model is not implemented, thus the patches appear dark. Other than that, the mode-shapes show very good agreement and we conclude that the connection algorithm is working well for state space models retrieved from linearized PDEs.

5. Conclusion

The methods presented in this paper allow for a unified state space modeling of acoustic systems. This applies to models retrieved from analytical low order derivations, from linearized partial differential equations for aero-acoustic field variables and also from experimental or LES data. The respective translation to a generic state space formulation does not bring further approximations other than those introduced by the acoustic modeling in the first place. This distinguishes the procedure from methods that retrieve state space models from modal reduction techniques.

There is a generic algorithm to connect networks of interconnected state space models that results in one joint state space model of the interconnected system.

Due to the unified state space formulation, we can compute the eigenvalues and vectors of acoustic network models very efficiently by solving a standard or generalized linear eigenvalue problem. If one exploits the sparse structure of linear acoustic network models and an iterative eigenvalue solver, even solving for very large models is possible.

Therefore, we can determine stability, optimize using adjoint eigenvectors, carry out parameter studies and perform uncertainty quantification. Furthermore, power spectral density of noise emissions and acoustic wave scattering dynamics can be evaluated directly, without sampling, in frequency domain. At the same time, the simulation in time domain is possible, which is necessary for nonlinear simulations. For example limit cycles of a combustion test rig can be simulated by coupling a linear acoustic network model with an incompressible LES of the flame [22].

There are still some areas for improvements of this state space acoustic network modeling framework. Instead of appending all inputs to the state vector if the feedback is not entirely invertible, it would be better to partially invert the feedback and append just the ones that may not be inverted. On behalf of the interfaces between subsystems it would be possible to resolve non-planar waves. Such higher order interfaces would enable to divide systems into subsystems even if there are no acoustically compact regions for placing a planar-wave interface. Furthermore, multi physics systems can be easily included. For example active flow control can be incorporated into the network model directly by means of a sensor and actor model and a state space controller.

6. Acknowledgment

Financial support for S. Jaensch by the Research Association for Combustion Engines (Forschungsvereinigung Verbrennung e.V - FVV, project: 6011150) is gratefully acknowledged. We also like to thank A. Castagnotto, M. Cruz and B. Lohmann for the fruitful cooperation in developing the sparse state space toolbox.

References

[1] M. L. Munjal: Acoustics of Ducts and Mufflers. John Wiley & Sons, 1986.

ACTA ACUSTICA UNITED WITH ACUSTICA
Vol. 98 (2016)

[2] S. W. Rienstra, A. Hirschberg: An Introduction to Acoustics. Tech. Rept. IWDE 92-06, Eindhoven University of Technology, 2006.

[3] F. Nicoud, L. Benoit, C. Sensiau, T. Poinsot: Acoustic modes in combustors with complex impedances and multidimensional active flames. AIAA Journal **45** (2007) 426–441.

[4] G. Campa, S. M. Camporeale: Prediction of the Thermoacoustic Combustion Instabilities in Practical Annular Combustors. Journal of Engineering for Gas Turbines and Power **136** (2014) 091504–091504.

[5] C. Sovardi, S. Jaensch, W. Polifke: Concurrent Identification of Aero-acoustic Scattering and Noise Sources at a Flow Duct Singularity in low Mach Number Flow. Submitt. J. Sound Vib. (2015).

[6] J. Li, A. S. Morgans: Time domain simulations of nonlinear thermoacoustic behaviour in a simple combustor using a wave-based approach. Journal of Sound and Vibration (Juni 2015).

[7] J. J. Keller: Thermoacoustic Oscillations in Combustion Chambers of Gas Turbines. AIAA J. **33** (1995) 2280–2287.

[8] A. P. Dowling: The calculation of thermoacoustic oscillation. J Sound Vib. **180** (1995) 557–581.

[9] S. W. Yuen, A. M. G. Gentemann, W. Polifke: Influence of Boundary Reflection Coefficient on the System Identifiability of Acoustic Two-Ports. ICSV 11, Saint-Petersburg, Russia, July 5-8 2004, IIAV, 3501–3508.

[10] T. Elnady, M. Åbom: Sidlab : New 1d sound propagation simulation software for complex duct networks. ICSV 13, 2006, 4262–4269.

[11] M. Bothien, J. Moeck, A. Lacarelle, C. O. Paschereit: Time domain modelling and stability analysis of complex thermoacoustic systems. Proc. Inst. Mech. Eng. Part J. Power Energy **221** (Jan. 2007) 657–668.

[12] Professur für Thermofluiddynamik: tax. `https://tax.wiki.tum.de/`.

[13] P. R. Amestoy, I. S. Duff, J.-Y. L'Excellent, J. Koster: MUMPS: A General Purpose Distributed Memory Sparse Solver. – In: Applied Parallel Computing. New Paradigms for HPC in Industry and Academia. T. Sørevik, F. Manne, A. H. Gebremedhin, R. Moe (eds.). Springer Berlin Heidelberg, Juni 2000, 121–130.

[14] R. Lehoucq, D. Sorensen, C. Yang: ARPACK Users' Guide. Society for Industrial and Applied Mathematics, Jan. 1998, (Software, Environments and Tools).

[15] R. Ewert, W. Schröder: Acoustic perturbation equations based on flow decomposition via source filtering. J. Comput. Phys. **188** (Juli 2003) 365–398.

[16] B. Schuermans, V. Bellucci, C. O. Paschereit: Thermoacoustic Modeling and Control of Multi-Burner Combustion Systems. Int'l Gas Turbine and Aeroengine Congress & Exposition, Atlanta, GA, U.S.A., 2003, ASME, 509–519.

[17] T. Hummel, M. Schulze, B. Schuermans, T. Sattelmayer: Reduced-Order Modeling of transversal and non-compact Combustion Dynamics. ICSV 22, Juli 2015.

[18] S. Jaensch, C. Sovardi, W. Polifke: On the robust, flexible and consistent implementation of time domain impedance boundary conditions for compressible flow simulations. submitted to J. Comp. Phys. (2015).

[19] J. Lunze: Regelungstechnik 1. Springer Vieweg, Berlin, 2014.

[20] V. Duindam, A. Macchelli, S. Stramigioli, H. Bruyninckx: Modeling and Control of Complex Physical Systems. Springer Berlin Heidelberg, Berlin, Heidelberg, 2009.

[21] S. Evesque, W. Polifke: Low-Order Acoustic Modelling for Annular Combustors: Validation and Inclusion of Modal Coupling. Int'l Gas Turbine and Aeroengine Congress & Exposition, Amsterdam, NL, 2002.

[22] S. Jaensch, M. Merk, E. Gopalakrishnan, S. Bomberg, T. Emmert, R. I. Sujith, W. Polifke: Hybrid CFD/ low-order modeling of nonlinear thermoacoustic oscillations. submitted to the 36th Symposium of the Combustion Institute, Seoul, Korea, 2016.

Hybrid CFD/ low-order modeling of nonlinear thermoacoustic oscillations

S. Jaensch[a], M. Merk[a], E. A. Gopalakrishnan[b], S. Bomberg[a], T. Emmert[a], R. I. Sujith[b], W. Polifke[a,*]

[a]*Professur für Thermofluiddynamik, Fakultät für Maschinenwesen, Technische Universität München, Boltzmannstr. 15, D-85748 Garching, Germany*
[b]*Department of Aerospace Engineering, Indian Institute of Technology Madras, Chennai, 600036, India*

Abstract

This paper proposes and compares two nonlinear time-domain models of self-excited thermoacoustic oscillations of laminar premixed flames. The flame and its immediate vicinity are resolved with reactive flow simulations. Simultaneously, the acoustic field is modeled with low-order models, which are coupled to the reactive flow simulations. On the one hand a flame model based on the fully compressible Navier-Stokes equations is investigated. Here, the simulation is coupled to the low-order model via the characteristic wave amplitudes at the inlet boundary. The other model resolves the flame with a low Mach number reactive flow simulation. In order to include thermoacoustic feedback, this flame model is coupled with an acoustic network model by the global heat release rate and the fluctuation of the axial velocity at a reference position upstream of the flame. A bifurcation analysis using the plenum length as bifurcation parameter is conducted. Both models exhibit complex nonlinear oscillations and are in good agreement with each other. Therefore, we conclude that the coupling of a linear acoustic model and a nonlinear flame model via reference velocity and global heat release rate is sufficient to accurately capture thermoacoustic oscillations of the configuration investigated. This implies that the most important nonlinearities can be attributed to hydrodynamic effects and the flame kinematics. Additionally, the study provides further evidence that premixed flames respond predominantly to fluctuations of the upstream velocity.

Keywords: nonlinear combustion dynamics, premixed flame, causality, state-space, nonlinear time series analysis

1. Introduction

The development of gas turbines or rocket engines is often impeded by thermoacoustic instabilities. Feedback between the unsteady heat release rate of the combustion and the acoustic field results in very large oscillations of pressure, heat release and velocity. These oscillations can reach amplitude levels at which gas turbines have to be shut down, or rockets are destroyed. To decide whether a thermoacoustic instability reaches such amplitude levels, nonlinear models are required.

This modeling is a challenging task, as complex nonlinear phenomena are involved. Durox et al. [1] studied the response of various laminar flame configurations to fluctuations of the inflow velocity. It was observed that the fluctuations of the global heat release rate saturate for high forcing amplitudes. Correspondingly, Kabiraj et al. [2] studied self-excited thermoacoustic oscillations of a laminar flame and observed periodic, aperiodic, or chaotic oscillations as well as hysteresis. In order to obtain qualitative and quantitative agreement with these experimental results, a model of thermoacoustic instabilities has to account for all effects observed. Dowling [3] proposed to model the nonlinear flame dynamics with a flame describing function (FDF). Noiray et al. [4] showed that the FDF combined with an acoustic network model provides a useful estimate of limit cycle amplitudes in many cases. However, it is a frequency domain approach and considers only a single unstable acoustic mode. Therefore, it can only predict harmonic oscillations. The advantage of time-domain models is that they can account for multi-modal coupling, which is necessary to describe complex types of oscillations. A time-domain model that has enjoyed recent interest uses a *G*-equation based flame model coupled with a low-order acoustic model [3, 5–7]. This model shows complex nonlinear oscillations. However, the results depend strongly on the velocity model used

*Corresponding author
Email address: polifke@tfd.mw.tum.de (W. Polifke)
URL: http://www.tfd.mw.tum.de (W. Polifke)

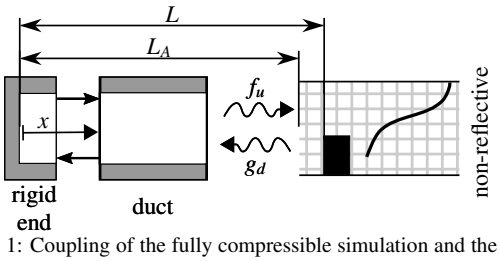

Fig. 1: Coupling of the fully compressible simulation and the corresponding acoustic model. (Model: C-fg)

[8, 9]. Indeed, the *G*-equation models found in the literature do not account for vortex shedding or vortex-flame interaction. Additionally, gas expansion and shear layer effects were reported to have a significant influence on the flame response [10]. These effect are also not considered by state-of-the art *G*-equation implementations. Therefore, quantitative agreement with experiment is not obtained and more sophisticated models are needed.

A suitable low-order model has to account for the complex interaction between flame, flow and acoustics. In the present study we propose and compare two models which account for these effects: Firstly, a model which resolves the flame and its vicinity with a fully compressible, reactive flow simulation. As shown in Fig. 1, the simulation is coupled to the acoustic low order model via the characteristic wave amplitudes in order to model the full acoustic field of the plenum. In the following we denote this simulation "C-fg". Secondly, a model which utilizes a low Mach number, reactive flow simulation. Here, the density depends only on the temperature, but not on pressure. As shown in Fig. 2, this model is coupled to a low-order network model via a reference velocity and the global heat release rate. Consequently, we denote this model "LM-uq".

Please note that in the literature [11–14] other hybrid models for thermoacoustic oscillations have been proposed. However, the coupling used by these hybrid models has not been cross-validated in a systematic manner against a fully compressible simulation. This cross-validation allows to directly verify the coupling between flame, hydrodynamics and acoustics.

In the following section the two formulations are explained in detail. Thereafter, in Section 3 the results of the two models are compared via a bifurcation analysis. Although, complex thermoacoustic oscillations are observed, the two models are in good agreement with each other. Thus it is concluded that the coupling of a nonlinear flame model and a linear acoustic model is sufficient to describe the thermoacoustic oscillation of the configuration investigated.

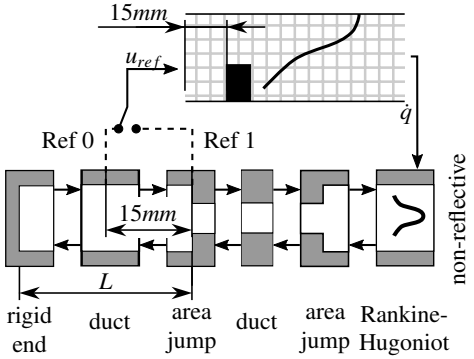

Fig. 2: Coupling of the low Mach number simulation and the corresponding acoustic model. The reference velocity is measured at two different locations (compare Tab. 1). (Model: LM-uq)

2. Numerical setup

The laminar slit burner considered in the present study is shown in Fig. 3. Kornilov et al. [15] and Duchaine et al. [16] investigated the linear dynamics of this configuration by experiment and simulation, respectively. Good agreement between experimental and numerical results was found. The CFD setup used in the present work corresponds to the one used in [16]. Only one half of one flame is resolved within the two dimensional CFD domain and symmetry boundary conditions are used. The outlet BC is non-reflective. This corresponds to a flame positioned in the middle of the burner plate. The influence of asymmetry on the nonlinear dynamics is expected to be complex and necessitates a separate study. At the inflow, we impose a mean velocity of 0.4 m/s and a temperature of 293 K. The plate on which the flame is stabilized is modeled as no-slip wall with a fixed temperature of 373 K as measured in [15]. The fuel is methane with an equivalence ratio of 0.8. For a detailed description of the two-step reaction mechanism we refer to [16]. As sketched in Fig. 3, a structured grid with 122300 cells was used. In the region of the steady-state position of the flame and of the area contractions, the grid is uniform with a cell size of 0.025 mm. This corresponds to about 18 grid points in the reactive zone. Outside this region the cells were stretched in the axial direction.

In order to model thermoacoustic instabilities of the configuration correctly, it is crucial to capture the coupling between combustion, hydrodynamics and acoustics. In this regard the treatment of the model C-fg and LM-uq differs from each other.

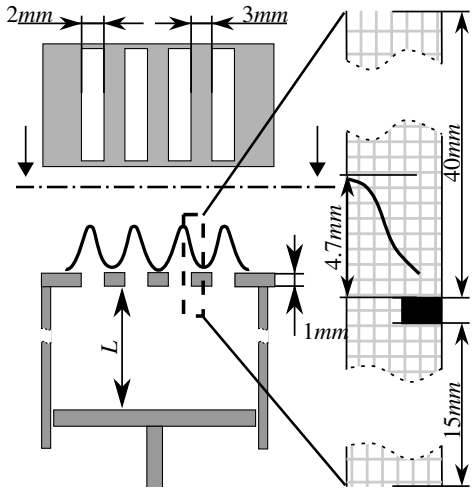

Fig. 3: Left: Sketch of the experimental configuration considered. Right: Truncated CFD domain.

2.1. Compressible simulation – plenum modeled via acoustic boundary conditions

By its nature, the compressible simulation used by the model C-fg captures the coupling between combustion, hydrodynamics and acoustics. However, the plenum length L determines the acoustic impedance at the burner plate and thus, is crucial for the thermoacoustic stability of the configuration. In order to capture thermoacoustic instabilities the full plenum length has to be modeled. The most straight-forward way to model the plenum is to resolve it within the CFD domain. However, this approach has two important drawbacks: (1) The impedance at the inlet of the extended CFD domain can be imposed in a very limited manner, only. (2) Changing the length of the plenum requires to create a new mesh. In oder to overcome these drawbacks, in the present study Characteristic Based State-Space Boundary Conditions (CBSBC), as proposed in [17], are utilized to effectively extend the plenum to the full plenum length (compare Fig. 1).

CBSBC provide a robust and consistent implementation of time-domain impedance boundary conditions. This BC allows to impose an impedance and ensures that the CFD simulation exhibits the impedance imposed, accurately. CBSBC are based on a model of the reflection coefficient which can be considered as equivalent to the acoustic impedance. The reflection coefficient has to be provided in state-space representation. We will first explain how the state-space model for the present study is determined. Afterwards, we show how the model is coupled with the compressible CFD simulation.

Plane acoustic waves can be described by means of the characteristic waves amplitudes

$$f = \frac{1}{2}\left(p'/\bar{\rho}\bar{c} + u'\right), \quad g = \frac{1}{2}\left(p'/\bar{\rho}\bar{c} - u'\right), \tag{1}$$

with density $\bar{\rho}$, speed of sound $\bar{c}$. p' and u' are the acoustic pressure and velocity fluctuations, respectively. f corresponds to the wave traveling in the downstream direction and g to the wave traveling in the upstream direction. The one-dimensional, linearized Euler equations

$$\frac{\partial f}{\partial t} + (\bar{u} + \bar{c})\frac{\partial f}{\partial x} = 0 \text{ and } \frac{\partial g}{\partial t} + (\bar{u} - \bar{c})\frac{\partial g}{\partial x} = 0, \tag{2}$$

describe the propagation of the acoustic wave amplitudes. At the inlet of the acoustic model the boundary condition

$$u'(x = 0) = 0 \Leftrightarrow f(x = 0) = g(x = 0), \tag{3}$$

models a rigid wall. At the outlet of the acoustic model the boundary condition

$$g(t, x = L_A) = g_u(t) \tag{4}$$

allows to impose an arbitrary incoming wave $g_u(t)$. The discretization of Eq. (2) with a third-order upwind scheme in space under consideration of the boundary conditions (3) and (4) can be written in state-space form

$$\dot{\mathbf{x}}_{\text{C-fg}} = A_{\text{C-fg}}\mathbf{x}_{\text{C-fg}} + B_{\text{C-fg}}g_u \tag{5a}$$
$$f_u = C_{\text{C-fg}}\mathbf{x}_{\text{C-fg}}, \tag{5b}$$

with the state-space matrices $A_{\text{C-fg}}$,$B_{\text{C-fg}}$ and $C_{\text{C-fg}}$ and the state-vector $x_{\text{C-fg}}$. The index "C-fg" emphasizes that the state space model belongs to the model C-fg. For a tutorial explanation of how these matrices can be determined we refer to [17].

The second step is to couple the model (5) with the CFD simulation. CBSBC extends the well-known Navier-Stokes characteristic boundary conditions (NSCBC) [18]. As in the NSCBC framework, CBSBC define the derivative of pressure p and velocity u according to

$$\frac{\partial p}{\partial t} + \frac{1}{2}(\mathcal{L}_5 + \mathcal{L}_1) = 0, \quad \frac{\partial u}{\partial t} + \frac{1}{2}(\mathcal{L}_5 - \mathcal{L}_1) = 0. \tag{6}$$

Here, $\mathcal{L}_5$ and $\mathcal{L}_1$ are the temporal derivatives of the characteristic wave amplitudes f and g, respectively. With a setup as shown in Fig. 1, $\mathcal{L}_1$ corresponds to the wave leaving the CFD domain and is given as

$$\mathcal{L}_1 = (u - c)\left(\frac{\partial p}{\partial x} - \rho c \frac{\partial u}{\partial x}\right). \tag{7}$$

$\mathcal{L}_5$ corresponds to the f-wave entering the domain and has to be imposed

$$\mathcal{L}_5 = \sigma\left(u - (f_u - g_d) - u_T\right) + 2\frac{\partial f_u}{\partial t}, \tag{8}$$

The term $(f_u - g_d)$ is equal to the acoustic velocity fluctuation. Including this term in the relaxation term avoids artificial reflections at the boundaries of the CFD domain as it compensates the effect of the acoustic fluctuation on the relaxation term. The term $\partial f_u/\partial t$ allows to impose an ingoing wave. Please note that equation (8) is equal to the formulation given in [19].

Solving equations (5) to (8) at every time step allows to extend the acoustic domain to the full plenum length. Please note, by changing the length L_A we can change the plenum length without the requirement of a new mesh. At the outlet of the compressible simulation we impose non-reflective boundary conditions as proposed in [19]. The fully compressible simulations were conducted using AVBP [1] (Cerfacs and IFP). The Lax-Wendroff scheme was used for the discretization. This scheme is second-order accurate in both time and space. The time step was set to ensure an acoustic CFL number of 0.7.

2.2. *Low Mach number simulation – coupled to acoustics via Rankine-Hugoniot*

The model LM-uq is based on a low Mach number simulation. This means that the density depends only on the temperature, but not on pressure. In this way acoustic waves and hence, thermoacoustic feedback inside the CFD domain is suppressed. These kind of simulation is also called weakly compressible. In order to account for the thermoacoustic feedback, the low Mach number simulation is coupled with an acoustic network model via the linearized Rankine-Hugoniot equations [20] for a compact heat source. As shown in Fig. 2, the network model and the low Mach number simulation are coupled via the global heat release rate $\dot{q}'$ and a reference velocity u_{ref}. Please note, it can be shown that the coupling is equivalent to the one proposed by Moeck et al. [12]. As the acoustic model is linear it can be written in state space form

$$\dot{\mathbf{x}}_{LM-uq} = A_{\text{LM-uq}}\mathbf{x}_{\text{LM-uq}} + B_{\text{LM-uq}}\dot{q}' \tag{9a}$$

$$u_{ref} = C_{\text{LM-uq}}\mathbf{x}_{\text{LM-uq}} + D_{LM-uq}\dot{q}' \tag{9b}$$

With the state-space matrices $A_{\text{LM-uq}}$, $B_{\text{LM-uq}}$ and, $C_{\text{LM-uq}}$ and the state-vector $x_{\text{LM-uq}}$. Here, the index "LM-uq" emphasizes that the state space model belongs to the low Mach number simulation. A detailed description of how these matrices may be formulated can be found in [21–23]. The elements of the network model are shown in Fig. 2. As for the C-fg case the duct sections are modeled using the linearized Euler equations. The model for the area jump is based on the continuity equation and does not include acoustic losses. The inlet BC of the acoustic network model is a reflection coefficient of 1, which corresponds to a rigid wall. The outlet BC is a non-reflective boundary condition. The temperature ratio across the flame is 6.1. Overfall, the same configuration, shown in Fig. 3, as with the model C-fg is modeled.

The Rankine-Hugoniot equations assumes that the flame is compact with respect to the acoustic wavelength. Considering the height of the flame of about 5 *mm* and the length of the plenum which is the characteristic dimension of the acoustics for longitudinal modes, varying between 200 *mm* and 1000 *mm*, this assumption is fulfilled with good accuracy. The flame acts as an acoustic point source while the real flame has some spacial extent. The exact position of this source is a model parameter. In the present study this position was chosen 2.6 *mm* after the burner plate. Additionally, it is assumed that the flame responds only to fluctuations of the reference velocity. Again, due to the spatial extent of the real flame, the position at which this reference velocity is extracted is a model parameter. As indicated in Fig. 2, two different positions were investigated: (1) 15 *mm* upstream of the burner plate. This position coincides with the inlet boundary of the low Mach number simulation and is denoted as reference 0 (compare Fig. 2 and Tab. 1). (2) The reference velocity was chosen at the upstream side of the burner plate. In Fig. 2 and Tab. 1 this position is denoted as reference 1. The open-source finite volume code OpenFOAM[2] was used as low Mach number CFD solver. For the temporal integration the implicit Euler scheme with a (hydrodynamic) CFL number of 0.3 was employed. A transient

[1] http://cerfacs.fr/en/computational-fluid-dynamics-softwares/

[2] http://www.openfoam.org/

Table 1:
Model settings considered. Compare Fig. 2 for the reference position of the model LM-uq. Abbreviation: perturbation (pert.)

case name	model	initial condition	reference position
C-fg-low	C-fg	low pert.	—
C-fg-high	C-fg	high pert.	—
LM-uq-low-0	LM-uq	low pert.	0
LM-uq-high-0	LM-uq	high pert.	0
LM-uq-high-1	LM-uq	high pert.	1

SIMPLEC algorithm [24] which stopped iterating once the residuals were lower than 10^{-6} was used.

3. Numerical results

The model settings for which self-excited thermoacoustic instabilities were observed are listed in Tab. 1. Simulations with two different initial conditions were conducted. (1) The simulations denoted with "low" were started from a converged mean field. Here, only a small initial acoustic excitation was applied. This speeds up the development of a thermoacoustic oscillation and allows to reduce the computational costs significantly. (2) The simulations denoted with "high" were started from a initial condition taken from a snapshot with developed thermoacoustic oscillations. For all plenum length the same snapshot is used. The two different reference positions for the model LM-uq were explained in the previous section and are shown in Fig. 2. Depending on the complexity of the oscillations observed for each case, time series between 100 *ms* and 500 *ms* were generated. The first part of the time series at which the thermoacoustic oscillations are not yet fully developed were removed before the post processing. The two models were compared w.r.t. the normalized fluctuation of the reference velocity:

$$u' = \left(u'_{ref} - \bar{u}'_{ref}\right) / \bar{u}'_{ref} \tag{10}$$

Here, u'_{ref} is the area averaged velocity measured at a plane 15 *mm* upstream of the burner plate. $\bar{u}'_{ref}$ is the temporal average of u'_{ref}. In the remainder of this section the two models are first compared via a bifurcation analysis. Thereafter, the cases with a plenum length of $L = 200$ *mm* and $L = 700$ *mm* are investigated in detail.

3.1. Bifurcation analysis

In Fig. 4 (top) and Fig. 5 the variation of the root mean square (RMS) value with plenum length and the bifurcation diagram are shown, respectively. The amplitudes predicted by the two models are in good agreement with each other. This holds in particular for short plenum lengths L. For long plenum lengths the amplitudes predicted by the model LM-uq are slightly lower than the amplitudes predicted by the model C-fg. The corresponding velocities yield a Reynolds number of about 1000. Thus, the flow is in the transition to turbulence and better agreement cannot be expected.

It is interesting to note that the simulations with and without initial perturbation yield the same thermoacoustic oscillations. In contrast to experiments [2, 4] hysteresis is not observed. Several possible reasons can be named: E.g. the assumption of symmetry, the neglect of conjugate heat transfer, (unsteady) uncertainties in the boundary conditions [25] and the flow properties. However, also G-equation based models predict hysteresis, qualitatively. Therefore, the most likely reasons why the models proposed in the present study do not show hysteresis are: (1) The flame considered in the present study is very small. As shown in Fig. 3, the flame height is only 4.7 *mm*. This reduces the size of the computational domain and thus, the computational costs, significantly. However, the flame wrinkling is reduced which can prevent hysteresis to occur. (2) In [2] and [6] a Rijke tube configuration was investigated. Both acoustic boundary conditions of these configurations are open ends. This is in contrast to the closed end -non-reflective BC investigated in the present study. This changes the shape of the acoustic modes in the configuration, which again may prevent hysteresis to occur.

Another interesting point is the onset of the thermoacoustic oscillations. It is observed that the model C-fg and the LM-uq with reference position 1 (compare Fig. 2) become unstable at a plenum length of $L = 160$ *mm*. The models LM-uq with reference position 0, however, exhibit a thermoacoustic instability starting at a plenum length of 170 *mm*. Therefore, the less intuitive coupling using a reference position which is right before the burner plate is more accurate than the coupling using a reference position that coincides with the inlet boundary of the low Mach number simulation. The reason is that due to the low Mach number formulation, a velocity fluctuation imposed at the inlet will act immediately on the whole CFD domain. Therefore, the reference position should be chosen at the location where acoustic fluctuations create hydrodynamic fluctuations, which in general does not coincide with the position of the inlet of the CFD domain.

In Fig. 5 bifurcation diagrams of the two models are shown. In Fig. 4 (bottom) the dominant frequencies f_u predicted with the different setups investigated are

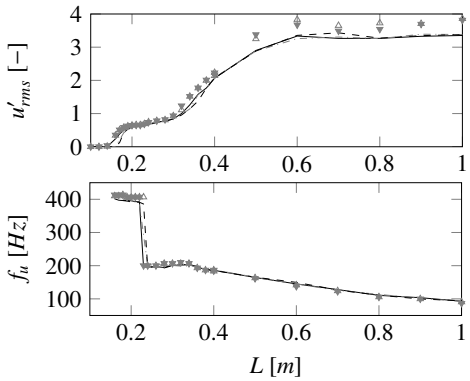

Fig. 4: RMS (top) and dominant frequency (bottom) of the reference velocity for different plenum length. ·····: LM-uq-low-0, - - - : LM-uq-high-0, ——: LM-uq-high-1, △: C-fg-low, ▽: C-fg-high

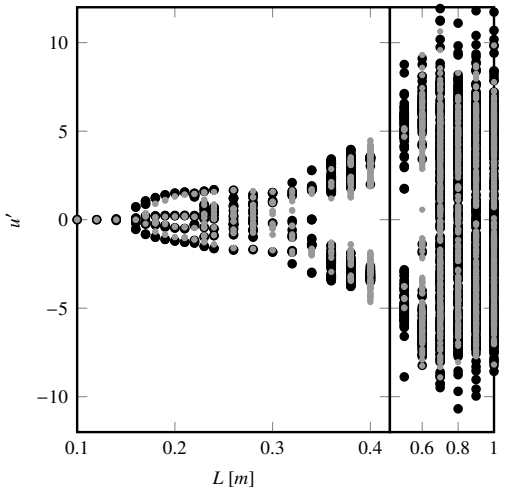

Fig. 5: Bifurcation diagram showing the minima and maxima of the normalized fluctuation of the reference velocity. The black dots show the result obtained with C-fg-low and C-fg-high and the gray dots the one obtained with LM-uq-low-0 and LM-uq-high-0

shown. The comparison shows that also the nature of the oscillations predicted by the two models is in good agreement with each other. A significant difference is observed at a plenum length of $L = 500mm$.

3.2. Comparison of time series

In Fig. 6 the time series (top plots) and the power spectrum (bottom plots) of the unsteady velocity for a plenum length of 200 *mm* and 700 *mm* are shown. Both plots show that the simulations are in good agreement which each other. Consistent with the bifurcation diagram, the amplitude at a plenum length of 700 *mm* is significantly larger than the amplitude at $L = 200$ *mm*. In the power spectrum for $L = 700$ *mm* a noise content is observed, which can be attributed to the onset of turbulence due to the high oscillation amplitudes. The corresponding maximum Reynolds number observed inside the slit of the burner plate is about 1000. The oscillation observed can be categorized as period-2 oscillations at $L = 200$ *mm* and limit cycle oscillations at $L = 700$ *mm*.

4. Summary and Conclusion

Two nonlinear, time-domain models of self-excited thermoacoustic instabilities of a laminar premixed flame (see Fig. 3) were proposed and compared: On the one hand the model C-fg shown in Fig. 1 resolves the flame with a fully compressible and reactive simulation. A low-order model of the plenum of the burner is coupled to the simulation via the characteristic wave amplitudes. This allows to change the length of the plenum without modifying the computational grid. On the other hand the model LM-uq (see Fig. 2) uses a low Mach number formulation of the Navier-Stokes equations to describe the flame dynamics. In order to account for the thermoacoustic feedback this simulation is coupled to an acoustic network model. Here, the coupling is based on the Rankine-Hugoniot equations and uses a reference velocity measured upstream of the flame and the global heat release rate.

A bifurcation analysis with the plenum length as bifurcation parameter was conducted. The two models were in good agreement with each other. The compressible simulation on which the model C-fg is based on resolves the flame acoustic interaction, possible nonlinear scattering of acoustic waves and hydrodynamic effects. On the other hand, the low Mach number simulation utilized by the model LM-uq, suppresses all acoustic effects inside the CFD domain. Thus, in this model the acoustic is acting on the flame only via fluctuations of the reference velocity. As the bifurcation analysis shows good agreement of the two models, we conclude that the flame investigated indeed responds predominantly to fluctuations of the reference velocity. This holds even while the flame exhibits complex thermoacoustic oscillations. Consequently, the acoustic pressure and acoustic waves act on the flame only indirectly, as they cause fluctuations of the reference velocity. This sequence of cause and effect has been questioned in the context of the recent discussion on the intrinsic thermoacoustic

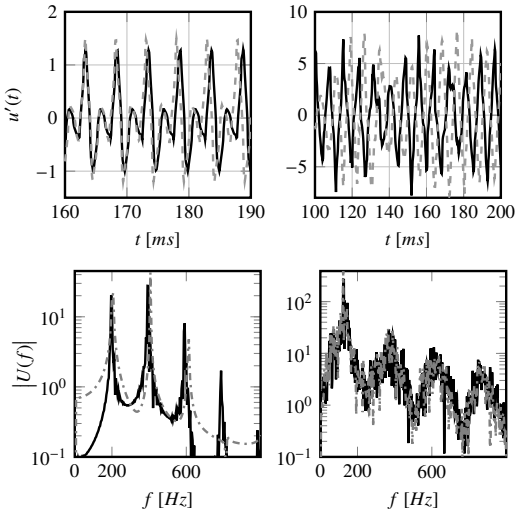

Fig. 6: Time series (top), power spectrum (bottom) of the velocity signal for $L = 200$ *mm* (left) and $L = 700$ *mm* (right). Dashed gray line: Compressible simulation (case: C-fg-low), Full black line: Low Mach number simulation (case: LM-uq-low-0)

feedback [26–31]. Furthermore, the comparison shows that the nonlinearities observed can be attributed to hydrodynamic effects or to the flame kinematics.

The models investigated in the present study form a basis for further research. On the one hand the two models can be extended in a straightforward manner, in order to account for effects like for conjugate heat transfer or for three dimensional effects. This is expected to be necessary in order to obtain models which reproduce experimental results, quantitatively. Here, the most critical limitations are that both models are restricted to the low-frequency regime and that the model LM-uq is valid only for velocity sensitive heat sources. On the other hand the models can serve as reference for nonlinear reduced-order models for the dynamics of laminar flames. Furthermore, both coupling methods also work with LES and therefore, allow a detailed numerical study of thermoacoustic oscillations of turbulent flames. This is of significant applied interest and will be subject of future investigations.

5. Acknowledgment

The financial support for S. Jaensch has been provided by the Research Association for Combustion Engines (Forschungsvereinigung Verbrennung e.V - FVV, project number: 6011150). Financial support for M. Merk and E. A. Gopalakrishan was provided by the German Research Foundation (DFG) via the project PO 710/16-1 and the SFB/TRR40 summer program, respectively. Financial support for S. Bomberg was provided by Technische Universitt München Institute for Advanced Study, funded by the German Excellence Initiative, and DFG, project PO 710/12-1. This support is gratefully acknowledged. We thank CERFACS and IFP for providing the solver AVBP. The authors gratefully acknowledge the Gauss Centre for Supercomputing e.V. (www.gauss-centre.eu) for funding this project by providing computing time on the GCS Supercomputer SuperMUC at Leibniz Supercomputing Centre (LRZ, www.lrz.de).

References

[1] D. Durox, T. Schuller, N. Noiray, S. Candel, Proceedings of the Combustion Institute 32 (2009) 1391 – 1398. doi:DOI:\%002010.1016/j.proci.2008.06.204.

[2] L. Kabiraj, R. Sujith, P. Wahi, Journal of Engineering for Gas Turbines and Power 134 (2012) 031502.

[3] A. P. Dowling, Journal of Fluid Mechanics 394 (1999) 51–72.

[4] N. Noiray, D. Durox, T. Schuller, S. Candel, Journal of Fluid Mechanics 615 (2008) 139–167. doi:10.1017/S0022112008003613.

[5] K. Kashinath, S. Hemchandra, M. P. Juniper, Journal of Engineering for Gas Turbines and Power 135 (2013) 061502.

[6] K. Kashinath, I. C. Waugh, M. P. Juniper, Journal of Fluid Mechanics 761 (2014) 399–430. doi:10.1017/jfm.2014.601.

[7] A. Orchini, S. Illingworth, M. Juniper, Journal of Fluid Mechanics 775 (2015) 387–414.

[8] T. Schuller, S. Ducruix, D. Durox, S. Candel, Proceedings of the Combustion Institute 29 (2002) 107–113.

[9] K. Kashinath, S. Hemchandra, M. P. Juniper, Combustion and Flame 160 (2013) 2856–2865.

[10] S. Schlimpert, S. Hemchandra, M. Meinke, W. Schröder, Combustion and Flame (2014) 1–23. doi:10.1016/j.combustflame.2014.08.001.

[11] S. R. Chakravarthy, C. Balaji, R. K. R. Katreddy, A. Nath, in: n3l - Int'l Summer School and Workshop on Non-Normal and Nonlinear Effects In Aero- and Thermoacoustics, Munich, Germany, p. 12.

[12] J. Moeck, C. Scharfenberg, O. Paschereit, R. Klein, in: Active Flow Control II, volume 108 of *Notes on Numerical Fluid Mechanics and Multidisciplinary Design*, 2010, pp. 291–306.

[13] B. Schuermans, H. Luebcke, D. Bajusz, P. Flohr, in: Proc. of ASME Turbo Expo 2005 Power for Land, Sea and AirIGTI, GT2005-68393, ASME, Reno, Nevada, USA, 2005.

[14] C. T. Wall, Numerical Methods for Large Eddy Simulation of Acoustic Combustion Instabilities, Phd thesis, Stanford University, 2005.

[15] V. N. Kornilov, R. Rook, J. H. M. ten Thije Boonkkamp, L. P. H. de Goey, Combustion and Flame 156 (2009) 1957 – 1970. doi:http://dx.doi.org/10.1016/j.combustflame.2009.07.017.

[16] F. Duchaine, F. Boudy, D. Durox, T. Poinsot, Combustion and Flame 158 (2011) 2384–2394. doi:10.1016/j.combustflame.2011.05.013.

[17] S. Jaensch, C. Sovardi, W. Polifke, Journal of Computational Physics 314 (2016) 145–159. doi:http://dx.doi.org/10.1016/j.jcp.2016.03.010.
[18] T. Poinsot, S. K. Lele, Journal of Computational Physics 101 (1992) 104–129.
[19] W. Polifke, C. Wall, P. Moin, Journal of Computational Physics 213 (2006) 437–449. doi:doi:10.1016/j.jcp.2005.08.016.
[20] B. T. Chu, in: 4th Symposium (International) on Combustion, volume 4, pp. 603–612. doi:10.1016/S0082-0784(53)80081-0.
[21] T. Emmert, S. Jaensch, C. Sovardi, W. Polifke, in: 7th Forum Acusticum, DEGA, Krakow, 2014.
[22] T. Emmert, M. Meindl, S. Jaensch, W. Polifke, submitted to Acta Acustica united with Acustica (2016).
[23] M. Meindl, T. Emmert, W. Polifke, in: Abstract submitted to ICSV23.
[24] H. K. Versteeg, W. Malalasekera, An introduction to computational fluid dynamics: the finite volume method, 2nd ed ed., Pearson Education Ltd, Harlow, England ; New York, 2007.
[25] V. Nair, S. Sarkar, R. Sujith, Probabilistic Engineering Mechanics 34 (2013) 177–188.
[26] M. Hoeijmakers, V. Kornilov, I. Lopez Arteaga, P. de Goey, H. Nijmeijer, Combustion and Flame 161 (2014) 2860–2867. doi:10.1016/j.combustflame.2014.05.009.
[27] M. Hoeijmakers, V. Kornilov, I. L. Arteaga, P. de Goey, H. Nijmeijer, Proceedings of the Combustion Institute 35 (2015) 1073–1078. doi:10.1016/j.proci.2014.06.059.
[28] S. Bomberg, T. Emmert, W. Polifke, in: 35th Symposium on Combustion, volume 35, The Combustion Institute, San Francisco, CA, USA, 2014. doi:10.1016/j.proci.2014.07.032.
[29] E. Courtine, L. Selle, T. Poinsot, Combustion and Flame 162 (2015) 4331–4341. doi:10.1016/j.combustflame.2015.07.002.
[30] T. Emmert, S. Bomberg, W. Polifke, Combustion and Flame 162 (2015) 75–85. doi:10.1016/j.combustflame.2014.06.008.
[31] C. F. Silva, T. Emmert, S. Jaensch, W. Polifke, Combustion and Flame 162 (2015) 3370 – 3378. doi:10.1016/j.combustflame.2015.06.003.

Combustion and Flame 162 (2015) 75–85

Contents lists available at ScienceDirect

Combustion and Flame

journal homepage: www.elsevier.com/locate/combustflame

Intrinsic thermoacoustic instability of premixed flames

Thomas Emmert, Sebastian Bomberg, Wolfgang Polifke *

Lehrstuhl für Thermodynamik, Technische Universität München, D-85747 Garching, Germany

ARTICLE INFO

Article history:
Received 31 October 2013
Received in revised form 31 January 2014
Accepted 4 June 2014
Available online 4 August 2014

Keywords:
Intrinsic instability
Premixed flame
Acoustic energy
Thermoacoustics
Frequency response
Combustion dynamics

ABSTRACT

The thermoacoustic stability of velocity sensitive premixed flames is investigated. A causal representation of the flow-flame-acoustic interactions reveals a flame-intrinsic feedback mechanism. The feedback loop may be described as follows: An upstream velocity disturbance induces a modulation of the heat release rate, which in turn generates an acoustic wave traveling in the upstream direction, where it influences the acoustic velocity and thus closes the feedback loop. The resonances of this feedback dynamics, which are identified as *intrinsic eigenmodes* of the flame, have important consequences for the dynamics and stability of the combustion process in general and the flame in particular. It is found that the amplification of acoustic power by flame-acoustic interactions can reach very high levels at frequencies close to the intrinsic eigenvalues due to the flame-internal feedback mechanism. This is shown rigorously by evaluating the "instability potentiality" from a balance of acoustic energy fluxes across the flame. One obtains factors of maximum (as well as minimum) power amplification. Based on the acoustic energy amplification, the small gain theorem is introduced as a stability criterion for the combustion system. It allows to formulate an optimization criterion for the acoustic characteristics of burners or flames without regard of the boundary conditions offered by combustor or plenum. The concepts and methods are exemplified first with a simplistic $n-\tau$ model and then with a flame transfer function that is representative of turbulent swirl burners.

1. Introduction

The dynamics and stability of flames are fascinating and multifaceted phenomena, which have been important and popular topics in combustion research [1,2]. From a fundamental point of view, thermo-diffusive or hydrodynamic flame instabilities might be most interesting [3–5], while phenomena such as blow off or flash back are very relevant for combustion engineering, see e.g. Kröner et al. [6], Aggarwal [7], Cavaliere et al. [8].

The present paper focuses on thermoacoustic instabilities, which result from an interaction between fluctuations of heat release rate and acoustic waves [9]. Starting with the development of rocket engines in the 1930s, thermoacoustic instabilities have impeded severely the development of reliable combustion equipment. The development of lean-premixed, low-emission combustion technology for stationary gas turbines has increased the technological relevance of these instabilities, their prediction and control remains a challenging task with great scientific appeal [10,11].

Thermoacoustic instabilities are usually conceptualized as a coupled feedback loop involving burner, flame, combustion chamber and plenum (possibly also fuel or air supply, etc): Fluctuations of heat release act as a monopole source of sound [12], the resulting acoustic waves are reflected by the combustion chamber or the plenum and in turn modulate the flow conditions at the burner, which successively perturb the flame and thus close the feedback loop [10,13]. If the resulting relative phase between fluctuations of heat release and pressure at the flame are favorable, a self-excited instability may occur [9]. In this well-established framework, thermoacoustic instabilities are considered a result of the *combined* dynamics of the flame and its acoustic environment, i.e. plenum, burner, combustor, supply lines, etc.; a flame placed in a anechoic environment should not be able to develop a thermoacoustic instability.

The present paper develops a different point of view: thermoacoustic interactions at the flame are analyzed in a framework that properly respects the causal relationships between "excitation" and "responses", respectively. With this perspective, it becomes evident that *flame-intrinsic feedback* between acoustics-flow-flame-acoustics may give rise to *intrinsic flame instabilities*, which are distinct from the resonating acoustic eigenmodes of the environment of the flame. Nevertheless, these instabilities are

* Corresponding author.
E-mail address: polifke@tum.de (W. Polifke).

http://dx.doi.org/10.1016/j.combustflame.2014.06.008
0010-2180/

Nomenclature

CWA	characteristic wave amplitude
$F(s)$	flame transfer function, –
f	downstream traveling CWA, m s^{-1}
g	upstream traveling CWA, m s^{-1}
$\mathbf{H}$	energy amplification matrix, –
λ_{max}	maximum sound power amplification, –
n	interaction index, –
ω	frequency, rad s^{-1}
Ω	closed loop denominator of flame feedback, –
OLTF	open loop transfer function of flame feedback, –
p'	acoustic pressure fluctuation, Pa
$\vec{q}$	vector of emitted rescaled CWAs, W
s	laplace variable $(= j\omega + \sigma)$, rad s^{-1}
σ	growth rate, rad s^{-1}
$\vec{\xi}$	vector of incident rescaled CWAs, W
$\mathbf{S}$	scattering matrix, –
$\mathbf{\Sigma}$	energy scaled scattering matrix, –
τ	time delay, s
θ	relative temperature jump $(= T_d/T_u - 1)$, –
u'	acoustic velocity fluctuation, m s^{-1}
ξ	ratio of specific impedances $(= \rho_u c_u/\rho_d c_d)$, –

Subscript indices

bf	burner and flame
f	flame
u	upstream
d	downstream

thermoacoustic in nature, and thus differ essentially from other types of "intrinsic flame instabilities in premixed and non-premixed combustion", as reviewed by Matalon [5].

In an independent study, Hoeijmakers et al. [14] explored strategies for preventing thermoacoustic instabilities by breaking the aforementioned feedback loop and also observed that a flame can be intrinsically unstable. Experiments were carried out in a setup with significant acoustic losses, induced by acoustic horns. The stability behavior was investigated for three different burners, and a range of operating conditions. It was observed that despite the significant acoustic losses present, thermoacoustic instabilities may still occur [15]. Of course, these results are very closely related to the ideas developed in the present paper. Lending further support to the argument, Bomberg et al. [16] have identified intrinsic flame eigenmodes in experimental setups investigated previously by Noiray et al. [17] and Komarek and Polifke [18], respectively.

The paper is organized as follows: The next chapter introduces first the low-order modeling concepts that are used to formulate ideas. Then the intrinsic thermoacoustic feedback structure of a velocity-sensitive premixed flame is identified. The corresponding spectrum of intrinsic eigenmodes is determined for the simple example of an $n - \tau$ flame transfer function. In the subsequent section, a balance for the flow rates of acoustic energy at a premixed flame is formulated, introducing the "instability potentiality" [19,20]. It is found that frequencies where generation of perturbation energy by fluctuating heat release is maximal correlate with the intrinsic eigenfrequencies of the flame. Invoking the small gain theorem originally deduced by Zames [21], it is then shown how these results are related to a general stability criterion for network models. This leads to an optimization criterion for individual elements in acoustic networks, which might be used to optimize burner designs independently from up- or downstream acoustic conditions at an early stage of combustor development. The tools and concepts developed up to that point are then applied to a more realistic flame transfer function, which is representative of turbulent premixed swirl flames. The analysis in the present paper is formulated in terms of a low-order model for velocity sensitive premixed flames. Nevertheless, implications should go beyond the limitations of the present study and indeed be fairly general, as discussed in the conclusions.

2. Intrinsic thermoacoustic feedback in a velocity-sensitive premixed flame

Our investigation is focused on the dynamics of the coupling between the heat release of the flame and the acoustic waves incident to and emitted from the flame. There is a causal chain of events, consisting of the acoustic waves altering the flow field, which leads to a fluctuation in heat release, which in turn generates acoustic waves. For premixed flames, the heat release fluctuation is typically caused by a velocity perturbation u' upstream of the flame. Thus the flame does not respond directly to incident acoustic waves, but to an upstream flow perturbation. The physical mechanism involved may be flame front kinematics, a convective transport of fuel inhomogeneities or a swirl modulation and possibly other effects.

For example in the case of premixed flames with technical fuel injection, a modulation of air velocity u' at the location of fuel injection results in an equivalence ratio modulation ϕ', which convects downstream. For an acoustically "stiff" injector, positive u' gives a leaner mixture and negative u' a richer mixture, whereas pressure p' has no effect. Once the fuel inhomogeneities arrive at the flame, they cause heat release rate fluctuations.

On the other hand, inside a swirler, in response to a perturbation of velocity, a wave in swirl number (or circulation) is set up, and the flame responds later to the swirl modulation as shown by Straub and Richards [22] as well as Komarek and Polifke [18]. Palies et al. [23] have coined the term "mode conversion" for this effect where an acoustic wave generates a vortical wave. Again, the cause for this generation of swirl modulation is u' at the swirler, p' at the swirler is unimportant.

As a last example, according to the Unit Impulse Response model of the G-equation by Blumenthal et al. [24], the "restoration term" of the flame front kinematics is triggered by movement of the flame at the anchoring point. The physical mechanism for this generic flame model may be vortex shedding at a backward facing step. So again, u' at the anchoring point is important and the flame transfer functions respect this causality as they relate u' to $\dot{Q}'$.

Other than deducing causality from first principles, it is substantially harder to retrieve it from experiments. The reason is, that in frequency domain, no discrimination between causes and consequences is possible and therefore, no causality can be inferred from measured results of harmonic solutions. But there is also numerical evidence for the causal relation between a velocity perturbation and heat release fluctuations of laminar premixed flames. Jaensch et al. [25] have identified and validated causal time domain models for the flame transfer function of such a flame from random time series simulation of a CFD model.

Low-order modeling concepts are used throughout this paper to formulate ideas. The present chapter introduces very briefly pertinent nomenclature and concepts, more details are found, e.g.

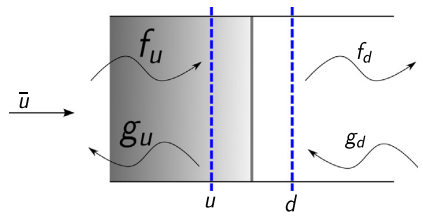

Fig. 1. Velocity sensitive premixed flame anchored in a duct section.

in [26,13,10,27,28]. Then the intrinsic thermoacoustic feedback structure of a ducted, velocity-sensitive premixed flame as depicted in Fig. 1 is identified. The corresponding spectrum of eigenmodes is determined for the simplistic example of an $n-\tau$ flame transfer function. In Section 4 the method will be applied to a more complex model of a turbulent premixed swirl burner.

2.1. Low-order thermoacoustic flame model

The diameter of the combustor configurations investigated is assumed to be much smaller than relevant acoustic wave lengths. Therefore, acoustic modes are considered to consist of one dimensional plane waves. Under the assumption of an acoustically compact flame with Helmholtz number $\mathrm{He} \equiv L_{flame}/\lambda \ll 1$, the conservation equations for mass, momentum and energy may be linearized to relate fluctuations of heat release $\dot{Q}'$ and acoustic perturbations of velocity u' and pressure p' upstream (u) and downstream (d) of the flame to each other. To simplify the derivation, terms of order $\mathcal{O}(2)$ in Mach number and higher are neglected and two non-dimensional parameters are introduced: Ratio of specific impedances $\xi \equiv \frac{\rho_u c_u}{\rho_d c_d}$, and the relative temperature increase $\theta \equiv T_d/T_u - 1$. Fluctuating quantities are denoted with a ', mean flow quantities do not carry indices:

$$\begin{pmatrix} \frac{p'}{\rho c} \\ u' \end{pmatrix}_d = \begin{pmatrix} \xi & 0 \\ 0 & 1 \end{pmatrix} \begin{pmatrix} \frac{p'}{\rho c} \\ u' \end{pmatrix}_u + \begin{pmatrix} 0 \\ \theta u_u \end{pmatrix} \frac{\dot{Q}'}{\dot{Q}}. \tag{1}$$

The first term on the r.h.s. describes the coupling of acoustic pressure p' and velocity u' across the discontinuity in specific impedances, the second term accounts for the effect of fluctuating heat release $\dot{Q}'$. The original derivation of these relations – known also as "acoustic Rankine–Hugoniot jump conditions" – was given by Chu [29], a detailed derivation using the same notation as this paper is found in [30,27].

The system of Eqs. (1) has constant coefficients and is not closed as $\dot{Q}'$ is unknown. Closure is achieved – and non-trivial dynamics are introduced – with a model for the heat release fluctuations of the flame: The flame transfer function $F(s)$. As we are assuming a velocity sensitive flame, the heat release fluctuations $\dot{Q}'$ are related to a velocity perturbation u'_u upstream of the flame:

$$\frac{\dot{Q}'}{\dot{Q}} = F(s)\frac{u'_u}{u_u}, \tag{2}$$

where $s = j\omega + \sigma$ is the Laplace variable. Various strategies to retrieve the flame transfer function $F(s)$ are described in the literature. The most popular methods are based on parametrized models such as the kinematic G-equation [31,11], and identification of non-parametric models from experiments [32] or reactive flow simulations [28].

With the flame transfer function, closure of Eq. (1) is achieved and one can introduce a flame transfer matrix $\mathbf{T}(s)$:

$$\begin{pmatrix} \frac{p'}{\rho c} \\ u' \end{pmatrix}_d = \underbrace{\begin{pmatrix} \xi & 0 \\ 0 & 1+\theta F(s) \end{pmatrix}}_{\mathbf{T}(s)} \begin{pmatrix} \frac{p'}{\rho c} \\ u' \end{pmatrix}_u \tag{3}$$

2.2. Causal representation of flame dynamcis and intrinsic feedback

The solution of the 1D wave equation can be represented as superposition of characteristic waves traveling in opposite directions. On the perspective of the acoustic subsystem containing the flame, acoustic waves that are entering the domain are causal inputs "excitation", while acoustic waves that are leaving the domain are causal outputs "responses". The direction of propagation ensures causality in the sense that waves that are leaving the domain are caused by waves that entered the domain at former times. Polifke and Gentemann [33] have shown, however, that the analysis of transmission and reflection of acoustic waves by a multi-port is facilitated by using a causal representation. The primitive acoustic variables p' and u' on the other hand are non-causal quantities in the sense that it is not possible to associate unambiguously a direction of propagation with either of them.

The *scattering matrix formulation* provides a representation of acoustic interactions at an element. Characteristic acoustic wave amplitudes f, g are introduced

$$f \equiv \frac{1}{2}\left(\frac{p'}{\rho c} + u'\right); \quad g \equiv \frac{1}{2}\left(\frac{p'}{\rho c} - u'\right) \tag{4}$$

and the scattering matrix $\mathbf{S}(s)$ describes how the outgoing waves g_u, f_d (see Fig. 1) depend on the incident waves f_u, g_d:

$$\begin{pmatrix} g_u \\ f_d \end{pmatrix} = \underbrace{\begin{pmatrix} r_u & t_d \\ t_u & r_d \end{pmatrix}}_{\mathbf{S}(s)} \begin{pmatrix} f_u \\ g_d \end{pmatrix}. \tag{5}$$

Obviously, the coefficients of the scattering matrix **S** can be identified as transmission and reflection factors for the waves incident from the upstream side u (left side in Fig. 1) or downstream side d (right side) of the multi-port. Note that the notation for the wave vectors and the scattering matrix in Eq. (5) is the one used by Aurégan and Starobinski [19]: The waves are sorted by port (location), upstream waves come first in the signal and response wave vectors, respectively. This notation allows a more natural formulation of the acoustic energy balance, see Section 3, but differs from the one used in other publications [33,27].

Mathematically, the coefficients of the scattering matrix **S** (reflection and transmission up- and downstream) are obtained by a coordinate transformation of the transfer matrix **T**:

$$r_u = (-T_{11} - T_{12} + T_{21} + T_{22})/\Omega, \tag{6}$$
$$t_d = 2/\Omega, \tag{7}$$
$$t_u = 2(T_{11}T_{22} - T_{12}T_{21})/\Omega, \tag{8}$$
$$r_d = (T_{11} - T_{12} + T_{21} - T_{22})/\Omega, \tag{9}$$

where T_{ij} are the coefficients of the transfer matrix and

$$\Omega \equiv (T_{11} - T_{12} - T_{21} + T_{22}) \tag{10}$$

is the common denominator of all scattering matrix coefficients.

For the special case of a flame transfer matrix – see Eq. (3) – the common denominator is $\Omega(s) = \xi + 1 + \theta F(s)$. In general, a low value of Ω should result in a high gain of the transmission or reflection of acoustic signals, as already observed by Gentemann and Polifke [34] and Polifke [20]. Zeros of the denominator $\Omega(s) \to 0$ are poles of the flame scattering matrix. It will be shown in the following that the poles of the flame scattering matrix are not artifacts due to mathematical conversions from transfer to scattering matrix formulation, but indeed are due to intrinsic eigenmodes of the flame and associated resonances.

A re-formulation of the system of equations allows to develop a distinct physical interpretation of the intrinsic modes: Instead of directly transforming the closed form flame transfer matrix Eq. (3) to scattering matrix formulation Eq. (5), the open form of the

Rankine–Hugoniot jump conditions Eq. (1) is first rewritten in scattering matrix representation to obtain $\mathbf{S}_\xi$, i.e. the scattering matrix of the jump in specific impedances due to the steady heat release. The thermoacoustic effect of the unsteady heat release is subsequently introduced, using again the flame transfer function Eq. (2). The following intermediate system of equations is obtained:

$$\begin{pmatrix} \boldsymbol{g_u} \\ f_d \end{pmatrix} = \underbrace{\frac{1}{\xi+1}\begin{pmatrix} 1-\xi & 2 \\ 2\xi & \xi-1 \end{pmatrix}}_{\mathbf{S}_\xi} \begin{pmatrix} f_u \\ g_d \end{pmatrix} + \frac{\theta}{\xi+1}\begin{pmatrix} 1 \\ \xi \end{pmatrix} F(s)(f_u - \boldsymbol{g_u}). \tag{11}$$

The g_u wave, which is propagating away from the flame in the upstream direction, is present on both sides of the equations. In the context of a causal representation of the system dynamics, with excitation on the r.h.s. and response on the l.h.s. [33], this means that the wave amplitude g_u appears as a cause as well as an effect and thus it causes feed back within the flame model.

The structure of this intrinsic feedback cycle is illustrated by the thick red lines in the dynamic system sketch of the flame in Fig. 2. The feedback mechanism involves the upstream traveling wave g_u, which contributes to the velocity perturbation at the reference position "u" (see the lower left corner of the figure). The flame, which is velocity sensitive, responds with a fluctuation in heat release rate $\dot{Q}'$, which in turn generates an upstream traveling wave g_u.

It is important to notice that this intrinsic feedback is not visible in transfermatrix representation of the system in Eq. (3). The reason for this discrepancy between scattering- and transfermatrix is that the transfermatrix is presuming $g_u = \frac{p'_u}{\rho c} - u'_u$ as a input and therefore ignores the causal intrinsic feedback mechanism.

2.3. Stability of intrinsic eigenmodes

The open loop dynamics of the feedback cycle introduced in the previous subsection is described by the open loop transfer function (OLTF) and a negative feedback:

$$g_u = -\underbrace{\frac{\theta}{\xi+1}F(s)}_{\text{OLTF}} g_u. \tag{12}$$

When solving for the closed loop transfer function dynamics of the scattering matrix of the flame, it is necessary to rewrite Eq. (11) such that g_u appears as output on the l.h.s.:

$$\begin{pmatrix} g_u \\ f_d \end{pmatrix} = \underbrace{\frac{1}{\xi+1+\theta F(s)}\begin{pmatrix} \theta F(s)-\xi+1 & 2 \\ 2\xi(\theta F(s)+1) & \xi-1-\theta F(s) \end{pmatrix}}_{\mathbf{S}_f} \begin{pmatrix} f_u \\ g_d \end{pmatrix} = \frac{\tilde{\mathbf{S}}_f}{\Omega}\begin{pmatrix} f_u \\ g_d \end{pmatrix}. \tag{13}$$

The matrix inversion involves a division of all coefficients of the scattering matrix with the factor Ω, which was introduced in Eq. (10). Now this factor can be identified as the closed loop feedback dynamics corresponding to the open loop feedback cycle of the flame (Eq. 12):

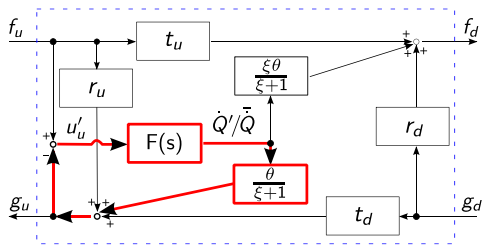

Fig. 2. Structure of the intrinsic feedback mechanism of a velocity sensitive premixed flame with the flame transfer function $F(s)$ and the transmission and reflection coefficients of the scattering matrix $\mathbf{S}_\xi$.

$$\Omega = \xi + 1 + \theta F(s) = (\xi+1)\cdot(1+\text{OLTF}(s)). \tag{14}$$

Thus, the roots s (zeros) of the closed loop denominator $\Omega(s) = 0$ are the eigenvalues (poles) of the flame scattering matrix $\mathbf{S}_f(s)$. Roots of Ω correspond to OLTF $= -1$. The point $P_{crit} = -1$ is called critical point. The eigenmodes of the flame dynamics are stable if all eigenfrequencies correspond to negative growth rates and are unstable if they have positive growth rates.

2.4. Example: intrinsic modes of the $n-\tau$ model

By way of illustration, the intrinsic eigenfrequencies of a simplistic velocity sensitive premixed flame model, i.e. the $n-\tau$ model with flame transfer function

$$F(s) = n e^{-s\tau}, \tag{15}$$

where n is the "interaction index" and τ the time lag, are computed next. The eigenvalues are found by solving the characteristic equation $\Omega(s) = 0$:

$$\xi + 1 + \theta n e^{-s\tau} = 0. \tag{16}$$

Infinitely many complex-valued eigenvalues are found for integers $z = 0, 1, \ldots$ (see B):

$$s_z = \underbrace{j\frac{(2z+1)\pi}{\tau}}_{\omega_z} + \underbrace{\frac{1}{\tau}\ln\left(\frac{n\theta}{1+\xi}\right)}_{\sigma}. \tag{17}$$

Normalizing time by choosing: $\tau = 1$ gives eigenfrequencies

$$\omega_z/(2\pi) = 0.5 + 1z. \tag{18}$$

The intrinsic eigenmodes of the flame are stable if the growth rates are negative $\sigma < 0$. As the growth rate is the same for all eigenfrequencies ω_z, this condition is globally fulfilled if $n < (\xi+1)/\theta$. An energy argument for low frequencies derived by Polifke and Lawn [35] requires that the interaction index be equal to unity, $n = 1$. Using the ideal gas law (C) the condition for stability of the intrinsic eigenmodes of the $n-\tau$ flame model simplifies to $\theta < 3$.

Figure 3 allows a graphical assessment of the stability of the system. According to Nyquist [36], unstable eigenfrequencies do not exist if the frequency response of the open loop transfer function OLTF($s \equiv j\omega$) does not encircle the critical point (see Eg. (14)) in clockwise direction. Thus, the Nyquist plot confirms that $\theta = 2$ is stable, $\theta = 3$ is marginally stable and $\theta = 4$ is unstable.

In an independent study, Hoeijmakers et al. [14] computed eigenmodes of a simple thermoacoustic model system, with an $n-\tau$ heat source placed in a duct. Even in the limit of zero

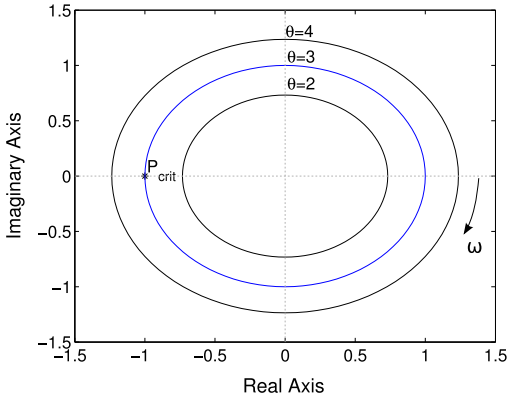

Fig. 3. Nyquist plot with critical point of the open loop transfer function OLTF(s) of the $n-\tau$ flame model for various values of the relative temperature increment θ.

reflection coefficients, eigenmodes were found. It is evident that these eigenmodes are associated with the instabilities resulting from flame-intrinsic feedback identified in the present study.

Given the stability of the flame alone, conclusions about the stability of the combustion system containing the flame cannot be drawn directly. It is a well known result from control theory that due to feedback, the stability of a linear system is undetermined even if all parts of a system are individually stable. In the present context, this means that even though a flame itself might be stable, given the right feedback of acoustic waves by the upstream an downstream boundaries, the interconnected combustion system might be unstable. Thus there is the need for a weaker (more conservative) stability criterion that allows to draw conclusions concerning thermoacoustic stability without regarding its boundaries. Such a criterion will be developed in Section 3.

3. Stability criteria based on a balance of acoustic power

As stated in the previous section, the stability of a linear acoustic system depends on all constitutive elements, and can be determined only by the analysis of the entire system. This approach can be tedious for large systems. At an early stage of the design process, when the acoustic dynamics of all components are not yet known, it may even be impossible. Thus it is of interest to develop a stability criterion based on perturbation energy or sound power, which allows to optimize individual elements of the combustion system independently.

Derivations of perturbation energy in increasingly complex flows were developed by Chu [37], Cantrell et al. [38], Morfey [39], Myers [40], Giauque et al. [41], and Brear et al. [42]. A definition of perturbation energy implies a decomposition of flow perturbations into acoustics, vortices and entropy, but this decomposition is not unambiguously. More recently George and Sujith [43] have pointed out, that in fact, Myers decomposition does not fulfill certain properties one should expect from an energy norm, whereas Chu's norm does, but it lacks the rigorous derivation.

The core issue is however that none of the norms leads to a conservative energy potential, which is needed for the construction of a rigorous stability criterion. Strictly speaking, energy provides a stability criterion only if it is monotonously decreasing for stable systems [44,45]. This does in general not apply to (acoustic) perturbation energy. Investigations by Subramanian and Sujith [46], Blumenthal et al. [47], as well as Wieczorek et al. [48] show that due to the acoustic-flow-flame-acoustic interaction even low order linear thermoacoustic systems are non-normal. As a consequence (acoustic) perturbation energy may rise even if the thermoacoustic system is asymptotically stable ("transient growth"). The method we propose instead does not rely on the acoustic energy in the field and is therefore not affected by the issues mentioned above.

Based on a balance for sound power, Aurégan and Starobinski [19] introduced the *whistling potentiality*, which provides a necessary-but-not-sufficient criterion for instability in (aero-) acoustic multi-port systems. Polifke [20] linked the argument of Aurégan and Starobinski to commonly used acoustic scattering matrices and applied the criterion under the name *instability potentiality* to a flame system. As *instability potentiality* is sound power based, it is also linked to the Rayleigh criterion (see [42]), though not limited by the strong assumptions of the latter. In this section it will be shown that strong amplification "gain" of sound power and thus strong potentiality of thermoacoustic instability occurs in the vicinity of the intrinsic eigenmodes of the flame.

Eventually, a rigorous theoretical science base is provided by linking the energy or sound power based stability criterion to the small gain theorem, which was originally developed by Zames [21] in the domain of control system theory.

3.1. Sound power balance

According to the energy corollary of Myers [40], the flux of acoustic energy p_a in 1-D flow equals

$$p_a = (p' + \rho u u')\left(u' + p'\frac{u}{\rho c^2}\right). \tag{19}$$

Correspondingly, for plane wave propagation along a duct with cross-sectional area A at negligible mean flow Mach number, the sound power P – i.e. the flow rate of acoustic energy with units Watt – evaluates to [49]

$$P = \frac{1}{2}A\ \mathrm{Re}(p'\ u'^{*}) = \frac{1}{2}\rho\ c\ A\ (|f|^2 - |g|^2). \tag{20}$$

In this notation the superscript asterisk in "u'^{*}" denotes the complex conjugate of u'.

In order to formulate a balance of acoustic energy at an acoustic two-port with ports "u" and "d", it is convenient to re-scale the characteristic wave amplitudes f and g as follows

$$\vec{\varsigma} \equiv \mathbf{V}\begin{pmatrix} f_u \\ g_d \end{pmatrix}, \quad \vec{\varrho} \equiv \mathbf{V}\begin{pmatrix} g_u \\ f_d \end{pmatrix}, \tag{21}$$

where

$$\mathbf{V} \equiv \begin{bmatrix} \chi_c & 0 \\ 0 & \chi_h \end{bmatrix} \quad \text{with} \quad \chi \equiv \sqrt{\frac{\rho c A}{2}}. \tag{22}$$

Note that the acoustic state vectors $\vec{\varsigma}$ and $\vec{\varrho}$ represent the incident "excitation" and outgoing "responses", respectively. Both vectors contain the upstream and downstream contributions needed for the net acoustic power balance deduced below (see Fig. 1).

Of course, with these variables the scattering matrix $\mathbf{S}$ has to be re-scaled, too. Defining

$$\mathbf{\Sigma} \equiv \mathbf{V}\mathbf{S}\mathbf{V}^{-1}, \tag{23}$$

one formulates concisely for the scattering of acoustic waves by a two-port:

$$\vec{\varrho} = \mathbf{\Sigma}\vec{\varsigma}. \tag{24}$$

The re-scaled acoustic variables are energy-extensive, i.e. the 2-norm of an acoustic state vector $\vec{\varsigma}$ or $\vec{\varrho}$ represents the corresponding flow rate of acoustic energy P incident upon or emanating from a two-port, respectively:

$$P_{\mathrm{in}} = \|\vec{\varsigma}\|_2 = \vec{\varsigma}^{\,\dagger}\vec{\varsigma}, \tag{25}$$

$$P_{\mathrm{out}} = \|\vec{\varrho}\|_2 = \vec{\varrho}^{\,\dagger}\vec{\varrho}. \tag{26}$$

where $(\cdot)^{\dagger}$ denotes the complex conjugate transpose (the "adjoint") of a vector or matrix. The steady-state balance of acoustic power for a two-port now reads as follows,

$$P_{\mathrm{gen}} = P_{\mathrm{out}} - P_{\mathrm{in}}. \tag{27}$$

The rate of generation of acoustic energy P_{gen} is the difference between incident and outgoing acoustic flow rates. If $P_{\mathrm{gen}} > 0$ incident acoustic power is amplified, i.e. there is overall generation of acoustic energy by the acoustic two-port, if $P_{\mathrm{gen}} < 0$ more power is dissipated than produced. Combining Eqs. 24, 26, 25 and 27, one finds that

$$P_{\mathrm{gen}} = \vec{\varsigma}^{\dagger}(\underbrace{\mathbf{\Sigma}^{\dagger}\mathbf{\Sigma}}_{\mathbf{H}})\vec{\varsigma} - \vec{\varsigma}^{\,\dagger}\vec{\varsigma}. \tag{28}$$

This formulation makes explicit that the generation of acoustic energy by a two-port is related to the non-unitary character of its scattering matrix $\mathbf{\Sigma}$: Production $P_{\mathrm{gen}} = 0$ if the scattering matrix is unitary, i.e. if its adjoint is equal to its inverse, $\mathbf{\Sigma}^{\dagger} = \mathbf{\Sigma}^{-1}$.

Acoustic states that correspond to maximal (or minimal) generation of acoustic energy can be identified by determining the

eigenvectors $\vec{\varepsilon}_i$ and eigenvalues $\lambda_i, i = 1, 2$ of the energy amplification matrix $\mathbf{H} \equiv \mathbf{\Sigma}^\dagger \mathbf{\Sigma}$. Following Aurégan and Starobinski [19], the sum of the energy of the incoming waves is conveniently normalized to unity, $\|\vec{\varsigma}\|_2 = 1$. Then the energy of the outgoing waves is equal to the value of the quadratic form $\vec{\varsigma}^\dagger \mathbf{H} \vec{\varsigma}$ on the unit sphere, which can be reduced to a sum of squares:

$$\vec{\varsigma}^\dagger \mathbf{H} \vec{\varsigma} = \sum_{i=1}^{2} \lambda_i \mid \eta_i \mid^2. \tag{29}$$

The energy amplification matrix $\mathbf{H}$ is positive definite and symmetric. Thus its eigenvectors $\vec{\varepsilon}_i$ are orthogonal, the left and right eigenvectors are identical and all eigenvalues λ_i are real and positive. Note that the eigenvalues λ_i of the energy amplification matrix $\mathbf{H}$ are equivalent to the squares of the singular values of the energy scattering matrix $\mathbf{\Sigma}$.

The acoustic energy balance at a two-port may be visualized as follows: Let

$$\mathbf{U} = \begin{pmatrix} \vec{\varepsilon}_1 \\ \vec{\varepsilon}_2 \end{pmatrix} \tag{30}$$

denote the unitary matrix that diagonalizes the scattering matrix, $\mathbf{U}^\dagger \mathbf{H} \mathbf{U} = \mathrm{diag}(\lambda_{\max}, \lambda_{\min})$, and let $\vec{\eta} \equiv \mathbf{U}^\dagger \vec{\varsigma}$. The unit sphere in variables $\vec{\varsigma}$ – i.e. all acoustic states with incoming acoustic power P_{in} normalized to unity – is mapped by $\mathbf{U}$ to a unit sphere in variables $\vec{\eta}$. The scattering of acoustic waves corresponds to stretching (generation) or shrinking (dissipation) of the acoustic state vector, the eigenvectors $\vec{\varepsilon}$ identify the states that result in maximal or minimal amplification of acoustic energy, see Fig. 4. All other possible acoustic states are linear combinations of the two orthonormal eigenvectors $\vec{\varepsilon}_1$ and $\vec{\varepsilon}_2$.

An eigenvalue $\lambda = 1$ would correspond to zero net generation of acoustic energy $P_{\mathrm{gen}} = 0$, eigenvalues larger (smaller) than unity represent generation (dissipation) of acoustic energy. The first eigenvalue $\lambda_{\max}$ of the matrix $\mathbf{H}$, gives the largest possible value of outgoing acoustic energy (maximum amplification) for all normalized acoustic signal states $\vec{\varsigma}$ with $\|\vec{\varsigma}\|_2 = 1$. The second eigenvalue $\lambda_{\min}$ corresponds to minimum outgoing energy (maximum dissipation). Obviously, a (thermo-) acoustic system may go unstable only if at least one of its two-ports has an eigenvalue $\lambda_{\max} > 1$. This condition is necessary, but not sufficient for instability to occur – dissipation of acoustic energy by other two-ports may exceed the generation – thus one may speak of "instability potentiality".

Keep in mind that the energy scaled scattering matrix $\mathbf{\Sigma}$ depends on frequency, thus all quantities deduced from it, in particular the eigenvalue λ_{max} are also functions of frequency.

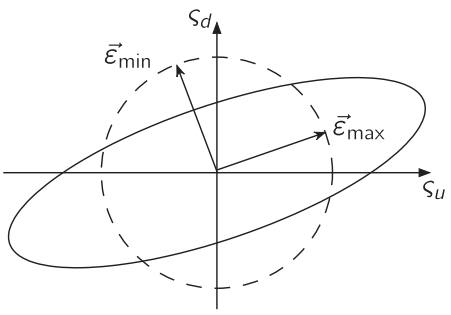

Fig. 4. Signal states on the unit sphere (dashed line) with $\|\vec{\varsigma}\|_2 = 1$ are mapped to states $\vec{\varrho} = \mathbf{\Sigma}\vec{\varsigma}$ (continuous line). The eigenvectors $\vec{\varepsilon}$ indicate which signal states give maximal/minimal amplification of acoustic energy.

3.2. Sound power balance of the $n - \tau$ model

As the common denominator Ω may be factored out of the scattering matrix of the flame in Eq. (13), poles of the scattering matrix $\mathbf{S}_f$ are also poles of the energy scaled scattering matrix $\mathbf{\Sigma}_f$.

$$\mathbf{S}_f = \frac{1}{\Omega}\tilde{\mathbf{S}}_f \rightarrow \mathbf{\Sigma}_f = \frac{1}{\Omega}\tilde{\mathbf{\Sigma}}_f \tag{31}$$

When computing the quadratic form $\mathbf{H}_f$, the matrix retains the common denominator Ω^2

$$\mathbf{H}_f = \frac{1}{\Omega^2}\tilde{\mathbf{H}}_f; \quad \tilde{\mathbf{H}}_f = \tilde{\mathbf{\Sigma}}_f^\dagger \tilde{\mathbf{\Sigma}}_f \tag{32}$$

and thus eigenfrequencies and poles of the scattering matrix are also maxima in amplification of perturbation energy.

Figure 5 shows the maximum acoustic power amplification eigenvalue λ_{max} of the $n - \tau$ model for a value of the relative temperature increment $\theta = 2$, which corresponds to an intrinsically stable flame. Repeated peaks in acoustic power amplification are observed at the respective eigenfrequencies $\omega_z/(2\pi) = 0.5 + 1z$ of the $n - \tau$ flame model, see Eq. (18). In the light of the above discussion of the intrinsic feedback structure of a velocity sensitive premixed flame, the interpretation of this result is quite straightforward: Near-resonance response of the flame to external excitation results in large amplification of acoustic energy.

3.3. Small gain theorem

Consider a combustion system partitioned into the combustion chamber section containing the flame (f) and upstream and downstream boundary conditions (bc) as sketched in Fig. 6. The reflections of acoustic waves up- and downstream (R_u, R_d) of the flame can be expressed as a diagonal scattering matrix $\mathbf{S}_{bc}$:

$$\begin{pmatrix} f_u \\ g_d \end{pmatrix} = \underbrace{\begin{pmatrix} R_u & 0 \\ 0 & R_d \end{pmatrix}}_{\mathbf{S}_{bc}} \begin{pmatrix} g_u \\ f_d \end{pmatrix}, \tag{33}$$

The scattering matrix of the flame $\mathbf{S}_f$ is described in Eq. (13). The entire open loop scattering matrix $\mathbf{S}_{ol}$ is the matrix of transfer functions that maps the characteristic wave amplitudes traveling into the flame domain onto themselves:

$$\begin{pmatrix} f_u \\ g_d \end{pmatrix} = \underbrace{\mathbf{S}_{bc}\mathbf{S}_f}_{\mathbf{S}_{ol}} \begin{pmatrix} f_u \\ g_d \end{pmatrix}. \tag{34}$$

The eigenfrequencies of the system may be determined from the characteristic equation:

$$\det(\mathbf{S}_{bc}\mathbf{S}_f - \mathbf{I}) = 0, \tag{35}$$

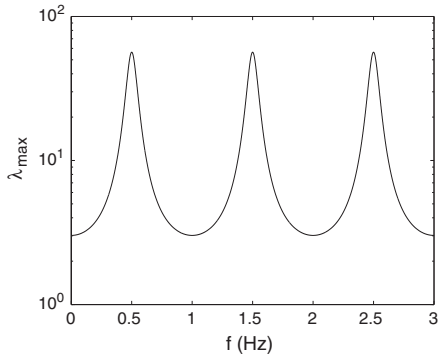

Fig. 5. Maximum energy amplification factor λ_{max} of the $n - \tau$ flame model ($\theta = 2$).

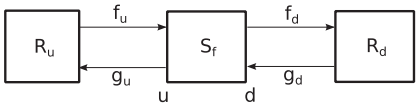

Fig. 6. Combustion system consisting of up and downstream reflection factors (R_u, R_d) and the flame scattering matrix $\mathbf{S}_f$.

which is, however, only possible if the boundary conditions as expressed through $\mathbf{S}_{bc}$ are known.

The small gain theorem allows to state a stability criterion for the interconnected system using only minimal assumptions on $\mathbf{S}_{bc}$. It states that a system is stable if all subsystems $(\mathbf{S}_{bc}, \mathbf{S}_f)$ are stable and the maximum gain $\gamma(\cdot)$ of the entire open loop system is less than unity for all frequencies:

$$\gamma(\mathbf{S}_{bc}\mathbf{S}_f) \leqslant \gamma(\mathbf{S}_{bc})\,\gamma(\mathbf{S}_f) < 1. \tag{36}$$

The norm γ which defines the gain only needs to satisfy some very general restrictions. Because of its ease of physical interpretation, it is convenient to use the maximum acoustic power amplification of the subsystems – i.e. the instability potentiality as introduced above – as a norm for the gain.

$$\gamma(\cdot) = \lambda_{max} = \max(\mathrm{eig}(\mathbf{H})) = \left(\|\mathbf{\Sigma}\|_\infty\right)^2. \tag{37}$$

The maximum eigenvalue of the acoustic power amplification matrix $\mathbf{H}$ is equivalent to the square of the maximum singular value of the energy scattering matrix $\mathbf{\Sigma}$. In control theory, the maximum singular value is known as the H_∞ norm, whereas it is known as spectral norm in mathematics.

The acoustic power of a unit input vector of acoustic invariants to the flame system is at maximum amplified by the maximum eigenvalue $\lambda_{f,max}$ of the $\mathbf{H}_f$ potentiality matrix. The same accounts for the boundary system and the stability criterion becomes:

$$\lambda_{f,max}\,\lambda_{bc,max} < 1 \tag{38}$$

In the limiting case of the minimal assumption of energy preserving, passive boundaries $(\lambda_{bc,max} = 1)$, the maximum eigenvalue of the flame potentiality matrix would need to be less than unity for all frequencies $\lambda_{f,max} < 1$ in order to ensure stability.

As the example of a premixed turbulent combustor in Section 4 will show, this restriction is met very rarely because the small gain theorem is very conservative.

Nevertheless it may give the opportunity to deduce burner design objectives even at a very early stage of development, when the acoustic properties of the subsystems (f, bc) are not known entirely, yet. By minimization of the instability potentiality $\lambda_{f,max}$, the burner designs may be optimized for minimum amplification of acoustic energy. For a smaller acoustic energy amplification, less damping by the boundaries $\lambda_{bc,max}$ is needed in order to ensure stability. Thus, minimizing $\lambda_{f,max}$ should enhance stability.

The more information on the acoustics of the combustion system becomes available, the less conservative the stability criterion becomes. If burner and flame scattering matrix are known, $\mathbf{S}_f$ can be replaced by $\mathbf{S}_{bf}$ instead of contributing the effect of the burner to the unknown boundaries. If eventually all elements of the system are known, the open loop scattering matrix of Eq. (34) is fully specified. Instead of directly solving for the eigenvalues of the closed system, one of the variables (f_u, g_d) may be eliminated. The resulting open loop transfer function may then be analyzed by a complex plane plot and the stability criterion developed by and named after Nyquist [36].

Here the connection between the small gain theorem and the Nyquist stability criterion becomes apparent: If the gain of the open loop transfer function (OLTF) is strictly less than 1, the critical point cannot be encircled by the path of the OLTF in the Nyquist plot.

The restriction to stable subsystems $(\mathbf{S}_{bc}, \mathbf{S}_f)$, again similar to the Nyquist criterion, is usually not limiting. The acoustic modes without flame interaction are stable and the inherent eigenmodes of the flame without acoustic boundary conditions are, in all physical meaningful cases we investigated, stable as well. The instability of thermoacoustic systems observed is established by the coupling between flame and acoustics.

4. Case study: turbulent premixed swirl flame

In this section, the amplification of acoustic power due to intrinsic resonance of a velocity sensitive premixed flame and related stability criteria, i.e. the instability potentiality and the small gain theorem, are scrutinized for a turbulent premixed swirl flame. The configuration under consideration is the "TD1 burner", which has been investigated extensively at the Lehrstuhl für Thermodynamik, both experimentally and numerically [50,51,34]. The burner, which is rated at approximately 60 kW, has a tangential swirl generated, followed by an annular flow passage with a centerbody. The flame is stabilized downstream of a sudden expansion in cross-sectional area, thanks to a recirculation zone that forms downstream of the centerbody in the swirling flow.

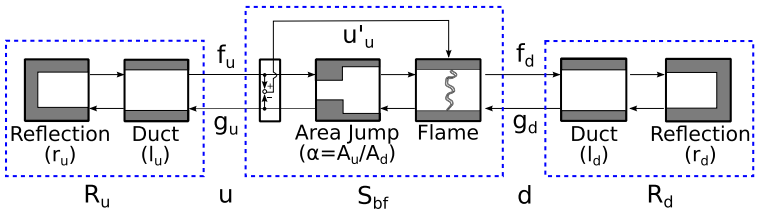

Fig. 7. Network model of the TD1 combustor.

Table 1
Parameters of the TD1 combustor network- and flame model.

l_u (m)	l_d (m)	$\lvert r_u\rvert$ (–)	$\lvert r_d\rvert$ (–)	α (–)	Ma_u (–)	c_u (m s^{-1})
$[0, 4.73]$	$[0, 10.67]$	$\{0, 0.0563\}$	$\{0, 0.0563\}$	0.294	0.0282	355
a (–)	τ_1 (m s^{-1})	σ_1 (m s^{-1})	τ_2 (m s^{-1})	σ_2 (m s^{-1})	ξ (–)	θ (–)
0.827	3.17	0.863	12.4	2.70	2.25	4.08

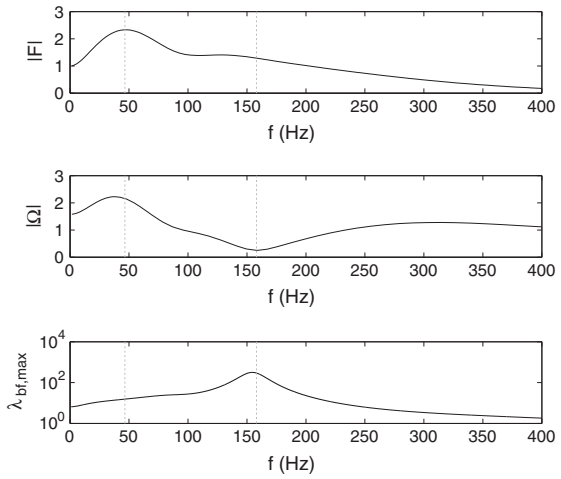

Fig. 8. Frequency response of the flame transfer function F, denominator Ω and maximum sound power amplification $\lambda_{bf,max}$.

The area expansion is acoustically modeled by a simplified scattering matrix, see e.g. Polifke [27], which takes into account only the effect of the change in cross-sectional area $\alpha = A_u/A_d$ on the acoustic velocities. The burner layout also implies that the reference velocity u'_u for the flame transfer function Eq. (2) and subsequently the flame model Eq. (11) is not located directly upstream of the flame, but inside the burner nozzle just upstream of the area jump. A sketch of the thermoacoustic network model used in this investigation is depicted in Fig. 7, the parameters of the geometry are listed in Table 1.

The flame transfer function $F(s)$ is modeled by the following expression:

$$F = (1+a)\,e^{(-s\,\tau_1 - \frac{s^2\sigma_1^2}{2})} - a\,e^{(-s\,\tau_2 - \frac{s^2\sigma_2^2}{2})} \tag{39}$$

Previous studies conducted by Lawn and Polifke [52], Schuermans et al. [53] and Hirsch et al. [54] have shown that this functional form of the flame transfer function in combination with the Rankine–Hugoniot jump equations reproduces quite well the flame dynamics of typical turbulent premixed swirl burners. Furthermore, this form ensures the correct value $|F| \to 1$ in the limit of low frequencies Polifke and Lawn [35]. The parameters for the TD1 flame considered in the present paper are also listed in Table 1. The gain $|F|$ of the flame transfer function is shown in Fig. 8 (top). It exhibits a characteristic local maximum in gain ("excess gain") at a frequency of around 50 Hz and then decays at higher frequencies.

Figure 9 depicts the absolute values of the coefficients of the scattering matrix $\mathbf{S}_{bf}$ of the acoustic system composed of burner and flame. The reference positions of the scattering matrix upstream (u) and downstream (d) are marked in the system sketch (Fig. 7). Remarkably, all four coefficients show typical resonance peaks at a frequency of $f_{res} = 150$ HZ Similar peaks were already observed by Gentemann and Polifke [34], who pointed out that the maxima in $|S_{ij}|$ coincide with minima of the common denominator Ω of the scattering matrix, see Eq. (10). Indeed, such a minimum is also observed in the present case, see Fig. 8, middle plot. However, while a proper physical explanation of these observations was not developed by Gentemann and Polifke [34], the large reflection and transmission coefficients at 150 HZ can now be interpreted physically as a near-resonant response of the flame to the incident acoustic excitation, where "resonant" refers, of course, to the intrinsic eigenmodes of the flame. This interpretation is strengthened further by re-writing the factor Ω such that its relation to the open loop transfer function of burner and flame is made explicit:

$$\Omega = (\xi+1)\left(1 + \underbrace{\frac{\theta\alpha}{\xi+1}F(s)}_{\text{OLTF}}\right) \tag{40}$$

Clearly, resonance $\Omega \to 0$ will occur as the OLTF approaches the critical point "-1". For the present configuration of burner and flame, with a flame transfer function according to Eq. (39) and model parameters as listed in Table 1, the Nyquist plot Fig. (10) shows indeed that at frequencies near 150 Hz the OLTF curve approaches the critical point. Following the Nyquist criterion, the

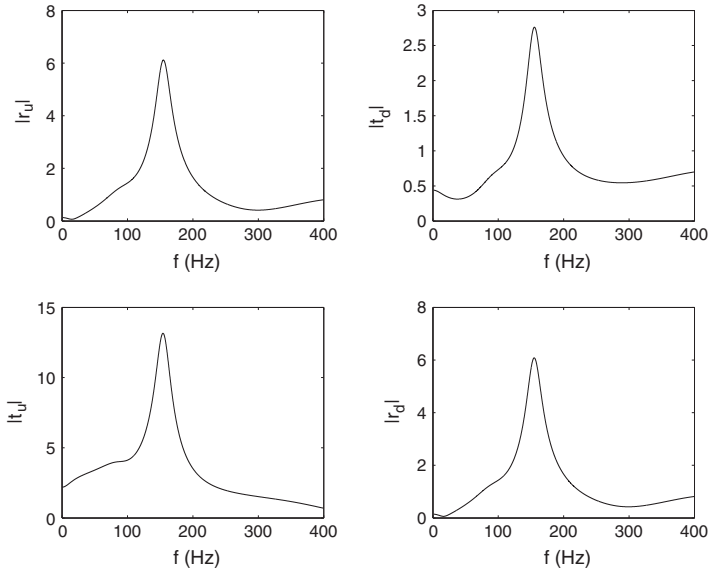

Fig. 9. Scattering matrix, computed from network model using analytical flame transfer function. Mind the different Y-scales.

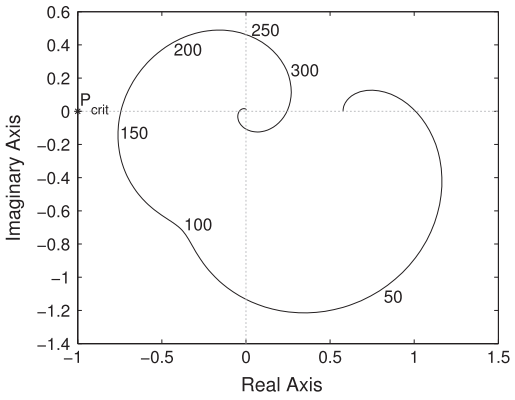

Fig. 10. Nyquist plot of the open loop transfer function OLTF(s) of the burner model.

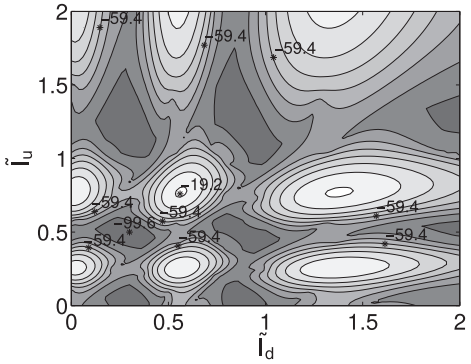

Fig. 11. Maximum growth rates of the modeled combustion system as a function of nondimensionalized duct lengths up- and downstream for stable reflection factors $r_u = r_d = 0.0563$. Numbers indicate the values on isolines.

flame is intrinsically stable, because the critical point is not encircled by the OLTF.

Correspondingly the maximum eigenvalue $\lambda_{bf,max}$ of the acoustic power amplification matrix $\mathbf{H}_{bf}$ peaks at 150 HZ (Fig. 8). Energy generation $\lambda_{bf,max}$ is larger than unity throughout the frequency range observed and peaks at a value $\max(\lambda_{bf,max}) \approx 315$ (!). Thus, the flame is able to produce acoustic energy throughout all frequencies, and in particular so at 150 Hz.

Considering Figs. 8–10 in the light of the arguments put forward in Section 3.2, one concludes that the peaks in scattering matrix coefficients $|r_u|, |t_d|, |t_u|, |r_d|$ and in acoustic power amplification λ_{max} are not due to excess gain of the flame transfer function $F(s)$, but due to the intrinsic feedback loop and the associated resonance, manifested as the minimum in Ω at 150 Hz.

Now we turn to the small gain theorem and its consequences for the present configuration. The boundary scattering Matrix $\mathbf{S}_{bc}$ is

$$\mathbf{S}_{bc} = \begin{pmatrix} r_u e^{-s\,2l_u/c_u} & 0 \\ 0 & r_d e^{-s\,2l_d/c_d} \end{pmatrix} \tag{41}$$

When evaluating the quadratic form $\mathbf{H}_{bc}$, the complex exponentials drop out and the maximum acoustic power amplification of the boundary is:

$$\gamma(\mathbf{S}_{bc}) = \lambda_{bc,max} = \max(r_u^2, r_d^2) \tag{42}$$

By evaluating the small gain stability criterion, a conservative limit for the reflection factors at the boundaries can be determined:

$$r_{u,d} < \sqrt{\frac{1}{\max(\lambda_{bf,max})}} \approx 0.0563. \tag{43}$$

For the given value of stable reflection factors $r_u = r_d = 0.0563$, a stability map of the combustion system is shown in Fig. 11. The maximum growth rate (smallest damping rate) is plotted as a function of the nondimensionalized lengths of the duct sections up- and downstream of the flame. The lengths were varied between 0 and about two times the wave lengths inside the respective ducts at the critical frequency of $f_{res} = 150$ HZ $\tilde{l} = lf_{res}/c$. In agreement with the small gain stability criterion, we observe that the system is stable for all parameters investigated with a maximum growth rate observed of -13.3. There are three resonant duct lengths up and downstream and maximum growth rates are observed when both duct sections are tuned to be resonating. Apparently, a resonance of one duct section can be damped by the other section if the corresponding length is set to a non-resonating length.

5. Conclusion

The thermoacoustic stability of velocity sensitive premixed flames was scrutinized. A causal representation of the acoustic-flow-flame-acoustic interactions revealed an intrinsic feedback mechanism: if an upstream velocity disturbance induces a modulation of the heat release rate, an acoustic wave will be generated that travels in the upstream direction, where it influences in turn the acoustic velocity, such that a closed feedback loop results.

Even if the *intrinsic eigenmodes* of the flame, which result from this feedback loop are stable, the flame system has peaks in its acoustic energy amplification when excited at resonant frequencies. This was shown rigorously by evaluating the "instability potentiality" from a balance of acoustic energy across the flame. One obtains factors of maximum (as well as minimum) power amplification over all possible acoustic states. The relation of maximum power amplification to peaks in the scattering matrix coefficients and the open loop transfer function of the internal flame dynamics was also elaborated.

Based on the acoustic power amplification, the small gain theorem was introduced and a corresponding energy-based stability criterion was formulated. Given passive boundaries, the gain – which is equivalent to the maximum sound power amplification – must be less than unity for all frequencies to ensure stability. The small gain theorem requires only minimal a priori assumptions on upstream and downstream acoustic boundary conditions.

The concepts were exemplified first with a simplistic $n-\tau$ model and then with a flame transfer function that is representative of turbulent swirl burners. It should be appreciated, however, that application of the ideas and methods developed here are not restricted to these configurations. Acoustic-flow-flame-acoustic interactions that involve fluctuations of equivalence ratio or a pressure sensitive flame transfer function should in general also exhibit intrinsic feedback, with similar consequences for amplification of acoustic power and combustor dynamics as presented here. The causal mechanisms involved in a pressure sensitive response of the flame may be resonances of an acoustically "soft" injection system as described by Huber and Polifke [55], or autoignition [56]. The impact of those processes on the flame intrinsic eigenmodes needs to be scrutinized and validated in future research, which involves numerical and experimental investigations yet to be done.

It is apparent that frequencies, where the acoustic power amplification of the flame is very high, may be critical frequencies for the stability of a combustion system. More research and a validation with experiments regarding critical burner frequencies are needed. First results have been presented by Bomberg et al. [16].

The small gain stability criterion is very conservative and therefore not immediately useful for stability prediction in an applied context. Nevertheless, it may be used as an optimization objective and comparison benchmark for combustor stability. Further studies to evaluate the effectiveness of this method are needed.

Furthermore, the small gain theorem is valid also for a large class of nonlinear systems. Thus an extension and application to nonlinear flame models seems possible and will be the subject of future research.

Acknowledgements

The authors acknowledge financial support by the German Research Foundation DFG, Project PO 710/12–1 and the Technische Universität München – Institute for Advanced Study, funded by the German Excellence Initiative.

Appendix A. Dynamic system of the flame model ($> \mathcal{O}(\boldsymbol{M}^{\mathbf{0}})$)

The flame transfer function according to linearized Rankine–Hugoniot equations including effects of Mach numbers:

$$\begin{bmatrix} \frac{p'}{\rho c_d} \\ u'_d \end{bmatrix} = \begin{bmatrix} \xi & -\theta M_d \\ -\gamma\theta M_u & 1 \end{bmatrix} \begin{bmatrix} \frac{p'}{\rho c_u} \\ u'_u \end{bmatrix} + \begin{bmatrix} -M_d \\ 1 \end{bmatrix} \left(\frac{T_d}{T_u} - 1\right) \bar{u}_u \frac{\dot{Q}'}{\dot{Q}} \tag{A.1}$$

Transformation to scattering matrix representation including full equations:

$$\begin{bmatrix} g_u \\ f_d \end{bmatrix} = \frac{1}{\xi + \theta M_d + \gamma\theta M_u + 1} \cdot \tag{A.2}$$

$$\begin{bmatrix} -\xi - (-\theta M_d) + (-\gamma\theta M_u) + 1 & 2 \\ 2 * (\xi - \theta M_d \gamma\theta M_u) & \xi + \theta M_d - \gamma\theta M_u - 1 \end{bmatrix} \begin{bmatrix} f_u \\ g_d \end{bmatrix} \tag{A.3}$$

$$+ \frac{\left(\frac{T_d}{T_u} - 1\right)}{\xi + \theta M_d + \gamma\theta M_u + 1} \begin{bmatrix} M_d + 1 \\ -M_d(\gamma\theta M_u + 1) + (\xi + \theta M_d) \end{bmatrix} F \bar{u}_u \frac{f_{ref} - g_{ref}}{\bar{u}_{ref}} \tag{A.4}$$

Appendix B. Derivation of the eigenvalues of the $n - \tau$ flame model

$$e^{-s\tau} = e^{-\lambda\tau}(\cos(-\omega\tau) + j\sin(-\omega\tau)) = e^{-\lambda\tau}(\cos(\omega\tau) - j\sin(\omega\tau)) = -\frac{1+\xi}{n\theta} \tag{B.1}$$

Imaginary part (integers k introduced):

$$\sin(\omega\tau) = 0 \tag{B.2}$$

$$\omega_k = \frac{k\pi}{\tau} \tag{B.3}$$

Real part:

$$\underbrace{e^{-\lambda\tau}(\cos(\frac{k\pi}{\tau}\tau)}_{=(-1)^k} = -\frac{1+\xi}{n\theta} \tag{B.4}$$

$$e^{\lambda\tau} = (-1)^{k+1}\frac{n\theta}{1+\xi} \tag{B.5}$$

λ and τ are real numbers, $\frac{n\theta}{1+\xi} > 0$ thus solutions only exist for $(-1)^{k+1} > 0$ and the exponent needs to be even $k + 1 = 2(z + 1) = 2z + 2$ with

$$\lambda_k = \frac{1}{\tau}\ln\left(\underbrace{(-1)^{2z+2}}_{=1}\frac{n\theta}{1+\xi}\right) \tag{B.6}$$

$$\lambda_z = \lambda = \frac{1}{\tau}\ln\left(\frac{n\theta}{1+\xi}\right) \tag{B.7}$$

The growth rate λ is the same for all eigenfrequencies. And eigenfrequencies exist for:

$$\omega_z = \frac{(2z+1)\pi}{\tau} \tag{B.8}$$

The complex eigenfrequencies s_z of the inherent eigenmodes of the $n - \tau$ model are:

$$s_z = j\underbrace{\frac{(2z+1)\pi}{\tau}}_{\omega_z} + \underbrace{\frac{1}{\tau}\ln\left(\frac{n\theta}{1+\xi}\right)}_{\lambda}. \tag{B.9}$$

Appendix C. Characteristic equation of the flame model

The characteristic equation $\Omega = 0$:

$$F = -\frac{1+\xi}{\theta} \tag{C.1}$$

Eliminating ξ using ideal gas law as it was done by Polifke [20] ($\theta = \xi^2 - 1$):

$$\xi = \sqrt{\theta + 1} \tag{C.2}$$

and the definition of θ

$$\theta = \frac{T_d}{T_u} - 1 \tag{C.3}$$

in Eq. (C.1)

$$F = -\frac{1+\sqrt{\theta+1}}{\theta} = -\frac{1+\sqrt{\frac{T_d}{T_u}}}{\left(\sqrt{\frac{T_d}{T_u}}\right)^2 - 1} = -\frac{1}{\sqrt{\frac{T_d}{T_u}} - 1}. \tag{C.4}$$

References

[1] F.A. Williams, Combustion Theory, second ed., Addison-Wesley Publishing Company, 1985.
[2] B. Lewis, G. von Elbe, Combustion, Flames, and Explosion of Gases, third ed., Academic Press, New York, 1987.
[3] P. Clavin, Prog. Energy Combust. Sci. 11 (1985) 1–59.
[4] J. Buckmaster, Annu. Rev. Fluid Mech. 25 (1993) 21–53.
[5] M. Matalon, Annu. Rev. Fluid Mech. 39 (2007) 163–191.
[6] M. Kröner, J. Fritz, T. Sattelmayer, J. Eng. Gas Turb. Power 125 (2003) 693–700.
[7] S.K. Aggarwal, Progr. Energy Combust. Sci. 35 (2009) 528–570.
[8] D.E. Cavaliere, J. Kariuki, E. Mastorakos, Flow Turbul. Combust. 91 (2013) 347–372.
[9] J.W.S. Rayleigh, Nature 18 (1878) 319–321.
[10] J.J. Keller, AIAA J. 33 (1995) 2280–2287.
[11] T. Lieuwen, V. Yang, Combustion instabilities in gas turbine engines: operational experience, fundamental mechanisms, and modeling, in: Progress in Astronautics and Aeronautics, AIAA, 2006 (Number ISBN 156347669X).
[12] W.C. Strahle, J. Fluid Mech. 49 (1971) 399–414.
[13] A. Dowling, J. Sound Vib. 180 (1995) 557–581.
[14] M. Hoeijmakers, V. Kornilov, I. Lopez Arteaga, P. de Goey, H. Nijmeijer, Combust. Flame (2014).
[15] M. Hoeijmakers, I. Lopez Arteaga, V. Kornilov, H. Nijmeijer, P. de Goey, in: Proceedings of the European Combustion Meeting, Lund, Sweden, 2013.
[16] S. Bomberg, T. Emmert, W. Polifke, in: 35th International Symposium on Combustion, The Combustion Institute, San Franciso, CA, USA, 2014.
[17] N. Noiray, D. Durox, T. Schuller, S. Candel, Proc. Combust. Inst. 31 (2007) 1283–1290.
[18] T. Komarek, W. Polifke, J. Eng. Gas Turb. Power 132 (2010). 061503-1,7.
[19] Y. Aurégan, R. Starobinski, Acta Acust. United Acust. 85 (1999) 5.
[20] W. Polifke, in: European Combustion Meeting, ECM2011, British Section of the Combustion Institute, Cardiff, UK, 2011.
[21] G. Zames, IEEE Trans. Autom. Control 11 (1966) 228–238.
[22] D.L. Straub, G.A. Richards, Int. Gas Turbine & Aeroengine Congress & Exhibition, ASME; 1999.
[23] P. Palies, D. Durox, T. Schuller, S. Candel, J. Fluid Mech. 672 (2011) 545–569.
[24] R.S. Blumenthal, P. Subramanian, R. Sujith, W. Polifke, Combust. Flame 160 (2013) 1215–1224.
[25] S. Jaensch, T. Emmert, W. Polifke, in: Proceedings of ASME Turbo Expo 2014, GT2014-27034, Düsseldorf, Germany, 2014.
[26] M.L. Munjal, Acoustics of Ducts and Mufflers, John Wiley & Sons, 1987.

[27] W. Polifke, in: Schram, C. (Ed.), Advances in Aero-Acoustics and Thermo-Acoustics, Van Karman Institute for Fluid Dynamics, Rhode-St-Genèse, Belgium, 2010.
[28] L. Tay-Wo-Chong, S. Bomberg, A. Ulhaq, T. Komarek, W. Polifke, J. Eng. Gas Turb. Power 134 (2012). 021502-1-8.
[29] B.T. Chu, vol. 4, 1953, pp. 603–612.
[30] J. Kopitz, W. Polifke, J. Comp. Phys 227 (2008) 6754–6778.
[31] T. Schuller, D. Durox, S. Candel, Combust. Flame 134 (2003) 21–34.
[32] C.O. Paschereit, B.B.H. Schuermans, W. Polifke, O. Mattson, J. Eng. Gas Turb. Power 124 (2002) 239–247 (Originally published as ASME 99-GT-133).
[33] W. Polifke, A.M.G. Gentemann, Int. J. Acoust. Vib. 9 (2004) 139–148.
[34] A. Gentemann, W. Polifke, in: Int'l Gas Turbine and Aeroengine Congress & Exposition, ASMEGT2007-27238, Montreal, Quebec, Canada, 2007.
[35] W. Polifke, C.J. Lawn, Combust. Flame 151 (2007) 437–451.
[36] H. Nyquist, Bell Syst. Tech. J. (1932) 1–24.
[37] B.T. Chu, Acta Mech. (1964) 215–234.
[38] H.R. Cantrell, R.W. Hart, F.T. McClure, AIAA 2 (1964) 1100–1105.
[39] C.L. Morfey, J. Sound Vib. 14 (1971) 159–170.
[40] M.K. Myers, J. Fluid Mech. 226 (1991) 383–400.
[41] A. Giauque, T. Poinsot, M. Brear, F. Nicoud, in: Proc. of the Summer Program, 2006, pp. 285–297.
[42] M.J. Brear, F. Nicoud, M. Talei, A. Giauque, E.R. Hawkes, J. Fluid Mech. 707 (2012) 53–73.
[43] K.J. George, R. Sujith, J. Sound Vib. 331 (2012) 1552–1566.
[44] A.M. Lyapunov, A.T. Fuller, The General Problem of the Stability of Motion, Tayor & Francis, London, Washington, DC, 1992.
[45] N. Rouche, P. Habets, M. LaLoy, Stability Theory by Liapunov's Direct Method, Number 22 in Applied Mathematical Sciences, Springer-Verlag, New York, 1977.
[46] P. Subramanian, R.I. Sujith, J. Fluid Mech. 679 (2011) 315–342.
[47] R.S. Blumenthal, A.K. Tangirala, R. Sujith, W. Polifke, in: n3l Workshop on Non-Normal and Nonlinear Effects in Aero- and Thermoacoustics, Munich, Germany, 2013.
[48] K. Wieczorek, C. Sensiau, W. Polifke, F. Nicoud, Phys. Fluids 23 (2011). 107013-1-14.
[49] A.P. Dowling, J.E. Ffowcs Williams, Sound and Sources of Sound, Ellis Horwood Limited, 1983.
[50] W. Polifke, A. Fischer, T. Sattelmayer, J. Eng. Gas Turb. Power 125 (2003) 20–27. Originally published as ASME2001-GT-35.
[51] A.M.G. Gentemann, C. Hirsch, K. Kunze, F. Kiesewetter, T. Sattelmayer, W. Polifke, in: Int'l Gas Turbine and Aeroengine Congress & Exposition, ASME GT-2004-53776, Vienna, Austria, 2004.
[52] C.J. Lawn, W. Polifke, Comb. Sci. Tech. 176 (2004) 1359–1390.
[53] B. Schuermans, V. Bellucci, F. Guethe, F. Meili, P. Flohr, O. Paschereit, 2004.
[54] C. Hirsch, D. Fanaca, P. Reddy, W. Polifke, T. Sattelmayer, in: Int'l Gas Turbine and Aeroengine Congress & Exposition, ASMEGT2005-68195 , Reno, NV, USA, 2005.
[55] A. Huber, W. Polifke, Int. J. Spray Comb. Dyn. 1 (2009) 199–250.
[56] M. Zellhuber, B. Schuermans, W. Polifke, Combust. Theory Modell. 18 (2014) 1–31.

Acoustic and Intrinsic Thermoacoustic Modes of a Premixed Combustor

T. Emmert, S. Bomberg, S. Jaensch, W. Polifke*

Professur für Thermofluiddynamik
Technische Universität München
D-85747, Garching, Germany

Abstract

Premixed flames are velocity sensitive, i.e. they react to a velocity perturbation at the burner mouth, say, with fluctuations in heat release rate. Unsteady heat release generates acoustic waves that travel back from the flame to the burner mouth, where they modulate the velocity and thereby close an *intrinsic thermoacoustic* (ITA) feedback loop. The present paper demonstrates that corresponding ITA eigenmodes are in general important for the dynamics and stability of premixed combustion systems. It is shown that the complete set of eigenmodes of a combustor test rig should be interpreted as the sum of acoustic and ITA eigenmodes. A procedure is presented which allows to distinguish between eigenmodes that may be considered as acoustic modes driven by the flame, versus those resulting from ITA feedback (but influenced by the acoustic properties of the combustor). This procedure is based on a factorization of the dispersion relation of the thermoacoustic model. Differences between the acoustic and intrinsic eigenmodes of a combustor test rig, in particular the corresponding mode shapes, are discussed. The paradoxical observation that increased acoustic losses at the boundaries may destabilize a combustion system is explained as an instability of the dominant ITA mode.

Keywords
intrinsic thermoacoustic feedback, premixed flame, thermoacoustics, combustion dynamics

1. Introduction

Thermoacoustic stability of combustion systems as diverse as gas turbines and domestic burners is important for emissions, noise and wear. Such devices possess acoustic modes (also known as "cavity modes"), which may be attenuated or amplified by the unsteady heat release. According to Rayleigh [1], the amplification is driven by heat release fluctuations in phase with pressure oscillations. The common perception is that instability occurs due to acoustic eigenmodes becoming unstable if the driving by the flame exceeds the damping by acoustic losses inside the device and at the boundaries [2].

Recently it was discovered that premixed flames can exhibit thermoacoustic instability even if non-reflective boundary conditions enforce that resonant acoustic modes cannot exist [3, 4, 5]. Bomberg et al. [6] identified the mechanism causing such instabilities as an intrinsic thermoacoustic (ITA) feedback, illustrated by Figure 3b. This mechanism may be summarized as follows: Premixed flames are *velocity sensitive*, i.e. they react with fluctuations in heat release to a perturbation of velocity at an upstream location, say at the burner mouth. Heat release fluctuations act as a volume source and generate upstream traveling acoustic waves, which in turn cause upstream velocity perturbations. Even if the ITA modes caused by the feedback are stable, they are associated with the amplification of acoustic power scattered by burner and flame of a system [7]. Therefore, ITA modes may be distinguished from the acoustic modes of the system. Note that they should not be confused with thermo-diffusive intrinsic instabilities of premixed flames.

In this paper we demonstrate that ITA modes are not only encountered in systems of dump combustor geometries with non reflecting boundaries as shown by [3, 4, 5]. They actually may be observed in combustor configurations of applied interest. At first the linear acoustic network model of the investigated combustor test rig as depicted in Fig. 1 is introduced. The pure acoustic modes are obtained by removing the flame dynamics from the full combustor model (Fig. 3a). Strip-

*Corresponding author
Email address: polifke@tfd.mw.tum.de (W. Polifke)
URL: http://www.tfd.mw.tum.de (W. Polifke)

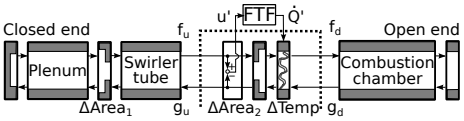

Fig. 1: Scheme of the premixed combustion test rig network model, flow from left to right.

ping the upstream and downstream sections of the full combustor results in a pure ITA system (Fig. 3b). Eventually a procedure is presented that shows how the eigenmodes of the full combustor system relate to the pure acoustic and the pure ITA modes (Fig. 3c). The total number of eigenmodes is exactly equal to the sum of acoustic and ITA modes. The frequency of the dominant ITA mode in the test rig we investigate is within the range, but different from the first two acoustic longitudinal eigenfrequencies. Its mode shape is similar to a combination of both of them. Eventually the paradox that damping of acoustic modes by introducing losses at the boundaries can destabilize a thermoacoustic system – as previously observed in numerical simulation by Silva et al.[5] – is explained as a result of ITA feedback.

2. The Premixed Combustion Test Rig Network Model

Linear, low-order acoustic network models have proven their capability to predict thermoacoustic instabilities in experiment [8, 9, 10, 11] and simulation [5]. By construction, such models take into consideration the relevant interactions between velocity, heat release rate and acoustics and thus capture also the effects of ITA feedback. This justifies the use of a low-order network model to demonstrate the existence and impact of ITA modes on the dynamics of a combustion system with reflective boundaries.

The configuration investigated in the present study is depicted in Figure 1, with model parameters specified in Table 1. It represents a perfectly premixed, single burner test rig that was experimentally investigated by Komarek and Polifke [12]. Tay-Wo-Chong et al. [11] analyzed a similar model of the test rig with a length of the combustion chamber $l_C = 0.7\,\mathrm{m}$. Whereas the model of [11] was a classical frequency domain low order network model, here linear state space models are used, as described by Emmert et al. [13]. Propagation of acoustic waves is modeled by 1D linearized Euler equations, which are spatially discretized using a third order upwind scheme. The frequency range of interest extends to 500 Hz, which is below the cut on frequency of the plenum $f_{co} = 1.84\,c/(2\pi r) \approx 1000\,\mathrm{Hz}$, with

Table 1: Parameters of the test rig network model.

Name	Parameters
Closed end	Reflection coefficient $r_C = 1$
	Inlet: Ma = 0.0011, $c = 343\,\mathrm{m\,s^{-1}}$
	$\rho = 1.2\,\mathrm{kg\,m^{-3}}$
Plenum	Duct, $l_P = 0.17\,\mathrm{m}$
Δ Area 1	Area ratio $\alpha_1 = A_u/A_d\|_1 = 29.76$
Swirler tube	Duct, $l_M = 0.18\,\mathrm{m}$
Δ Area 2	Area ratio $\alpha_2 = A_u/A_d\|_2 = 0.13$
Δ Temperature	Lin. energy equation,
	$\theta = (T_d - T_u)/T_u = 5.59$
	Ratio of specific impedances
	$\xi = \rho_u c_u/\rho_d c_d = 2.57$
Combustion chamber	Duct, $l_C = 0.70\,\mathrm{m}$
Open end	Reflection coefficient r_O = [-1, 0]
FTF	Identified from LES [11], see Fig. 2

$r = 0.10\,\mathrm{m}$. All area changes are modeled as acoustically compact elements without losses or correction factors. The axial swirler is assumed to be acoustically transparent.

As illustrated in Figure 1, the network model can be divided into four parts: the upstream and downstream sections (u,d), the acoustic part of the burner mouth and flame (b), and the unsteady heat release of the flame (f).

2.1. Upstream and Downstream Sections

As Figure 1 shows, the upstream and downstream sections are composite models. The upstream part consists of a closed end, two duct sections of plenum and swirler annulus and an area contraction in between. Downstream there is a duct section that represents the combustion chamber and an open end. Note that [11] imposed on the downstream side the reflection coefficient of a perforated plate, which was estimated to be in the range $R_x \in [-1, 0]$. The dynamics of these two sections are lumped into impedances $Z_u(s)$, $Z_d(s)$:

$$\frac{p}{\bar{\rho}\bar{c}}_u = Z_u(s)u_u\,; \quad \frac{p}{\bar{\rho}\bar{c}}_d = Z_d(s)u_d\,, \tag{1}$$

where $\bar{\rho}, \bar{c}$ are the mean density and speed of sound and p, u the acoustic pressure and velocity fluctuations. The Laplace variable $s = j\omega + \sigma$ is defined by the angular frequency ω and the growth rate σ.

2.2. Burner Mouth and Flame

The burner mouth (see Fig. 3) comprises the area expansion into the combustion chamber and the acoustic flame model. As the distance between the burner mouth and flame $l_f \approx 0.074\,\mathrm{m}$ is much smaller than the wavelength at the maximum frequency of interest 500 Hz: $\lambda = c/f \approx 0.7\,\mathrm{m}$, it is modeled acoustically compact.

The velocity fluctuations at the burner mouth are retrieved as input signal for the heat release model. For simplicity zero Mach number is assumed and the transfer matrix of the area expansion Δ Area$_2$ is:

$$\begin{bmatrix} \frac{p}{\bar{\rho}\bar{c}}_i \\ u_i \end{bmatrix} = \begin{bmatrix} 1 & 0 \\ 0 & \alpha \end{bmatrix} = \begin{bmatrix} \frac{p}{\bar{\rho}\bar{c}}_u \\ u_u \end{bmatrix} \tag{2}$$

with $\alpha_2 = A_u/A_d$ the area ratio between the cross section of the mixing tube and the combustion chamber. An intermediate node $p/(\bar{\rho}\bar{c})_i$, u_i is located between area change and flame.

The acoustic flame model Δ Temp is based on linearized *Rankine Hugoniot* jump equations across a compact heat source [14], [7] with heat release fluctuations:

$$\begin{bmatrix} \frac{p}{\bar{\rho}\bar{c}}_d \\ u_d \end{bmatrix} = \begin{bmatrix} \xi & 0 & 0 \\ 0 & 1 & \theta \end{bmatrix} \begin{bmatrix} \frac{p}{\bar{\rho}\bar{c}}_i \\ u_i \\ \dot{q}' \end{bmatrix} \tag{3}$$

where $\xi = \rho_u c_u/\rho_d c_d$ is the ratio of specific impedances and $\theta = (T_d - T_u)/T_u$ is the normalized temperature ratio. Combining Eq. 2 and Eq. 3, we obtain the burner mouth and flame transfer matrix:

$$\begin{bmatrix} \frac{p}{\bar{\rho}\bar{c}}_d \\ u_d \end{bmatrix} = \begin{bmatrix} \xi & 0 & 0 \\ 0 & \alpha & \theta \end{bmatrix} \begin{bmatrix} \frac{p}{\bar{\rho}\bar{c}}_u \\ u_u \\ \dot{q}' \end{bmatrix}. \tag{4}$$

2.3. Unsteady Heat Release

The model is closed by a flame transfer function (FTF). It relates velocity fluctuations $u_u$at the burner mouth with the normalized global heat release fluctuations of the flame $\dot{q}' = \dot{Q}'\bar{u}_u/\bar{\dot{Q}}$:

$$\dot{q}' = F(s)u_u \tag{5}$$

This FTF is a finite impulse response model that was retrieved from LES simulation of a 30 kW perfectly premixed turbulent swirl flame and system identification (SI) techniques. It was validated against experimental results [11, Fig. 6,7] and its frequency response is shown in Fig. 2.

3. Pure Acoustic, Pure ITA and Full System Modes

Subsequently, the dynamics and stability of the test rig network model are investigated. For this purpose, the eigenmodes of the full linear system are derived. In addition, two simplified systems are investigated. At first, the unsteady heat release is removed from the system in order to obtain *pure acoustic* modes. Then the acoustic reflections at the up- and downstream sections

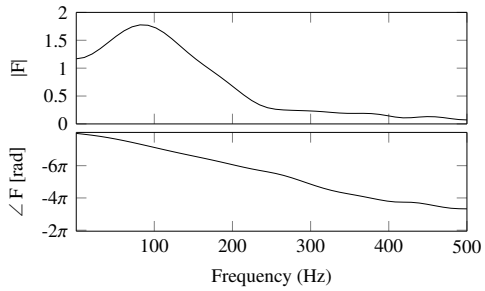

Fig. 2: Frequency response of the FTF.

are suppressed and *pure ITA* modes remain. Finally the corresponding eigenvalues are computed and compared against each other and validated using previously published results.

3.1. Full system modes

In order to solve for the dynamics of the full test rig network model, the equations (1),(4) and (5) are reordered:

$$0 = \underbrace{\begin{bmatrix} -1 & Z_u & 0 & 0 & 0 \\ 0 & 0 & -1 & Z_d & 0 \\ \xi & 0 & -1 & 0 & 0 \\ 0 & \alpha & 0 & -1 & \theta \\ 0 & F & 0 & 0 & -1 \end{bmatrix}}_{A(s)} \begin{bmatrix} \frac{p}{\bar{\rho}\bar{c}}_u \\ u_u \\ \frac{p}{\bar{\rho}\bar{c}}_d \\ u_d \\ \dot{q}' \end{bmatrix} \tag{6}$$

Now the eigenvalues can be computed as the roots s of the characteristic equation

$$\det(A(s)) = Z_d(s)\alpha - Z_u(s)\xi + Z_d(s)F(s)\theta = 0. \tag{7}$$

A similar formulation is given in [15, Eq. 7], where instead of an impedance, an upstream admittance is considered. The eigenvalues of the full system are related to the acoustics as well as to the flame dynamics.

3.2. Pure Acoustic Modes

The burner mouth and flame section is influenced by acoustic reflections up- and downstream as well as the heat release model. Eliminating the flame dynamics by setting the FTF to zero, $F = 0$ in Eq. (7), results in a pure acoustic system as shown in Fig. 3a with eigenvalues:

$$0 = Z_d(s)\alpha - Z_u(s)\xi\,. \tag{8}$$

For high frequencies, the flame response typically dies out $F(s) \approx 0$ and the characteristic equation of the full system (7) becomes the same as the one of the pure acoustic system (8). Therefore, at high frequencies acoustic modes are not affected by the flame.

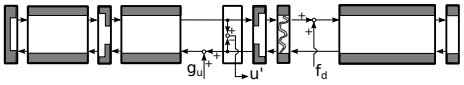

(a) Acoustic system.

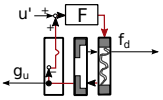

(b) ITA system feedback: heat release, upstream traveling wave and velocity fluctuation.

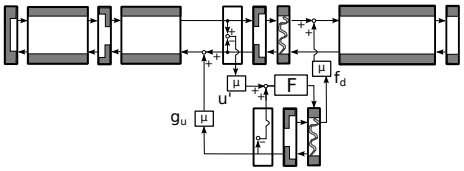

(c) Coupled, modulated system.

Fig. 3: Partitioning of the test rig network model.

3.3. *Pure Intrinsic Thermoacoustic Modes*

Eliminating acoustic reflections from the up- and downstream section instead imposes $Z_u = -1$, $Z_d = +1$ in Eq. (7). In this case, the system reduces to the ITA feedback system depicted in Fig. 3b with dispersion relation:

$$0 = \alpha + \xi + F(s)\theta\,. \tag{9}$$

This equation, which was previously reported by [4], [16, Eq. (14)] and [7, Eq. (14)], is clearly distinct from the acoustic modes of the system (8).

3.4. *Validation and Comparison of Full, Acoustic and Intrinsic System*

The eigenvalues of the full, the pure acoustic and the pure ITA system are displayed in Fig. 4. We observe that the number of the pure acoustic plus the number of the pure ITA eigenvalues is equal to the total number of full system eigenmodes. This suggests that the full set of system eigenmodes comprises acoustic and ITA modes.

There are three dominant – i.e. least decaying – modes of the full system (×) at approximately 42 Hz, 111 Hz and 315 Hz, delimited by the dashed line in Fig. 4. The growth rates of all eigenfrequencies are negative, thus the full system is stable. This is in agreement with [11], where it is mentioned that in the burner test rig an instability close to 100 Hz was observed. In the present model this mode is dominant and marginally stable.

According to a preliminary estimation [11], only two acoustic modes are expected in the frequency range under investigation. This is in agreement with the pure

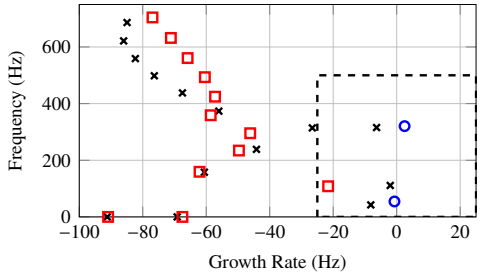

Fig. 4: Eigenfrequencies of full (×), acoustic (○) and ITA (□) system of the test rig model are corresponding but distinct.

acoustic modes (○) computed from Eq. (8) and shown in Fig. 4. Tay-Wo-Chong et al. [11] attributed one of the three dominant modes to "flame dynamics", which in the light of recent developments should be interpreted as an ITA mode (□) (Eq. (9)) at ≈ 111 Hz in the vicinity.

4. The Link Between Pure Acoustic, Pure ITA and Full System Modes

Now we want to know which eigenmodes should be regarded as acoustic modes driven by the unsteady heat release of the flame, and which should be considered intrinsic thermoacoustic modes perturbed by acoustic reflections. This cannot be simply identified from the spectrum shown in Fig. 4, as the distance between the eigenvalues is not a unique criterion. In order to establish this relation, the full system model is reformulated and factorized into pure acoustic and pure ITA sub-systems, respectively.

At first we switch from primitive variables p, u to characteristic waves (CWA) f, g:

$$f = (p/(\bar{\rho}\bar{c}) + u)/2\,; \quad g = (p/(\bar{\rho}\bar{c}) - u)/2 \tag{10}$$

For the up- and downstream sections this implies the transformation from impedances to reflection factors:

$$f_u = R_u g_u\,; \quad R_u = (Z_u + 1)/(Z_u - 1)\,, \tag{11}$$
$$g_d = R_d f_d\,; \quad R_d = (Z_d - 1)/(Z_d + 1)\,. \tag{12}$$

The burner and flame transfer matrix is transformed to scattering matrix as well:

$$\begin{bmatrix} g_u \\ f_d \end{bmatrix} = \begin{bmatrix} \frac{\alpha-\xi}{\alpha+\xi} & \frac{2}{\alpha+\xi} & \frac{\theta}{\alpha+\xi} \\ \frac{2\alpha\xi}{\alpha+\xi} & \frac{\xi-\alpha}{\alpha+\xi} & \frac{\xi\theta}{\alpha+\xi} \end{bmatrix} \begin{bmatrix} f_u \\ g_d \\ \dot{q}' \end{bmatrix}. \tag{13}$$

In order to close the FTF model the relation between the reference velocity fluctuation and the CWA $u_u = f_u - g_u$

is used. Eqs. (11), (12), (13) and (5) are combined:

$$0 = \underbrace{\begin{bmatrix} -1 & \frac{Z_u+1}{Z_u-1} & 0 & 0 & 0 & 0 \\ \frac{\alpha-\xi}{\alpha+\xi} & -1 & 0 & \frac{2}{\alpha+\xi} & 0 & \frac{\theta}{\alpha+\xi} \\ \frac{2\alpha\xi}{\alpha+\xi} & 0 & -1 & \frac{\xi-\alpha}{\alpha+\xi} & 0 & \frac{\xi\theta}{\alpha+\xi} \\ 0 & 0 & \frac{Z_d-1}{Z_d+1} & -1 & 0 & 0 \\ 1 & -1 & 0 & 0 & -1 & 0 \\ 0 & 0 & 0 & 0 & F & -1 \end{bmatrix}}_{A(s)} \begin{bmatrix} f_u \\ g_u \\ f_d \\ g_d \\ u_u \\ \dot{q}' \end{bmatrix}. \quad (14)$$

Each line of the system reflects the open loop transfer functions relating inputs and outputs of the network model and its closure on the right hand side by -1. The characteristic equation is

$$\det(A(s)) = 0 = \frac{-4(Z_d(s)\alpha - Z_u(s)\xi + Z_d(s)F(s)\theta)}{(\alpha+\xi)(Z_d(s)+1)(Z_u(s)-1)}. \quad (15)$$

The denominator is always non-zero. $Z_u = 1$ and $Z_d = -1$ would imply the respective reflection factors being infinite, while the parameters α and ξ are positive and bounded. Thus the eigenvalues need to fulfill the condition

$$0 = Z_d(s)\alpha - Z_u(s)\xi + Z_d(s)F(s)\theta, \quad (16)$$

which is the same as the characteristic equation of the system defined in primitive variables (compare Eq. (7)).

In contrast to the transfer matrix formulation in primitive acoustic variables p', u' we can now separate out the g_u waves caused by the flame. In Eq. (14) the heat release $\dot{q}'$ is driving g_u by $\theta/(\alpha+\xi)$ (column 6, row 2) and g_u in turn is acting on f_u by $(Z_u+1)/(Z_u-1)$ and u_u by -1 (column 2 and rows 1, 5). We rearrange the equations such that in Eq. (17) $\dot{q}'$ directly affects f_u by $(Z_u+1)/(Z_u-1)\cdot\theta/(\alpha+\xi)$ (column 6, row 1) and u_u by $-\theta/(\alpha+\xi)$ (column 6, row 5).

$$0 = \underbrace{\left[\begin{array}{cccc|cc} -1 & \frac{Z_u+1}{Z_u-1} & 0 & 0 & 0 & \frac{Z_u+1}{Z_u-1}\frac{\theta}{\alpha+\xi} \\ \frac{\alpha-\xi}{\alpha+\xi} & -1 & 0 & \frac{2}{\alpha+\xi} & 0 & 0 \\ \frac{2\alpha\xi}{\alpha+\xi} & 0 & -1 & \frac{\xi-\alpha}{\alpha+\xi} & 0 & \frac{\xi\theta}{\alpha+\xi} \\ 0 & 0 & \frac{Z_d-1}{1+Z_d} & -1 & 0 & 0 \\ \hline 1 & -1 & 0 & 0 & -1 & -\frac{\theta}{\alpha+\xi} \\ 0 & 0 & 0 & 0 & F & -1 \end{array}\right]}_{\tilde{A}(s)} \begin{bmatrix} f_u \\ g_u \\ f_d \\ g_d \\ u_u \\ \dot{q}' \end{bmatrix} \quad (17)$$

By transforming the system, the dynamics are not affected, thus the characteristic equation and eigenvalues do not change. But now the system of equations $\tilde{A}(s)$ has a block matrix structure, which should be interpreted as follows: The upper left 4 by 4 matrix captures the pure acoustic dynamics, whereas the lower right 2 by 2 matrix, as we will show, models the intrinsic system. On the off diagonal there are coupling terms for the acoustic system acting on the intrinsic system (lower left) and the intrinsic system driving the acoustic system (upper right). This way to partition and interconnect the pure acoustic and pure ITA system is depicted in Fig. 3c. The acoustic system is feeding velocity perturbations at the burner mouth into the ITA system, where they contribute to the perturbations of the intrinsic system itself and resonate in ITA feedback. In turn, acoustic waves g_u, f_d generated by the ITA system are fed back into the acoustic system. As a final step a modulation parameter μ for the coupling terms is introduced:

$$0 = \underbrace{\begin{bmatrix} -1 & \frac{Z_u+1}{Z_u-1} & 0 & 0 & 0 & \boldsymbol{\mu}\frac{Z_u+1}{Z_u-1}\frac{\theta}{\alpha+\xi} \\ \frac{\alpha-\xi}{\alpha+\xi} & -1 & 0 & \frac{2}{\alpha+\xi} & 0 & 0 \\ \frac{2\alpha\xi}{\alpha+\xi} & 0 & -1 & \frac{\xi-\alpha}{\alpha+\xi} & 0 & \boldsymbol{\mu}\frac{\xi\theta}{\alpha+\xi} \\ 0 & 0 & \frac{Z_d-1}{1+Z_d} & -1 & 0 & 0 \\ \boldsymbol{\mu} & -\boldsymbol{\mu} & 0 & 0 & -1 & -\frac{\theta}{\alpha+\xi} \\ 0 & 0 & 0 & 0 & F & -1 \end{bmatrix}}_{\tilde{A}(s)} \begin{bmatrix} f_u \\ g_u \\ f_d \\ g_d \\ u_u \\ \dot{q}' \end{bmatrix}. \quad (18)$$

Sweeping the value of this parameter from $\mu = 0$ to $\mu = 1$ allows a continuous transition between the original full system ($\mu = 1$) and the pure acoustic and ITA systems. Choosing the parameter $\mu = 0$ results in the characteristic equation:

$$\det(\tilde{A}(s)) = (Z_d\alpha - Z_u\xi)(\alpha + \xi + F\theta) = 0, \quad (19)$$

which is factorized into the sum of pure acoustic and ITA eigenvalues (see Eq. (8),(9); Fig. 3).

This way to transform and rearrange the system seems tedious, however it would not be sufficient to simply modulate the FTF $F \to \mu F$. If one were to do so, $\mu = 1$ would give the full system, while $\mu = 0$ would result in pure acoustic, but not in pure ITA modes.

5. Numerical Results

Now the test rig system is examined using the derivations from the previous sections. For this purpose, the eigenvalues and eigenvectors of the systems under investigation are computed. At first the modulation parameter μ is used to discriminate between acoustic and ITA eigenmodes of the full system. Subsequently, the eigenvectors of the most dominant eigenmodes are analyzed. Eventually the influence of the downstream reflection coefficient on the eigenvalues of the system is investigated.

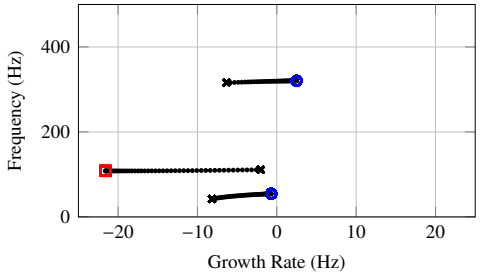

Fig. 5: Correspondence of acoustic (○) and ITA (□) to full system (×) eigenmodes. Modulation parameter μ is varied from 0 to 1 (•).

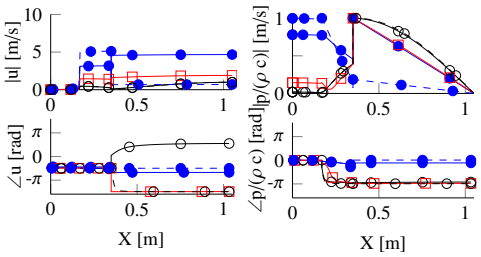

Fig. 6: Velocity and pressure mode shapes of the acoustic 1/4 wave (full: —●—, pure: - ●-), 3/4 wave (full: —○—, pure: - ○-) and ITA mode (full: —□—).

5.1. Correspondence of Eigenvalues

In the previous sections, we have shown that for $\mu = 0$ the eigenmodes of the pure acoustic and ITA systems emerge. For $\mu = 1$, the full system dynamics are recovered from the modulated system. Now a sweep of μ from 0 to 1 is performed and the resulting eigenvalues of the coupled system are shown in Figure 5. By doing so, a 1:1 relation between the eigenmodes of the full system and the pure acoustic and ITA modes is established. We observe, that the three dominant eigenmodes of the system stem in fact from two acoustic and one intrinsic mode, respectively. Both acoustic eigenmodes are stabilized by the coupling with the flame dynamics, i.e. the growth rates become more negative as μ increases. Conversely the ITA mode becomes more unstable.

5.2. Comparison of Mode Shapes

The eigenvectors of the first (1/4 wave) and second (3/4 wave) acoustic and the dominant ITA eigenmode are shown in Figure 6. The mode shapes of the pure acoustic system are drawn as dashed lines, wheres the full system modes are full lines.

The first acoustic mode (—●—,- ●-) has almost constant phase for both pressure and velocity and therefore is a quarter wave resonance of the system. Due to the coupling with the flame, it is shifted towards higher pressures and velocities in the combustion chamber and lower velocities in the swirler section. This is what is to be expected as the flame is mainly acting as a volume source.

We observe that the second acoustic mode (—○—,- ○-) has one phase jump of π in velocity at the temperature jump and a phase jump in pressure at the area contraction at the end of the plenum. Thus it can be identified as a three quarter wave resonance of the entire test rig. Overall, the second acoustic mode shape is not much affected by the coupling with the flame. The pure (- ○-) and the full (—○—) system mode shapes are very similar.

The ITA mode shape (—□—) can only be visualized for the full system, because the pure intrinsic mode is just due to flame dynamics and does not possess an acoustic field. It has features similar to both acoustic modes, which is remarkable given that the frequencies of the modes are so different. The pressure profile is similar to the one of the second acoustic mode (—○—), including the phase jump at the end of the plenum, whereas the velocity profile seems closer to the one of the first acoustic mode (—●—). Thus it is difficult to distinguish the intrinsic mode from acoustic modes by comparing mode shapes.

6. Destabilization of ITA Modes by Acoustic Losses

The investigations carried out in the previous chapters imposed a perfectly reflecting open end as downstream boundary condition. As mentioned by Tay-Wo-Chong et al. [11], in experiment the test rig is terminated by a perforated plate instead, which results in less acoustic reflections, which implies more loss of acoustic power. Traditionally, it is assumed that this leads to a more stable configuration. In order to find out whether this stabilizing effect is realized, we carry out a parameter study of the changes in eigenvalue due to changes in the reflection coefficient at the combustor exit. It is varied between $R_x = -1$, which is a fully reflective open end and $R_x = 0$, a non-reflective boundary condition. The level in the experiment is bounded by those values.

Figure 7 shows the eigenvalues of the full system as previously investigated (fully reflective open end $R_x = -1$, Eq. 7, Fig. 1). Eigenvalues of the full system attributed primarily to acoustic resonance (○) and ITA feedback (□) are indicated (compare with (×) in Fig 5). As the reflections are gradually lowered, the eigenvalues change and end up at positions denoted with a cross for the non reflective boundary condition ($R_x = 0$).

As expected, the reduction of the downstream reflection coefficient has a stabilizing effect on the two acous-

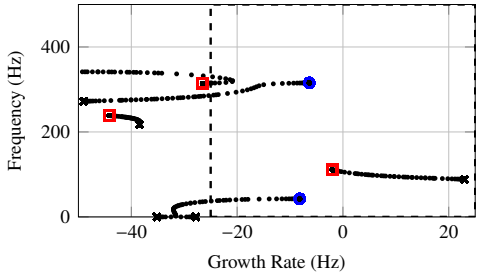

Fig. 7: Eigenvalue shift due to changes in downstream reflection factor. Fully reflective ($R_x = -1$) open end: acoustic modes (○), ITA modes (□); Gradually lower reflections (•) until non reflective (✖).

tic modes of the system. The first acoustic mode, which is a quarter wave mode, degenerates for a non reflective downstream boundary to a frequency of 0 Hz. Due to the plenum, the second acoustic mode remains resonating, but is heavily damped.

In contrast to the acoustic modes, the intrinsic mode is amplified and eventually becomes unstable as the reflection coefficient R_x is reduced. Similar observations were made by [5] in numerical simulations of laminar premixed flames. In the common perception of thermoacoustic instability, where only acoustic modes are considered to become unstable due to the driving by the flame, this is a surprising result. Typically one would assume that less reflections relate to more acoustic losses and therefore increased thermoacoustic stability. In closing it is mentioned that this result aligns with the assertion of [11] that in the experiment this mode is unstable despite the low reflection coefficient.

7. Conclusion

The paper shows that the set of thermoacoustic eigenmodes of a premixed combustion test rig should be interpreted as the sum of acoustic and intrinsic thermoacoustic (ITA) modes. The paradox that reducing acoustic reflections at the boundaries may render a thermoacoustic system unstable is explained by ITA feedback: increased losses damp acoustic modes, but may amplify an ITA mode.

ITA feedback and the corresponding modes must be taken into consideration in comprehensive thermoacoustic stability analysis. Note that this should not require a reformulation of thermoacoustic models, because typical implementations do consider all interactions that contribute to the ITA feedback loop. Results of previous investigations of thermoacoustic instabilities, which have sometimes produced inexplicable eigenfrequencies or eigenmodes, should be revisited and re-interpreted under the perspective of ITA modes.

The concept of intrinsic feedback and the associated eigenmodes is fairly general. It can be expected to apply to different combustion regimes and a wide range of phenomena related to sound generation and amplification. For example, in practical premixed flames acoustic waves generated by heat release fluctuations can couple with the fuel mixing process in an intrinsic manner. Similar feedback structures should exist for swirl fluctuations. Intrinsic feedback may also contribute to aeroacoustic whistling.

8. Acknowledgment

Financial support for S. Jaensch by the Research Association for Combustion Engines (Forschungsvereinigung Verbrennung e.V - FVV, project: 6011150) and for S. Bomberg by Technische Universität München Institute for Advanced Study, funded by the German Excellence Initiative, and German Research Foundation (DFG, project PO 710/12-1), is gratefully acknowledged. We also like to thank Dr. Luis Tay Wo Chong Hilares [11] for providing the LES data which was used to determine the FTF.

References

[1] J. W. S. Rayleigh, Nature 18 (1878) 319–321.
[2] T. Lieuwen, V. Yang (Eds.), Combustion Instabilities in Gas Turbine Engines, volume 210 of *Progress in Astronautics and Aeronautics*, AIAA, 2005.
[3] M. Hoeijmakers, V. Kornilov, I. Lopez Arteaga, P. de Goey, H. Nijmeijer, Combust. Flame 161 (2014) 2860–2867.
[4] E. Courtine, L. Selle, T. Poinsot, Combust. Flame 162 (2015) 4331–4341.
[5] C. F. Silva, T. Emmert, S. Jaensch, W. Polifke, Combust. Flame 162 (2015) 3370 – 3378.
[6] S. Bomberg, T. Emmert, W. Polifke, Proc. Combust. Inst. 35 (2015) 3185–3192.
[7] T. Emmert, S. Bomberg, W. Polifke, Combust. Flame 162 (2015) 75–85.
[8] A. Dowling, G. Bloxsidge, in: 9th Aeroacoustics Conference, AIAA-84-2321, AIAA/NASA, 1984, p. 1984.
[9] B. Schuermans, V. Bellucci, C. O. Paschereit, Proc. of ASME Turbo Expo 2003 Power for Land, Sea and Air, ASME, 2003, pp. 509–519.
[10] M. Bothien, J. Moeck, A. Lacarelle, C. O. Paschereit, Proc. Inst. Mech. Eng. Part J. Power Energy 221 (2007) 657–668.
[11] L. Tay-Wo-Chong, S. Bomberg, A. Ulhaq, T. Komarek, W. Polifke, J. Eng. Gas Turbines Power 134 (2012) 021502–1–8.
[12] T. Komarek, W. Polifke, J. Eng. Gas Turbines Power 132 (2010) 061503–1,7.
[13] T. Emmert, S. Jaensch, C. Sovardi, W. Polifke, in: 7th Forum Acusticum, Krakow.
[14] B. T. Chu, in: 4th Symposium (International) on Combustion, volume 4, pp. 603–612.

[15] J. Moeck, C. Scharfenberg, O. Paschereit, R. Klein, in: Active Flow Control II, volume 108 of *Notes on Numerical Fluid Mechanics and Multidisciplinary Design*, 2010, pp. 291–306.
[16] M. Hoeijmakers, V. Kornilov, I. L. Arteaga, P. de Goey, H. Nijmeijer, Proc. Combust. Inst. 35 (2015) 1073–1078.